TABLE OF CONTENTS

NASA Contractor Report 3355

Effect of Ambient Conditions on the Emissions From a Gas Turbine Combustor

C. W. Kauffman

GRANT NSG-3045
NOVEMBER 1980

NASA

NASA Contractor Report 3355

Effect of Ambient Conditions on the Emissions From a Gas Turbine Combustor

C. W. Kauffman
University of Cincinnati
Cincinnati, Ohio

Prepared for
Lewis Research Center
under Grant NSG-3045

National Aeronautics
and Space Administration

**Scientific and Technical
Information Branch**

1980

BLANK PAGE

BLANK PAGE

TABLE OF CONTENTS

INTRODUCTION

The 1979 Environmental Protection Agency aircraft emissions standards require that newly manufactured aircraft gas turbine engines be tested for compliance with emission standards. These standards are based upon engine testing at standard day conditions. It is extremely difficult to provide the enormous quantities of air necessary to operate large turbo-fan engines at standard day conditions, so preliminary emission certification testing commenced utilizing ambient air. A trend appeared that the engine to engine variations in emissions were greater than were thought to be attributable to manufacturing tolerances. It was postulated that this engine to engine variation was in part due to the varying atmospheric conditions on the days that the engines were tested.

The effect of inlet pressure, temperature, and humidity on the oxides of nitrogen produced by an engine operating at take-off power was noted quite early, and subsequent correlations were formulated by Lipfert[1]. A compilation and evaluation of these correlations has recently been given by Rubins and Marchionna[2]. For smoke, which is a pollutant of concern at high thrust settings, a recently reported result[3] indicates that the smoke number variability can be correlated to changes in the ambient inlet temperature. For a combustor operating at idle conditions, correlations were developed by Marzeski and Blazowski[4] to account for the effects of nonstandard inlet pressure and temperature on gaseous emissions. The effect of ambient

temperature and pressure on gaseous emissions over the complete thrust range for samples of a given production engine have been correlated by Sarli et al.[5] With the exception of some limited engine test data presented by Nelson et al.[6], Mosier and Roberts[7], and Allen and Slusher[8], the effect of humidity on idle emissions has received little attention even though the extreme sensitivity of CO oxidation to the presence of water vapor is well known.

This investigation was initiated in order to determine, in a systematic way and under controlled conditions, the effect of variations in the ambient conditions of pressure, temperature, and relative humidity upon the emissions of a gas turbine combustor. A single combustor can from a Pratt and Whitney JT8D-17 engine was run at parametric inlet conditions bracketing the actual engine idle conditions. Nonvitiated inlet air was used, and fuel was supplied through a flight certified fuel nozzle. These data were then correlated in order to determine the functional relationships between the emissions and ambient conditions.

These correlations, though useful to account for day to day variances in emissions, do not give any insight into the mechanism by which the generation of these pollutants is influenced by atmospheric conditions. It is for this reason that a mathematical modelling effort was initiated to explain the observed behavior of carbon monoxide and unburned hydrocarbons.

The carbon monoxide emissions were modelled using finite rate chemical kinetics in a plug flow scheme. The combustor was divided into three zones, primary, secondary, and dilution, and appropriate values were chosen for the local fuel-air ratio in

each zone. The initial species concentrations reflected not only the local combustor characteristics but also the effect of the changing inlet conditions.

Hydrocarbon emissions were believed to result from the failure of large droplets to completely vaporize. Vaporization calculations were performed for a Rosin-Rammler fuel drop distribution as it passed through the three zones of the combustor. The temperatures in each zone were based on the adiabatic flame temperature for that zone as determined by the local combustor characteristics and the changing inlet conditions.

EXPERIMENTAL EFFORT

Test Apparatus

The experimental program was conducted in a closed duct combustor test facility described in detail by Fear[9] and located in the Engine Research Building of the NASA Lewis Research Center. A single Pratt and Whitney JT8D-17 combustor can, shown in cross section in Figure 1, was supplied with the appropriate quantity of Jet A fuel and nonvitiated air. The combustor inlet conditions of pressure, temperature, and humidity were varied parametrically around the actual engine idle inlet conditions. The combustor installation and instrumentation are shown in Figure 2. The water content of the air furnished to the combustor was controlled by injecting demineralized water into the hot airstream approximately 5 meters upstream of the combustor. The water was injected through a pressure atomizing spray nozzle and complete vaporization of the water occurred before it entered the combustor. The water content of the air supplied by the preheater was continually monitored using an EGG optical sensor and it was nominally quite small, with a dew point of approximately 239 K. The combustor emissions were measured according to SAE specifications[10].

Test Conditions

The actual JT8D-17 idle operating conditions are shown in Table I. Table II lists the parametric inlet conditions investigated in this report. Compressor pressure ratios of 2, 3, 4,

and 5 were chosen, with the combustor inlet temperature, T_3, calculated assuming a compressor efficiency of 80%. The mass flow through the combustor was determined by maintaining a constant compressor discharge Mach number, M_3, or a constant reference velocity, V_3.

The mass flow into the combustor consists of both air and water, the combination of which may be considered an oxidizer. The fuel flow was set to maintain a constant fuel-air ratio and not a constant fuel-oxidizer ratio. A changing fuel flow rate was therefore dictated. This resulted in a different combustor discharge temperature, T_4, for each test point. Three different values of the overall fuel-air ratio were run in order to investigate the effect of local stoichiometry upon the emissions of the combustor.

Experimental Results

Unburned Hydrocarbon Emissions

The unburned hydrocarbon emission data is shown in Figures 3 to 11. Figures 3 to 7 present data obtained when the combustor reference velocity was maintained constant at 15.2 meters per second, and Figures 8 to 11 present data obtained holding combustor inlet Mach number constant at 0.42. Each set of data was obtained at the four different compressor pressure ratios of 2, 3, 4, and 5. Each figure presents data for one compressor pressure ratio and contains three sets of data, each corresponding to one of the three overall fuel-air ratios run. Within each fuel-air ratio grouping the ambient compressor inlet

temperature, T_o, and the relative humidity, RH, were varied. For each of the three ambient temperatures considered, data were obtained at three relative humidities with the exception of the T_o = 244 K condition where only one value of relative humidity was run due to extremely small water concentration necessary to cause saturation.

On all figures the ordinate is the emission index of unburned hydrocarbons in grams of CH_2 per kilogram of fuel burned, and the abscissa is the combustor discharge temperature, T_4. Early in the program it was thought that the combustor discharge temperature would be the dominant factor in determining the emissions.

On all figures a key to the data is presented. The shape of the symbol indicates the relative humidity, a circle for zero percent, a square for fifty percent, and a diamond for one hundred percent. A flag is used to indicate compressor inlet temperature. No flag indicates 244 K, a vertical flag 289 K, and a horizontal flag indicates 322 K compressor inlet temperature. The shading of the symbol indicates the overall fuel-air ratio. Bottom half shading indicates .007, top half shading indicates .011, and no shading indicates an overall fuel-air ratio of .015.

The following trends can be easily recognized for the combustor discharge temperature. A higher fuel-air ratio will result in a higher combustor discharge temperature if all other conditions are held constant. Increasing the ambient inlet temperature will result in an increased combustor discharge

temperature for a fixed relative humidity and fuel-air ratio. For a fixed fuel-air ratio and ambient inlet temperature, increasing the relative humidity decreases the combustor discharge temperature.

The following trends can be recognized for the hydrocarbon emissions. Curves A_1 and A_7 on Figure 3 show that an increase in fuel-air ratio results in a decrease in the hydrocarbon emission index if all other conditions are held constant. Connection of other points for identical ambient inlet conditions also gives the same trend. For a fixed fuel-air ratio, pressure ratio, and zero relative humidity, an increase in the compressor inlet temperature effects a decrease in the hydrocarbon emissions as shown by curves B_1, B_2, and B_3 on Figure 3. For a fixed fuel-air ratio, pressure ratio, and compressor inlet temperature an increase in the relative humidity effects an increase in the hydrocarbon emission index. This effect is especially noticeable for the 322 K inlet temperature data and is shown by curves C_1, C_2, and C_3 on Figure 3. At this condition saturation corresponds to 8.12 mass percent water vapor. For all conditions fixed except pressure, an increase in pressure effects a decrease in the hydrocarbon emission index. In a qualitative fashion one can see that for all fuel-air ratios the slope of $[\partial(EI\text{-}HC)/\partial T_4]_{RH=0}$, curves B_1, B_2, and B_3 of Figure 3,is less negative than the slope of $[\partial(EI\text{-}HC)/\partial T_4]_{RH=1}$, curves D_1, D_2 and D_3 of Figure 3. For all curves the slope becomes less negative with increasing fuel-air ratios. In other words, humidity affects the unburned

hydrocarbon emissions more strongly at lower adiabatic flame temperatures, and humidity has a stronger influence on emissions than compressor inlet air temperature.

This data clearly shows that the combustor exit temperature does not uniquely determine the overall emissions as was first postulated. In order to determine the repeatability of the data, the experimental conditions run for Figure 3 were rerun several weeks after the initial data collection. The results of this run are shown in Figure 4. Although slight variances in the actual emissions are detected, the qualitative trends from Figure 3 are clearly reproduced.

Figures 5, 6, and 7 depict the unburned hydrocarbon emissions for compressor pressure ratios of 3, 4, and 5 respectively. Figures 8, 9, 10, and 11 present the remaining unburned hydrocarbon emission data taken for a constant combustor inlet Mach number of 0.42. In all cases data were taken over the same pressure, inlet temperature, and humidity matrix. The constant inlet Mach number data displays the same qualitative trends as the constant reference velocity data.

Carbon Monoxide Emissions

The carbon monoxide emission data is presented in Figures 12 to 20. Figures 12 to 16 present data obtained at a constant combustor reference velocity of 15.2 meters per second, and Figures Figures 17 to 21 present data obtained holding combustor inlet Mach number constant at 0.42.

The test matrix for the carbon monoxide emissions was identical with that for the unburned hydrocarbons, as the two were

simultaneously measured. On all figures the ordinate is the emission index of carbon monoxide in grams of carbon monoxide per kilogram of fuel burned, and the abscissa is the combustor discharge temperature. A key to the data is presented on all figures.

The following trends can be recognized from the carbon monoxide emission data. Curves E_1 and E_7 on Figure 12 show that an increase in fuel-air ratio results in a decrease in the carbon monoxide emission index if all other conditions are held constant. For a fixed fuel-air ratio, pressure ratio, and zero relative humidity, an increase in the compressor inlet temperature effects a decrease in the carbon monoxide emissions as shown by curves F_1, F_2, and F_3 on Figure 12. For a fixed fuel-air ratio, pressure ratio, and compressor inlet temperature an increase in the relative humidity effects an increase in the carbon monoxide emission index. This effect is shown by curves G_1, G_2, and G_3 on Figure 12. In a qualitative fashion one can see that for all fuel-air ratios the slopes $[\partial(EI\text{-}CO)/\partial T_4)_{RH=0}$, curves F_1, F_2, and F_3 on Figure 12, are nearly identical; while the slopes $[\partial(EI\text{-}CO)/\partial T_4]_{RH=1}$, curves G_1, G_2, and G_3, becomes less negative with increasing fuel-air ratio. At the fuel-air ratio equal to 0.015 case the slopes are nearly identical. In other words, changes in relative humidity have a stronger influence upon the carbon monoxide emissions than do changes in the compressor inlet air temperature.

In general the trends shown by the carbon monoxide emissions are very similar to the trends displayed by the unburned hydrocarbons. Again one sees that the carbon monoxide emissions are not uniquely determined by the combustor exit temperature.

In order to determine the repeatability of the data, the pressure ratio two data was rerun several weeks after the initial data of Figure 12 was taken. The rerun data is presented in Figure 13. Although variations in the actual emissions are present, the qualitative trends are reproduced.

Figures 14, 15, and 16 present the carbon monoxide emissions for pressure ratios of 3, 4, and 5, respectively. Figures 17, 18, 19 and 20 present the remaining carbon monoxide data taken for the constant combustor inlet Mach number case. The data was taken over the same test matrix as for the previous figures presented. The constant inlet Mach number data display the same qualitative trends as the constant reference velocity data.

Oxides of Nitrogen Emissions

The oxides of nitrogen data is shown in Figures 21, 22, 23, and 24 for a constant reference velocity of 15.2 meters per second and in Figures 25, 26, 27, and 28 for a constant combustor inlet Mach number of 0.42. The test matrix for the oxides of nitrogen was identical with that for all other emissions. On all figures the ordinate is the emission index of total oxides of nitrogen in grams of nitrogen dioxide per kilogram of fuel burned. The abscissa is the combustor discharge temperature. A key to the data is presented on all the figures.

For the total oxides of nitrogen, the following trends are observed. For a given ambient condition the oxides of nitrogen may either remain constant or increase as shown in Figure 21 by curves I_1 and I_7. At a given pressure, a fixed fuel-air ratio, and zero humidity, an increase in the ambient compressor inlet temperature effects an increase in the emission index, as shown by curves J_1, J_2 and J_3 on Figure 21. For a fixed pressure, fuel-air ratio, and ambient compressor inlet temperature, an increase in relative humidity causes a decrease in the total oxides of nitrogen emission index. The effect is quite noticeable when the amount of water necessary for saturation is quite large, as shown by curves K_1, K_2, and K_3 on Figure 21. An increase in pressure, with all other parameters constant, increases the emission index. The slopes $[\partial(\text{EI-NOx})/\partial T_4]_{RH=0}$, curves J_1, J_2 and J_3 on Figure 21, and $[\partial(\text{EI-NOx})/\partial T_4]_{RH=1}$, curves L_1, L_2 and L_3 on Figure 21, are seen to be little affected by overall fuel-air ratio.

Figures 22, 23, and 24 present the remainder of the oxides of nitrogen emissions for the constant reference velocity case. Difficulty was experienced with the chemiluminescent instrumentation during portions of the overall test program. It is for this reason that incomplete data is presented in Figure 23. Figures 25, 26, 27, and 28 present the oxides of nitrogen emissions for the constant compressor inlet Mach number case. The constant inlet Mach number data display the same qualitative trends as the constant reference velocity data.

Nitrogen Dioxide Emissions

The nitrogen dioxide emissions are shown in Figures 29, 30, 31, and 32 for a constant combustor reference velocity of 15.2 meters per second and for compressor pressure ratios of 2, 3, 4 and 5, respectively. Figures 33, 34, 35, and 36 present the same data for a constant combustor inlet Mach number of 0.42. The test matrix for the nitrogen dioxide emissions is identical with that for all the other emissions. On all figures the ordinate is the emission index of nitrogen dioxide in grams of nitrogen dioxide per kilogram of fuel burned. The abscissa is the combustor discharge temperature. A key to the data is presented on all figures. Figure 31 presents incomplete data due to difficulty with the chemiluminescent instrumentation.

Most of the nitrogen dioxide emission plots display the same trends as the oxides of nitrogen emissions. This is shown by the similarity of the curves on Figure 29 with the curves on Figure 21. However, for data taken at pressure ratios of 4 and 5, Figures 31, 32, 35 and 36, it is difficult to recognize the functional dependence of the nitrogen dioxide emissions index on ambient inlet conditions. An examination of all the nitrogen dioxide emission data shows that the functional dependence of the nitrogen dioxide emissions is identical to the total oxides of nitrogen emissions as long as the combustor discharge temperature is less than 900 K. Below this temperature the nitrogen dioxide emissions are a substantial portion of the total oxides of nitrogen. Above this temperature nitrogen dioxide emissions are no longer a significant amount of the oxides of nitrogen emissions as the high temperature causes the nitrogen dioxide to form nitric oxide.

Empirical Emissions Correlations

For regulatory purposes the convenient independent variables in a correlation equation are the pressure, temperature, and humidity at the compressor discharge plane — p_3, T_3, and HUM, respectively — and the overall engine fuel-air ratio, FAR. The experimental data from this study was employed to generate such an equation for the emission index of each pollutant species. Because of the similarity between the constant velocity and constant Mach number data, separate correlations were not developed. The emission data were fit employing a stepwise multiple linear regression program to determine the coefficients in an equation of the following form:

$$EI = (p_3/6.894 \times 10^3)^a \exp [b + (FAR/c) + (9T_3/5d) + (HUM/e)]$$

where the respective dimensions are:

EI(gms/kg), p_3(pascals), T_3(K), and HUM(gms H_2O/kg air).

The coefficients as determined by the program are given in Table III for two extremes; all data collected, and various subcases selected to maximize the correlation. To maximize the correlations for the hydrocarbons and the carbon monoxide, the data collected at a compressor discharge pressure of two atmospheres was not included. The correlation consistently under-predicted the emissions at this pressure ratio due to marginal combustion in the burner can. For the case of total oxides of nitrogen only the data for a fuel-air ratio of .015 was included since the production of oxides of nitrogen is highest under these conditions.

Graphically the agreement between the measured emissions and the predicted emissions by regression analysis is shown in Figures 37, 38, and 39 for the selected data case. The relationship between the emissions and the chosen variables would appear to be adequately established as the correlation coefficients, R^2, clearly show.

Discussion

For a T-56 combustor the effect of ambient conditions on the gaseous emissions is surprisingly similar to that of the JT8D-17. The emission data of Marzeski and Blazowski[4], shown in Figures 40, 41, and 42, was collected using a T-56 combustor employing two different fuels, JP-4 and JP-8. Three different geometric modifications were run giving different primary zone fuel-air ratios of nominal, rich, and lean while maintaining a constant overall fuel-air ratio. The relative humidity of the inlet air was close to zero, the simulated compressor pressure ratio was three, and the compressor discharge Mach number was held constant. The changing combustor discharge temperature represents changes in ambient inlet temperature between 244 K and 322 K.

Although the absolute values of the emission indices for the T-56 vary slightly from the JT8D-17, at identical compressor pressure ratios and combustor discharge temperatures, the sensitivities of the emission index to changes in combustor discharge temperature, i.e. the slopes $[\partial(EI)/\partial T_4]_{RH=0.0}$, for hydrocarbons, carbon monoxide, and oxides of nitrogen are nearly identical. Perhaps this is not surprising considering that these two combustors are of a similar vintage, loading, air splits, and

reference velocity. Such a similarity among various combustors could ease the regulatory task of developing correction factors for each combustor for nonstandard inlet conditions.

ANALYTICAL EFFORT

Model

The experimental results indicate that the hydrocarbon and carbon monoxide emissions are decreased by increasing fuel-air ratio, pressure ratio, or ambient compressor inlet temperature; while they are increased by increasing relative humidity. For the oxides of nitrogen emissions the situation is just the reverse. The behavior of the oxides of nitrogen emissions have been modelled to account for all the observed effects by Blazowski et al.[12] Some of the mechanisms of carbon monoxide production within the gas turbine combustor have been previously modelled by Morr et al.[13] A less sophisticated model, but including a limited effect of ambient conditions, has been presented by Sarli[5].

In the model considered here and discussed in detail by Subramaniam[14], it is suggested that the combustor may be treated as a plug flow reactor in which there is homogeneous reaction between perfectly mixed fuel and oxidizer under the isothermal conditions corresponding to the adiabatic flame temperature. Since the kinetics representing the oxidation of a complex hydrocarbon fuel, such as Jet A, are only poorly understood, methane was chosen as the fuel for employment in the chemical kinetics scheme. In computing the carbon monoxide emissions it must be emphasized that instantaneous and complete evaporation of the fuel was assumed.

Previous hydrocarbon emission modelling conducted by Marchionna et al.[15] indicated that much of the unburned hydrocarbon emissions result from the escape of raw fuel. Therefore it is necessary to consider the vaporization of fuel droplets as they pass in a plug flow fashion through the combustor for the determination of the unburned hydrocarbon emissions.

For both pollutant species the calculation process is initiated by determining the adiabatic flame temperature within a particular combustor zone using the NASA CEC-71 computer program[16]. The combustor inlet conditions of temperature, pressure, and water content were the same as those used during the collection of the data. The fuel-air ratio within the combustor was determined by the total fuel flow rate and the air flow splits within the combustor as shown in Figure 1.

Carbon Monoxide Model

In the kinetic scheme for modelling the carbon monoxide emissions it was assumed that methane was instantaneously mixed with air and water vapor in the primary zone to obtain the desired fuel-air ratio within that zone. The mixture was then allowed to react for a period of time corresponding to the appropriate primary zone residence time at a temperature which corresponded to the adiabatic flame temperature. The primary zone combustion products were then instantaneously mixed with the quantity of additional air necessary to simulate entrance into the secondary combustion zone. The mixture was again allowed to react at the temperature representing the new adiabatic flame temperature for a period of time representing the appropriate

residence time in this zone. This process was again repeated in the dilution zone.

The methane-air kinetic scheme employed is that given by Ay and Sichel[17] and listed in Table IV. The second rate constant in reaction nine is similar in nature to that developed by Kollrack[18], but it is an order of magnitude smaller in order to prevent excessive oxidation of the carbon monoxide. It may be worthwhile to note that the species HO_2 and NO_2 are not included in the reaction scheme. Simultaneous solution of the rate equations for all species was done using the NASA GCKP-72 computer program[19]. The initial species composition utilized in this program differed for each ambient condition and for each combustor region.

Unburned Hydrocarbons Model

For modelling the unburned hydrocarbons a distribution of JP-4 fuel droplets was passed through the respective plug flow zones of the combustor. The amount of vaporization was determined by the local adiabatic flame temperature and the local residence time. Limited atomization data exists for the JT8D-17 fuel nozzle in the open literature. Therefore a Rosin-Rammler droplet size distribution function was assumed for the spray. This distribution gives the weight fraction of particles, R, having a diameter larger than a given diameter, d, i.e. $R = \exp(-bd^q)$. The value of the parameter indicating the monodisperse nature of the spray, q, was assumed to be similar to those determined for airblast atomizers[15]. The value of the parameter determining the mean drop size, b, of the spray was obtained by fitting experimentally measured emission data at one reference condition. To calculate

the amount of fuel vaporized, the drop distribution was divided into small segments and the diameter squared vaporization law was applied including corrections for convective enhancement, i.e.

$$d_o^2 - d^2 = Kt \quad ,$$

$$K_{static} = (8/\rho_\ell)(k_g/C_{pg}) \ln (B + 1) \quad ,$$

$$B = C_{pg} [(T - T_b)/L] \quad ,$$

and

$$K_{cov} = K_{static} (1 + .276 \, Re^{.5} \, Pr^{.33}) \quad .$$

The Reynolds number, Re, the Prandtl number, Pr, the gas conductivity, k_g, and the specific heat, C_{pg}, were determined by local conditions in each zone of the combustor. The droplets were allowed to remain in each zone for their characteristic residence time. All droplets were assumed to have an initial velocity of 60 m/s and the drag coefficient was parameterized by:

$$C_D = 28/Re^{.85} + .48 \quad .$$

Analytical Results

Because of limited computer access time, calculations were performed at a compressor pressure ratio of four only.

Values of the adiabatic flame temperature reflecting the effects of different ambient conditions are shown in Figure 43. The effect of humidity is to reduce the flame temperature. Lines of constant fuel-air ratio may be constructed on this figure using the data in Figure 44. For a given inlet temperature and relative humidity a fuel-air ratio is chosen and the value of the equivalence ratio is determined. This process may then be repeated for different inlet conditions but the same

fuel-air ratio. The results presented in Figure 45 relate the fuel-oxidizer and equivalence ratios.

It has not been clearly established where the cooling air from a given louver mixes with the main flow within the combustor. It may mix immediately within the zone in which it is introduced or it may not mix until subsequent zones. Hence for a given fuel flow a maximum and a minimum possible fuel-air ratio can be computed for each of the three combustor zones depending upon where the film cooling air is assumed to mix. For an overall fuel-air ratio of .011 the zone fuel-air ratios are given in Table V along with an upper and lower temperature and the residence time corresponding to these local conditions. For the primary zone a 2 ms residence time is typical while for the secondary and dilution zones a 4 ms and a 3 ms residence time, respectively, are more representative.

In the primary zone the carbon monoxide concentration is very near the equilibrium value as the computational results show in Figure 46. Using the plug flow reactor approach the effect of changing ambient conditions on the amount of carbon monoxide at the end of the primary zone is shown in Figure 47. Here the correction factor CF_{CO} is defined as the mole fraction of carbon monoxide at standard ambient conditions (T_o = 289 K, RH = 0%) divided by the mole fraction of carbon monoxide at nonstandard ambient conditions. Three different primary zone fuel-air ratios are considered, but the effects of ambient temperature and humidity changes are similar for each.

An increase in the ambient temperature causes an increase in the carbon monoxide mole fraction and an increase in the ambient humidity causes a decrease in the carbon monoxide mole fraction. These effects are precisely opposite to that observed in the experimental measurements but are in agreement with the burner measurements of Muller-Dethlefs and Schlader[20]. These results are simply explained by considering the effect of flame temperature on dissociation of CO_2. As the flame temperature increases due to increasing temperature or decreasing humidity, the formation of CO and O is favored. Miles also finds the same inverse ambient effects when the primary zone is treated as a perfectly stirred reactor employing a global hydrocarbon kinetic scheme. (Private communication from G. A. Miles, Detroit Diesel Allison Div., General Motors Corp., Indianapolis, Indiana in August 1976.)

In view of these results, it appears that the kinetics in the secondary and dilution zones are the ones primarily responsible for the overall effect of the changing ambient inlet conditions. Some results of modelling the complete combustor are shown in Figure 48. Here the carbon monoxide mole fraction is plotted against the combustor exit plane adiabatic flame temperature. Changing parameters are indicated in the identical fashion as done previously with the experimental data — symbol shape indicates ambient humidity, flag position indicates ambient temperature, and symbol shading indicates fuel-air ratio. The fuel-air ratios here though represent those in each zone of the combustor. In this particular case the fuel-air ratio of the secondary zone is varied within reasonable limits because of the cooling air ambiguity. The primary zone fuel-air ratio is taken

as .07 and the exit plane fuel-air ratio is .015. The residence time in each zone is 5 millseconds. The secondary zone with the lowest fuel-air ratio (0.025) produced more carbon monoxide than a secondary zone with a higher fuel-air ratio for all other parameters constant. This is not surprising for the colder secondary zone retards carbon monoxide oxidation. Examining the results for any one of the secondary zone fuel-air ratios, the effect of changing ambient conditions on the carbon monoxide is evident. For zero ambient humidity an increase in the ambient temperature decreases the emissions, curves A, while for a given ambient temperature an increase in the ambient humidity increases the emissions, curves B on Figure 48. The slopes, $[\partial(CO)/\partial T_4]_{RH=0.0}$ and $[\partial(CO)/\partial T_4]_{RH=1.0}$, are seen to depend upon the fuel-air ratio of the secondary zone.

Within each combustor zone for each operating condition the local fuel-air ratio is determined by the airflow splits and the overall fuel and air flows. As the exit plane fuel-air ratio is increased, the fuel-air ratio within each combustor zone will also increase. Figures 49, 50, and 51 show the calculated carbon monoxide emissions at an increased primary fuel-air ratio for the JT8D-17. The individual secondary zone data pairs with individual dilution zone data. The values of the fuel-air ratios used are representative of the ranges which may occur within the JT8D-17. As expected each figure shows that a higher exit fuel-air ratio produces less carbon monoxide. Also, within each dilution sequence the effect due to changing ambient conditions is discernible. Taking as a reference point the carbon monoxide emissions at T_o = 322 K and 0% relative humidity, for all cases

considered, an increase in the humidity or a decrease in the temperature causes an increase in the carbon monoxide emissions. The slopes $[\partial(CO)/\partial T_4]_{RH=0.0}$ and $[\partial(CO)/\partial T_4]_{RH=1.0}$ depend upon the particular primary zone and the dilution zone fuel-air ratios. In all cases the calculated emissions are more sensitive to changes in temperature than to changes in humidity.

For lean idle operating conditions corresponding to a combustor exit fuel-air ratio of 0.007 a slight modification of the modelling scheme was necessary. Consideration of only three combustor zones produced very little carbon monoxide at the combustor exit plane. An analysis of the problem indicated that too small a quantity of carbon monoxide was being produced in the homogeneous lean primary zone for fuel-air ratios varying between 0.30 and 0.45. In a lean actual combustion with a fuel spray, combustion will occur at approximately stoichiometric in the droplet diffusion flame of the primary zone. These products of combustion will then be further diluted by the excess air present in the primary zone. This has the effect of "freezing" the high carbon monoxide levels which occur during droplet combustion.

Experimental evidence given by Sullivan indicates that this type of primary zone quenching does occur. (Private communication from D. Sullivan, General Electric Co., Schenectady, New York in March 1979.) He found that under lean combustion conditions the exact placement of air holes in the secondary zone had very little effect on the carbon monoxide emission levels, suggesting that these levels are quenched by surrounding primary air itself and that any additional air would make very little difference in lowering the mass

fractions of carbon monoxide due to the additional amount of air introduced. A similar approach was employed in the current homogeneous combustion model. The methane and the oxidizer were allowed to react stoichiometrically for a short period of time (0.5 ms). This time was chosen to produce large amounts of carbon monoxide. Then an initial dilution was allowed to occur within the primary zone to some lower equivalence ratio where reactions were allowed to continue for the usual 5 ms. These products were then exhausted into the usual secondary and dilution zones. The results of such a calculation are shown in Figure 52 for subsequent primary zone fuel-air ratios of .06 and .03. Two different dilution schemes are then employed in arriving at the exit conditions. In this fashion adequate amounts of carbon monoxide may be produced, and the usual ambient effects may be recognized.

By the selection of typical primary zone and dilution zone fuel-air ratios, it is possible to simulate the JT8D-17 emissions at different overall fuel-air ratios, including the effect of differing ambient conditions. Results are presented in Figure 53 where the effects of different ambient conditions are shown on earlier dilution sequence presented.

For the hydrocarbon emissions, calculations were performed at one overall fuel-air ratio of 0.011 using the conditions of Table V. The effect of three different ambient inlet conditions on the evaporated mass fraction of the fuel spray at the combustor exit plane is presented in Figure 54 for drops of different

diameters. Because of the effect on adiabatic flame temperature, cold, wet ambient air is effective in suppressing vaporization. Through a combination of these results and the previously discussed Rosin-Rammler droplet distribution function, the total quantity of unburned hydrocarbon emissions may be calculated. The results are presented in Table VI. For both static and convectively enhanced vaporization, emissions are increased with respect to the reference level, 322 K and 0% RH, through either cooling of the ambient air or an increase in humidity. The emissions are more sensitive to wide humidity variations than to wide temperature changes.

EXPERIMENTAL AND ANALYTICAL COMPARISONS

Both experimental and analytical results show that for zero ambient relative humidity an increasing ambient inlet temperature decreases both the hydrocarbon and the carbon monoxide emissions. Also an increasing ambient relative humidity increases hydrocarbon and carbon monoxide emissions for a given ambient inlet temperature.

In order for increasing relative humidity or for decreasing ambient temperature to increase carbon monoxide production a modified CO-OH rate constant had to be used in the analytical model. It was also found that the analytical carbon monoxide emissions were extremely sensitive to the fuel-air ratio within each combustor zone. At this time only reasonable bounds may be placed on the local fuel-air ratio within each zone. As already indicated by Morr et al.[13], a Gaussian distribution should be considered for the local residence times as well as for the local fuel-air ratios. This was not done in this study.

A direct comparison between experimental and analytical results is given in Figure 55. The analytical values show too large an overall decrease in carbon monoxide emissions with increased overall fuel-air ratio, and too small a sensitivity to changing humidity and ambient inlet temperature. Additional comparisons are given in Figures 56, 57, and 58 where the carbon monoxide emissions at standard conditions are divided by those at nonstandard conditions and plotted as a function of ambient temperature. Relative humidity is also included as a parameter. The magnitude of the emission variation is reasonable. However,

the kinetic calculations are again unable to predict a sufficiently large increase in the carbon monoxide emissions with increasing humidity. Although no calculations were done for the T-56 combustor, the experimental data is shown in Figure 59 in the same format as the previous three figures for the JT8D-17. For no relative humidity the JT8D-17 shows a greater sensitivity to temperature changes than the T-56.

For the hydrocarbon emissions, as given in Table VI, the predicted effect of changing ambient conditions is much less than those actually observed. However, this disagreement is believed to be due in part to the changing character of the fuel spray as ambient inlet conditions vary. The data were obtained at a constant fuel-air ratio. Therefore as the water replaced the air with increasing humidity, it was necessary to decrease the fuel flow,which caused poorer fuel atomization. At test conditions for a pressure ratio of two, the entire combustor fuel flow was supplied by the primary portion of the duplex fuel nozzle. The Sauter mean diameter, SMD, of the spray is directly proportional to the fuel mass flow and inversely proportional to the nozzle pressure drop. It may be calculated by using a proprietary correlation. This correlation may also be used when there is fuel flow through the secondary nozzle as did occur for pressure ratios greater than two. The results however are less certain for this case. Calculated Sauter mean diameters are superimposed upon the emission data in Figures 60-63. Large variations do occur in its value, and for the case of the primary nozzle only fueled, the highest values of hydrocarbon emissions do

correspond to the largest values of the Sauter mean diameter. The hydrocarbon calculations presented in Table VI were done using a constant value for the Sauter mean diameter.

Although no explicit analytical predictions were made for the oxides of nitrogen an attempt was made to further collapse the experimental data through consideration of the combustion efficiency. On Figures 64-67 combustion efficiency is indicated for each oxides of nitrogen emission data point. It can be seen that for similar efficiency values there are still large differences in the oxides of nitrogen emission index.

CONCLUSIONS

Changing engine inlet conditions as produced by variations in the atmospheric temperature and relative humidity causes the amount of pollutants emitted by a gas turbine to vary. Increasing ambient temperature and decreasing relative humidity cause a decrease in the hydrocarbon and carbon monoxide emissions and an increase in the oxides of nitrogen emissions. Conversely, decreasing ambient temperature and increasing relative humidity cause an increase in the hydrocarbon and carbon monoxide emissions and a decrease in the oxides of nitrogen emissions. Increasing the engine pressure ratio or the engine fuel-air ratio decreases the hydrocarbon and carbon monoxide emissions and increases the oxides of nitrogen emissions and conversely.

For the JT8D-17 combustor these effects were experimentally quantized. It was found that the variations in the different emission indices could be correlated by an equation of the form

$$EI = (p_3/6.894 \times 10^3)^a \exp [b + (FAR/c) + (9T_3/5d) + (HUM/e)] ,$$

using appropriate constants for each pollutant species.

Analytically, it has been possible to determine the effect of ambient conditions on gas turbine engine emissions. The combustor is modelled as a plug flow reactor using an appropriate kinetic scheme along with the best available information concerning local values of the fuel-air ratio and the fuel spray size. Through the use of a smaller than generally accepted rate constant for the CO-OH reaction the magnitude and trend caused by changes

in ambient conditions of the carbon monoxide emission index were successfully predicted. This calculated value was found though to be quite sensitive to the values chosen for the fuel-air ratio within the different combustor zones. The magnitude and trend due to changes in ambient conditions of the hydrocarbon emission index did not reproduce experimental results. This is due to changes in the fuel spray drop size distribution which occur in conjunction with changing ambient conditions and which is not included in the model.

REFERENCES

1. Lipfert, F.W., "Correlation of Gas Turbine Emissions Data," ASME Gas Turbine and Fluids Engineering Conference, San Francisco, CA, Mar. 1972.

2. Rubins, P.M. and Marchionna, N.R., "Evaluation of NO_x Prediction Correlation Equations for Small Gas Turbines," AIAA/SAE 12th Propulsion Conference, Palo Alto, CA, July 1976.

3. Dieck, R.H., Western, E.E., and Reinhardt, A.H., Jr., "Aircraft Gas Turbine Smoke Measurement Uncertainty Using the SAE IEPA Method," J. of Aircraft, 15, 276, 1978.

4. Marzeski, J.M. and Blazowski, W.S., "Ambient Temperature and Pressure Corrections for Aircraft Gas Turbine Idle Pollutant Emissions," ASME Gas Turbine and Fluids Engineering Conference, New Orleans, LA, Mar. 1976.

5. Sarli, V.U., Eiler, D.C., and Marshall, R.I., "Effects of Operating Variables on Gaseous Emissions," APCA Conference on Air Pollution Measurement Accuracy, New Orleans, LA, Oct. 1975.

6. Nelson, A.W., Davis, J.C., and Medlin, C.H., "Progress in Techniques for Measurement of Gas Turbine Engine Exhaust Emissions," AIAA/SAE 8th Propulsion Conference, New Orleans, LA, Nov. 1972.

7. Mosier, S.A. and Roberts, R., "Low Power Turbopropulsion Combustor Exhaust Emissions," Technical Report AFAPL-TR-73/36, Vol. 3, July 1973.

8. Allen, L. and Slusher, G.R., "Ambient Temperature and Humidity Correction Factors for Exhaust Emissions from Two Classes of Aircraft Turbine Engines," FAA-RD-76-149, Oct. 1976.

9. Fear, J.S., "Performance of a Small Annular Turbojet Combustor Designed for Low Cost," NASA TM X-2476, 1972.

10. Anonymous, "Procedure for the Continuous Sampling and Measurements of Gaseous Emissions from Aircraft Gas Turbine Engines," SAE ARP 1256, 1971.

11. Roberts, R., Fiorentino, A.J., and Greene, W., "Pollution Technology Program Can-Annular Combustor Engines Final Report," NASA CR-135027, 1976.

12. Blazowski, W.S., Walsh, D.E., and Mach, K.D., "Operating and Ambient Condition Influences on Aircraft Gas Turbine NO_x Emissions," J. of Aircraft, 12, 2, 1975.

13. Morr, A.R., Heywood, J.G., and Fitch, A.H., "Measurements and Predictions of Carbon Monoxide Emissions from an Industrial Gas Turbine," Combustion Science and Technology, 11, 97, 1975.

14. Subramaniam, A.K., "The Effect of Ambient Conditions on Carbon Monoxide Emissions from an Idling Gas Turbine Combustor," Master of Science Thesis, University of Cincinnati, July 1977.

15. Marchionna, N., Watkins, S., and Opdyke, Jr., "Turbine Fuel Tolerance Study," Avco Lycoming TR 12090, Oct. 1975.

16. Gordon, S. and McBride, B.J., "Computer Program for Calculation of Complex Chemical Equilibrium Compositions, Rocket Performance, Incident and Reflected Shocks and Chapman-Jouguet Detonations," NASA SP-273, 1971.

17. Ay, J.H. and Sichel, M., "Theoretical Analysis of NO Formation Near the Primary Reaction Zone in Methane Combustion," Combustion and Flame, 26, 1, 1976.

18. Kollrack, R., "Model Calculations of the Combustion Product Distributions in the Primary Zone of a Gas Turbine Combustor," ASME Winter Annual Meeting, New York, 1976.

19. Bittker, D.A. and Scullin, V.D., "General Chemical Kinetics Computer Program for Static and Flow Reactions, with Application to Combustion and Shock Tube Kinetics," NASA TN D-6586, 1972.

20. Muller-Dethlefs, K. and Schlader, A.F., "The Effect of Steam on Flame Temperature, Burning Velocity, and Carbon Formation in Hydrocarbon Flames," Combustion and Flame, 27, 205, 1976.

TABLE I

Idle JT8D-17 Combustor Conditions

Nominal Operation

Total Inlet Pressure - 2.47 atm
Total Inlet Temperature - 393 K
Air Flow - 1.37 kg/sec
Fuel Flow - 0.0161 kg/sec
Fuel/Air Ratio - 0.0117

TABLE II

Test Operation

Compressor Efficiency - 0.8
Compressor Pressure Ratio - 2, 3, 4, 5
Compressor Inlet Pressure - 1 atm
Compressor Inlet Temperature - 244, 289, 322 K
Compressor Inlet Relative Humidity - 0, 50, 100%
Fuel/Air Ratio - 0.007, 0.011, 0.015
Constant Compressor Discharge Mach Number
$M_3 = 0.42$, or
Constant Reference Velocity, $V_3 = 15.2$ m/sec

TABLE III

Coefficients of Regression Analysis

Emission Index Coeff.	HC	CO	NO_x
All Data			
a	-1.2833	-0.9468	0.2547
b	15.806	11.552	-2.916
c	-0.00400	-0.00981	0.02074
d	-128.93	-243.48	324.67
e	43.30	76.39	-59.88
Multiple Correlation Coef. Squared	.934	.929	.824
Selected Data			
a	-1.9130	-1.1214	0.2552
b	20.135	13.411	-2.090
c	-0.00341	-0.00673	0.0
d	-107.35	-196.11	334.44
e	34.61	77.04	-54.31
Multiple Correlation Coef. Squared	.953	.940	.955

TABLE IV

Kinetic Scheme of Methane/Air Combustion

and Forward Rate Constants

$$k_f = A\ T^{a}\ e^{-\Delta E/RT}\ (cm^3/mole/sec)$$

	Reaction	A	a	ΔE
1	M + CH4 = CH3 + H	0.20E18	0.0	88332.5
2	CH4 + OH = CH3 + H2O	0.28E14	0.0	4962.5
3	CH4 + O = CH3 + OH	0.20E14	0.0	9210.4
4	CH4 + H = CH3 + H2	0.69E14	0.0	11810.8
5	CH3 + O2 = HCO + H2O	0.20E11	0.0	0.0
6	CH3 + O = HCO + H2	0.10E15	0.0	0.0
7	HCO + OH = CO + H2O	0.10E15	0.0	0.0
8	M + HCO = CO + H	0.20E13	0.5	28584.0
9	CO + OH = CO2 + H	0.56E12	0.0	600.0
		0.85E-14	7.0	-13895.0
10	H + O2 = O + OH	0.22E15	0.0	16554.9
11	O + H2 = OH + H	0.17E14	0.0	9428.8
12	O + H2O = OH + OH	0.58E14	0.0	18004.0
13	H + H2O = H2 + OH	0.84E14	0.0	20048.5
14	H + OH = H2O + M	0.40E20	-1.0	0.0
15	H + H = H2 + M	0.15E19	-1.0	0.0
16	O + O = O2 + M	0.40E18	-1.0	0.0
17	O + H = OH + M	0.53E16	0.0	5518.3
18	N + O2 = NO + O	0.64E10	1.0	6232.9
19	O + N2 = NO + N	0.14E15	0.0	75231.5
20	OH + N = NO + H	0.40E14	0.0	0.0

TABLE V

Typical Local Parameters, PR=4.0, F/A=.011

	Primary		Secondary		Dilution	
	High	Low	High	Low	High	Low
F/A	.0709	.0484	.0337	.0193	.0119	.0109
		T_O=244K 0% RH				
T	2370	1960	1580	1100	850	820 K
τ	1.77	1.51	4.20	3.50	2.59	2.48 MS
		T_O=289K 0% RH				
T	2400	2015	1635	1195	930	905
τ	1.90	1.59	4.40	3.50	2.58	2.44
			50% RH			
T	2390	2000	1605	1175	915	900
τ	1.90	1.60	4.47	3.54	2.62	2.45
			100% RH			
T	2380	1980	1580	1150	895	895
τ	1.90	1.61	4.52	3.61	2.67	2.45
		T_O=322K 0% RH				
T	2430	2050	1680	1235	980	950
τ	1.97	1.65	4.52	3.58	2.54	2.45
			50% RH			
T	2330	1960	1595	1180	940	925
τ	2.02	1.69	4.67	3.66	2.64	2.46
			100% RH			
T	2330	1870	1520	1130	920	875
τ	2.07	1.74	4.79	3.83	2.69	2.54

TABLE VI

HYDROCARBON EMISSIONS

Ambient Correlations	Hydrocarbon Emission Index		
	Static	Convective	Experimental
322 K, 0% RH	1.5	1.5	1.5
244 K, 0% RH	3.19	2.80	14.4
322 K, 100% RH	4.35	3.74	17.6

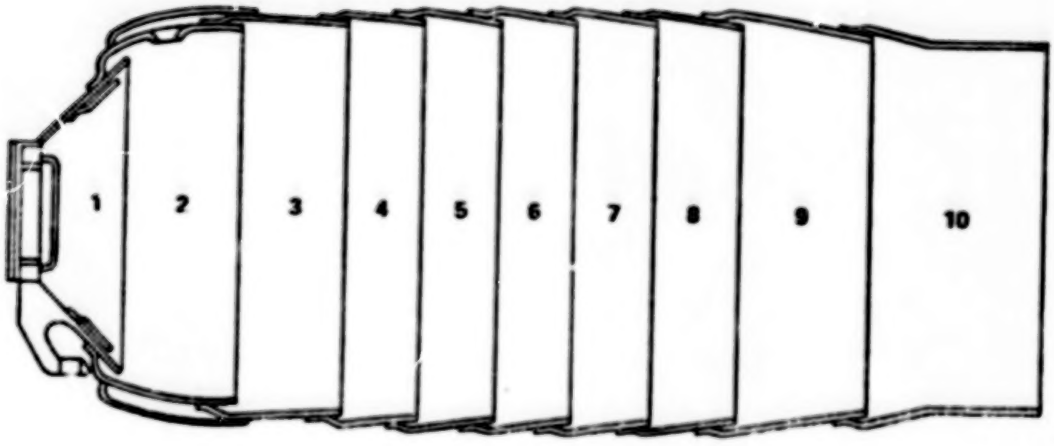

FUEL INJECTOR AND PRIMARY SWIRLER EQUIVALENT METERING AREA 7.61%

Equivalent Metering Area

Louver Cooling Air		Combustion Air	
Panel	%	Panel	%
1	1.53	2	7.93
2	5.62	3	1.92
3	7.56	5	8.00
4	5.69	8	15.85
5	4.24	9	18.09
6	3.41		
7	3.42		
8	3.43		
9	2.78		
10	1.81		

Figure 1. JT8D-17 Combustor

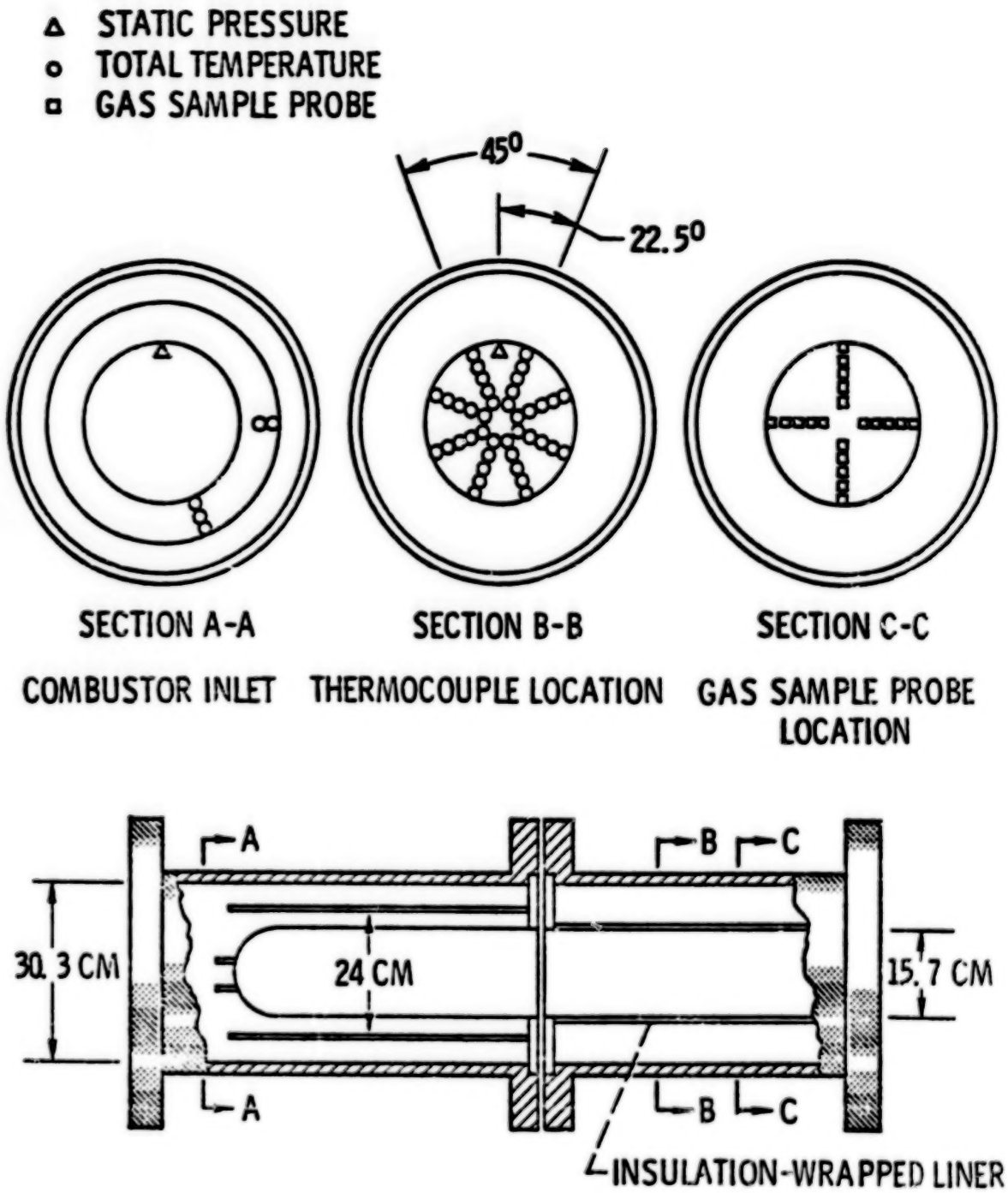

Figure 2. Combustor Test Section and Instrumentation Sections

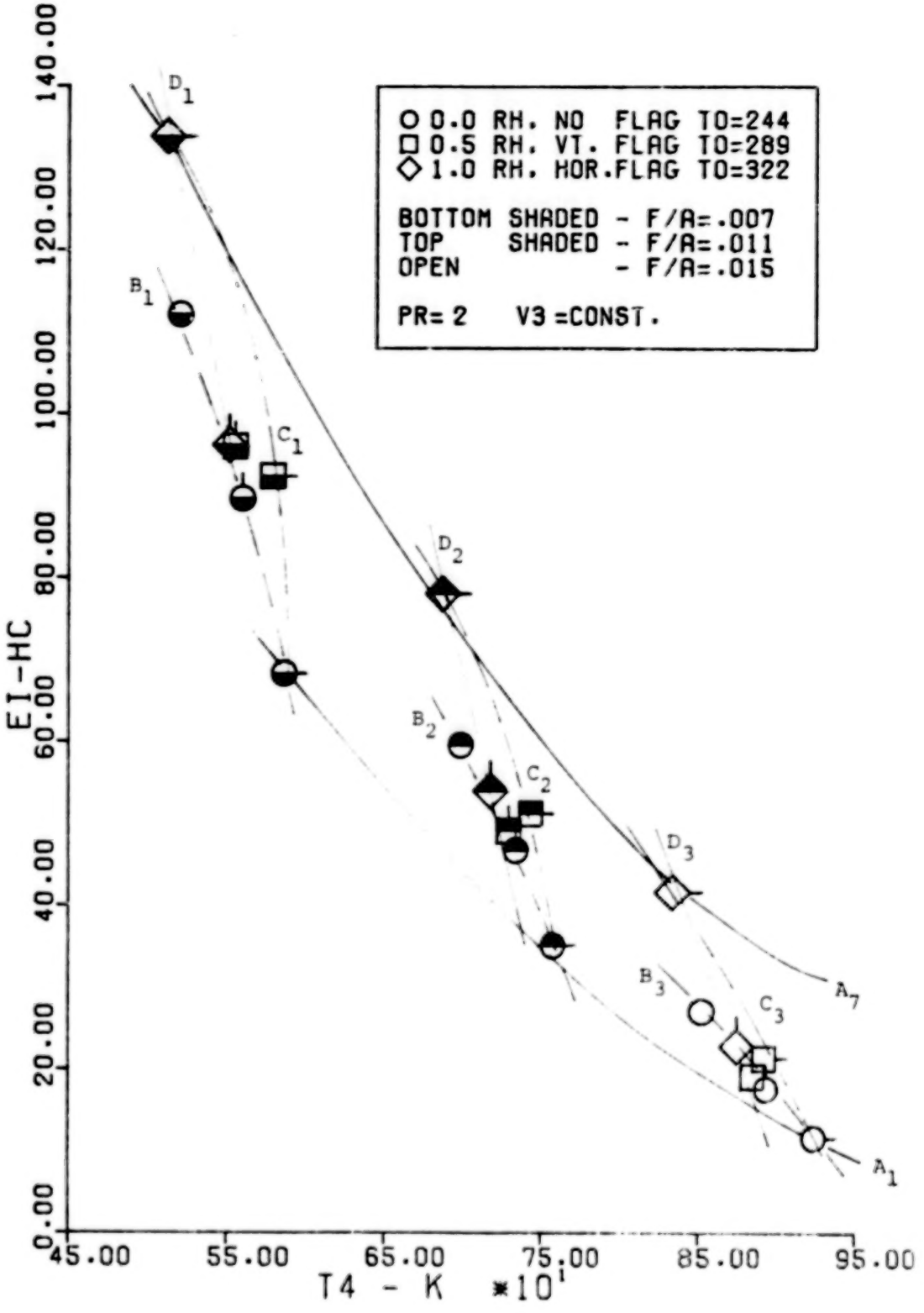

Figure 3. Hydrocarbon Emission Index for a Constant Reference Velocity at a Pressure Ratio of Two

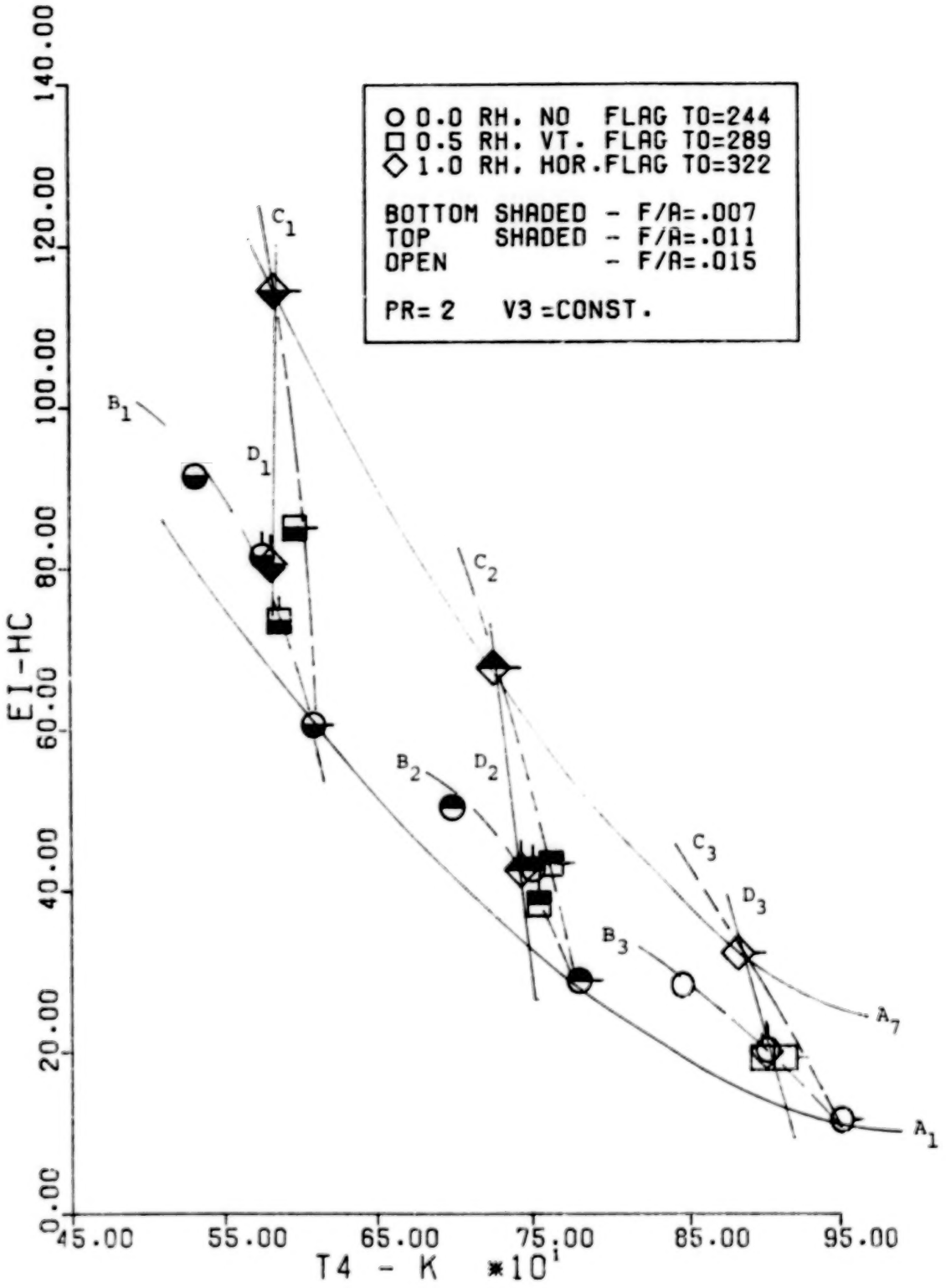

Figure 4. Hydrocarbon Emission Index Rerun for a Constant Reference Velocity at a Pressure Ratio of Two

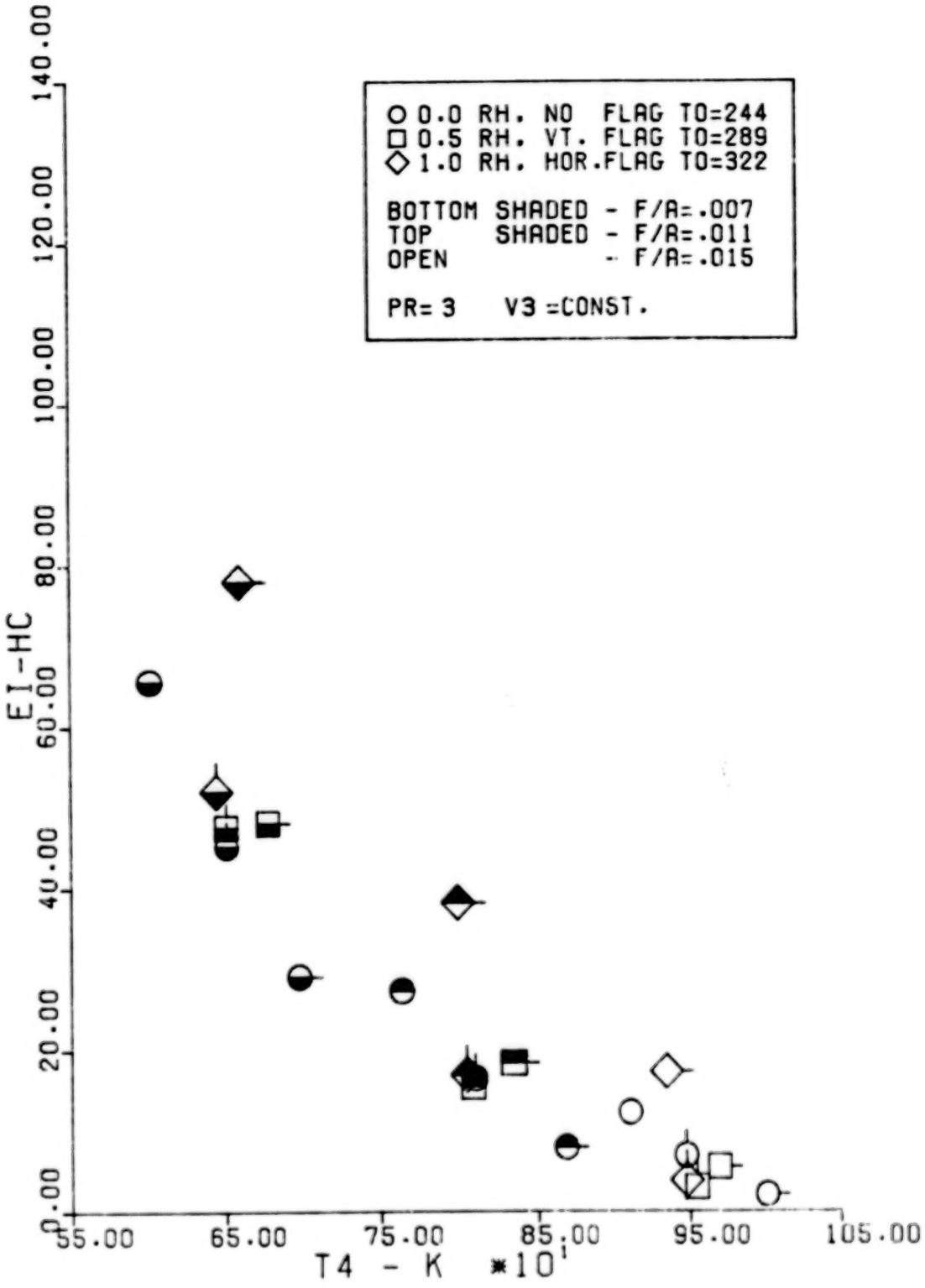

Figure 5. Hydrocarbon Emission Index for a Constant Reference Velocity at a Pressure Ratio of Three

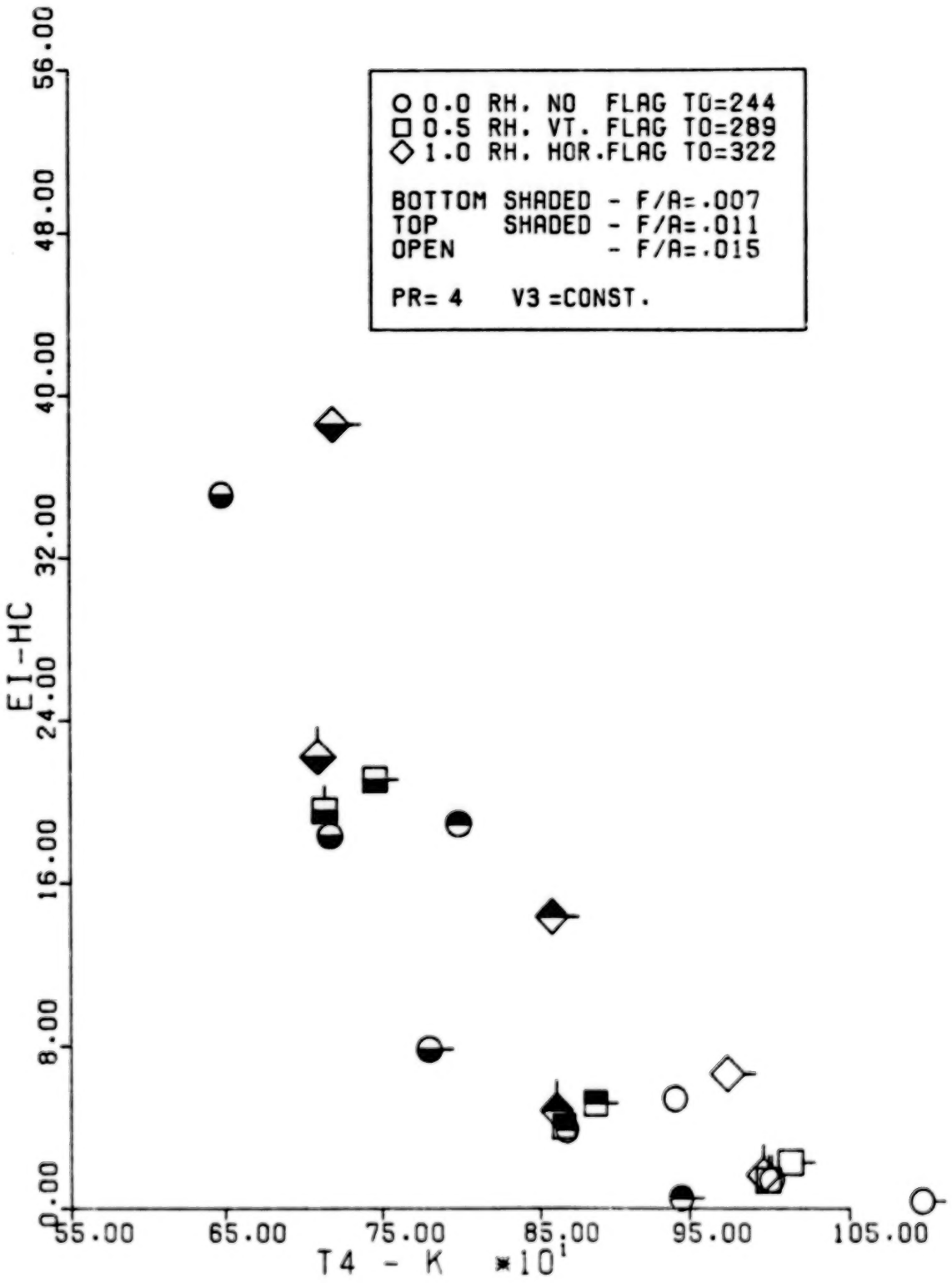

Figure 6. Hydrocarbon Emission Index for a Constant Reference Velocity at a Pressure Ratio of Four

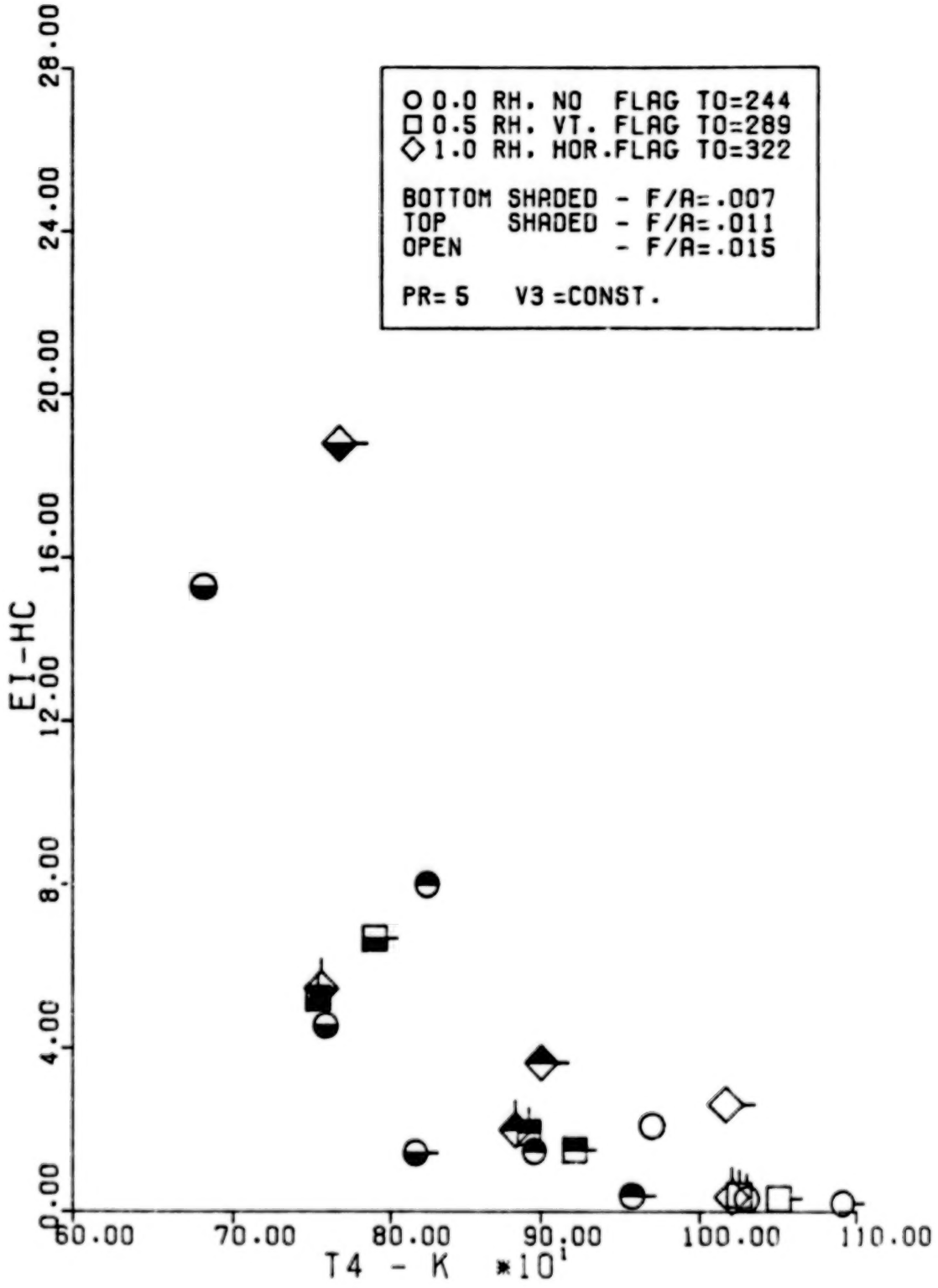

Figure 7. Hydrocarbon Emission Index for a Constant Reference Velocity at a Pressure Ratio of Five

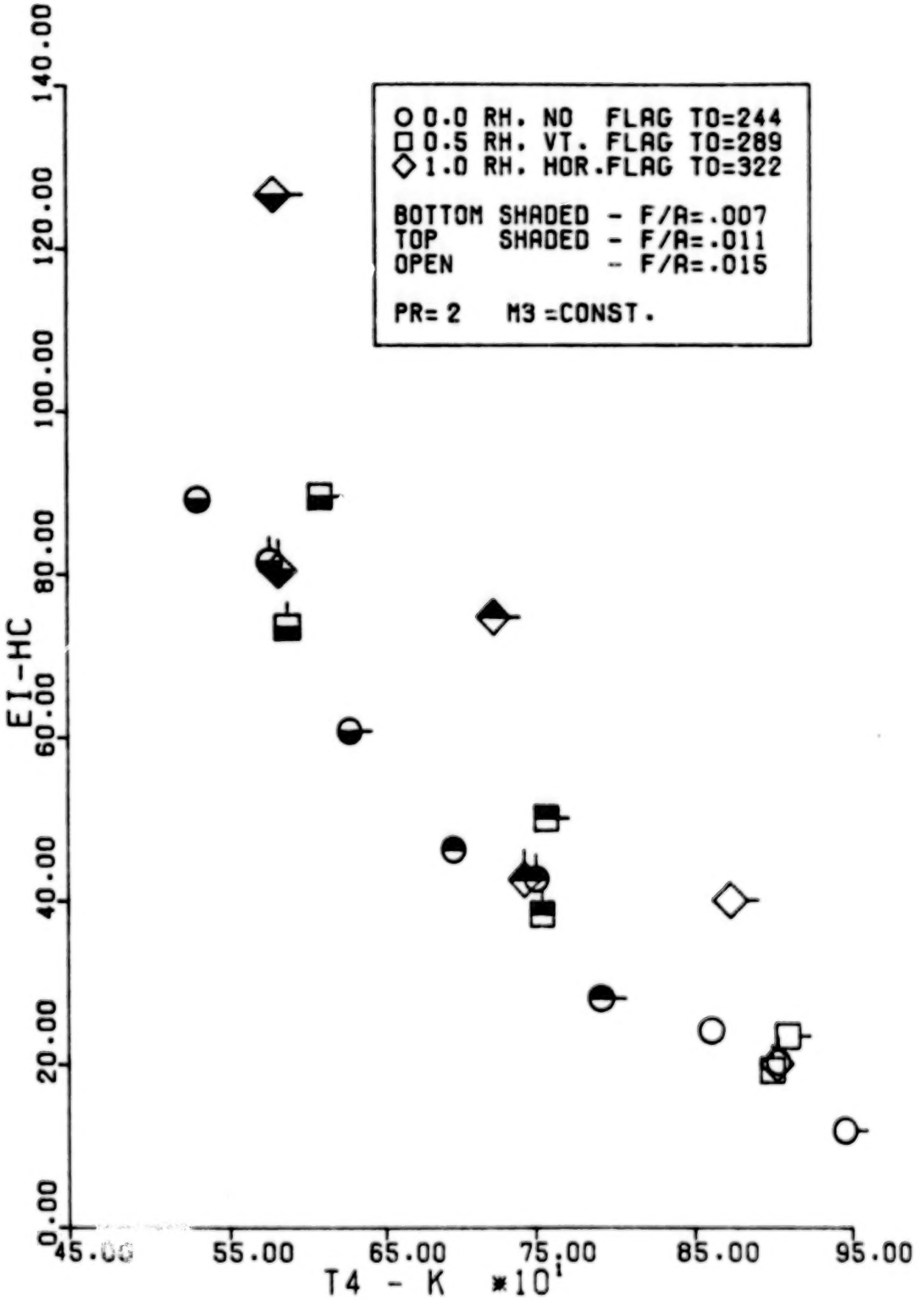

Figure 8. Hydrocarbon Emission Index for a Constant Compressor Discharge Mach Number at a Pressure Ratio of Two

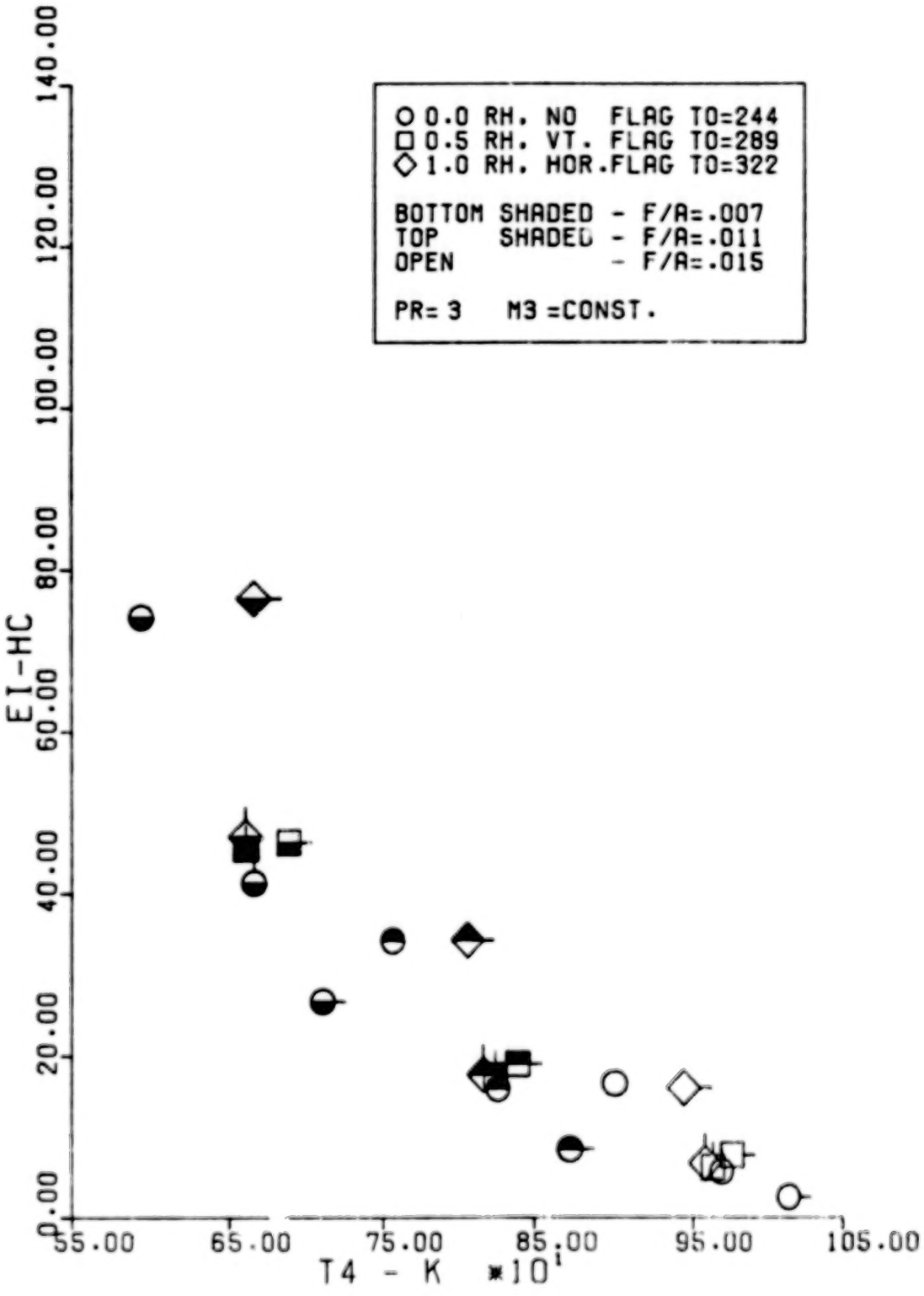

Figure 9. Hydrocarbon Emission Index for a Constant Compressor Discharge Mach Number at a Pressure Ratio of Three

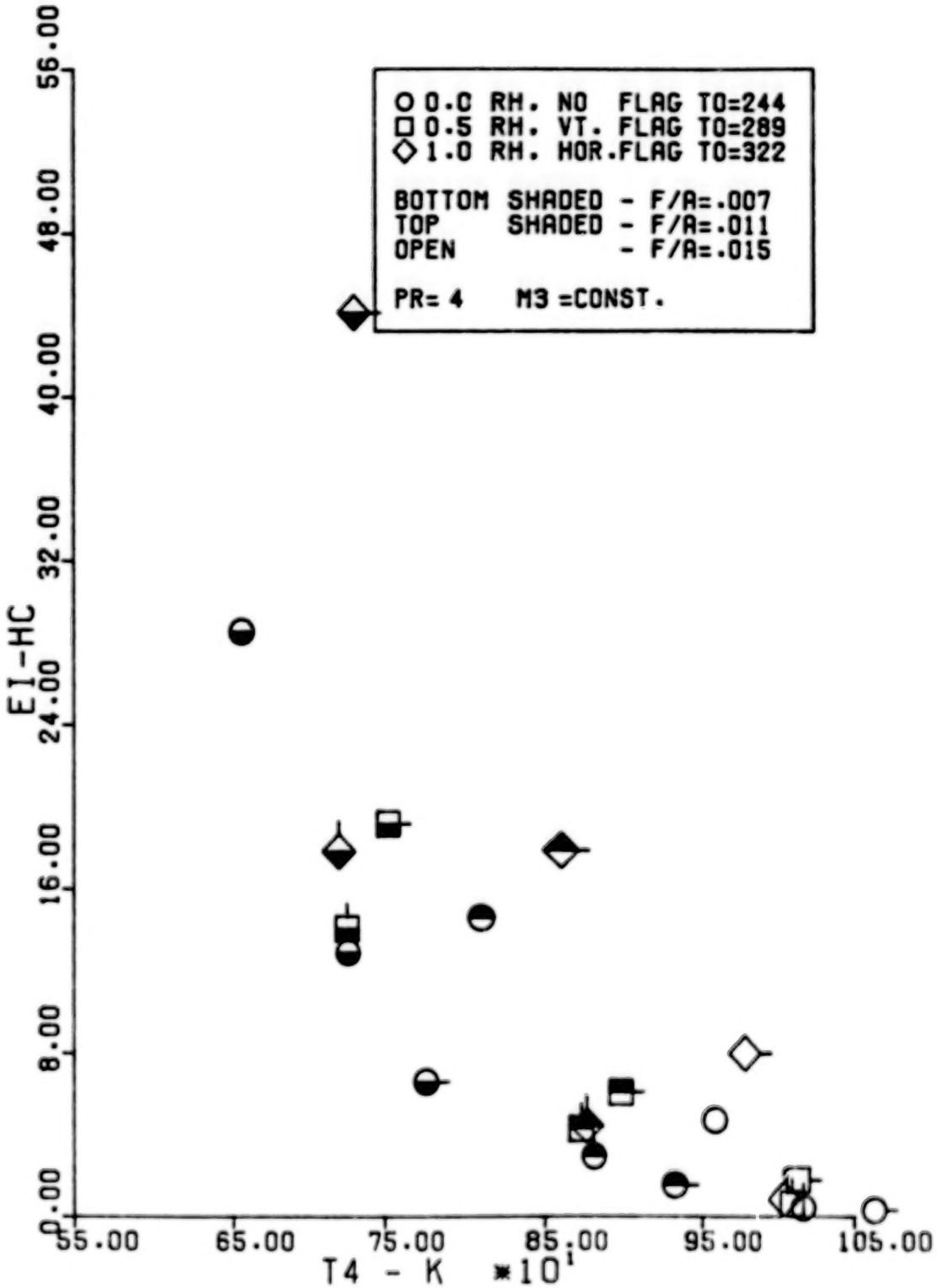

Figure 10. Hydrocarbon Emission Index for a Constant Compressor Discharge Mach Number at a Pressure Ratio of Four

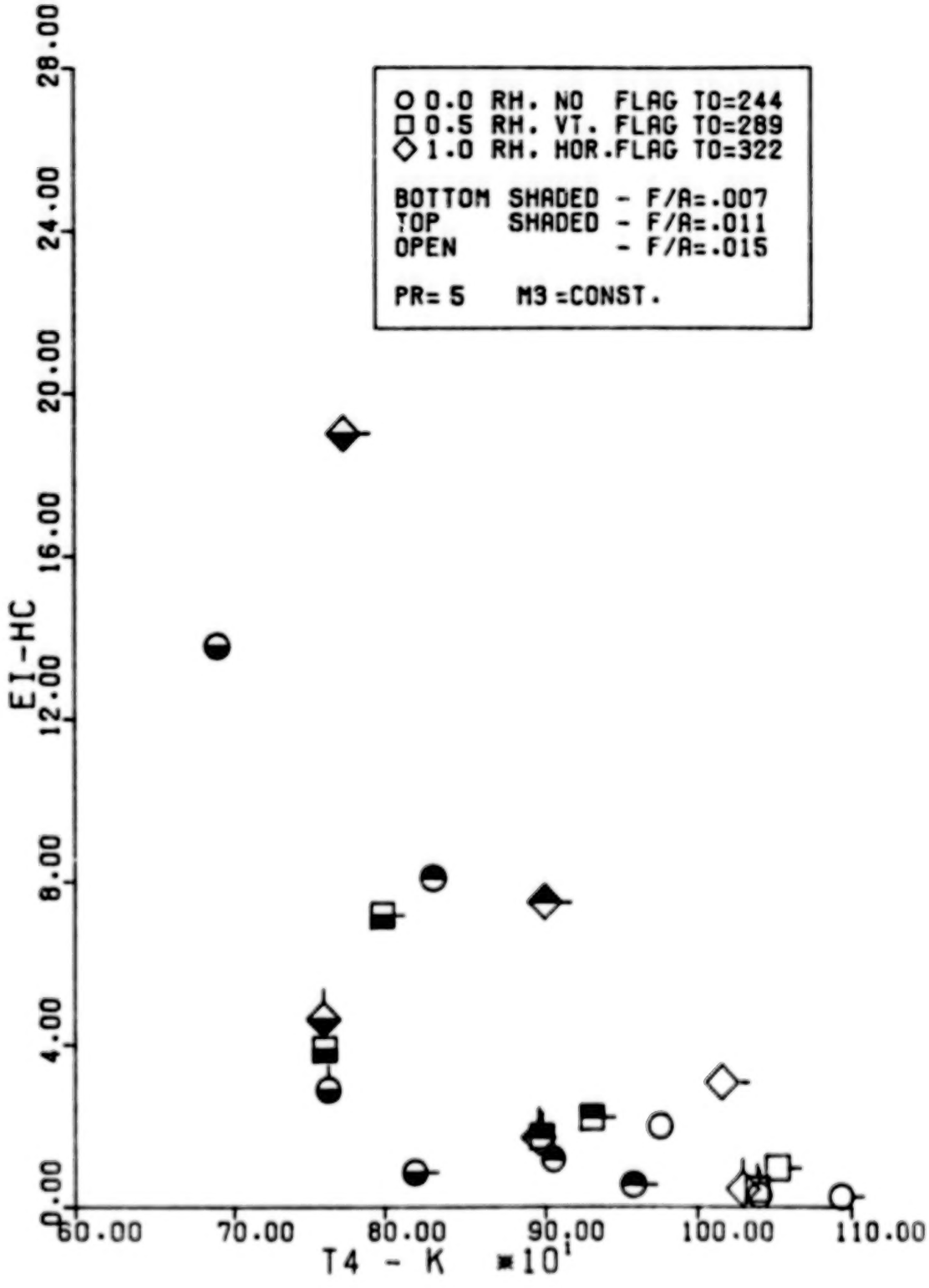

Figure 11. Hydrocarbon Emission Index for a Constant Compressor Discharge Mach Number at a Pressure Ratio of Five

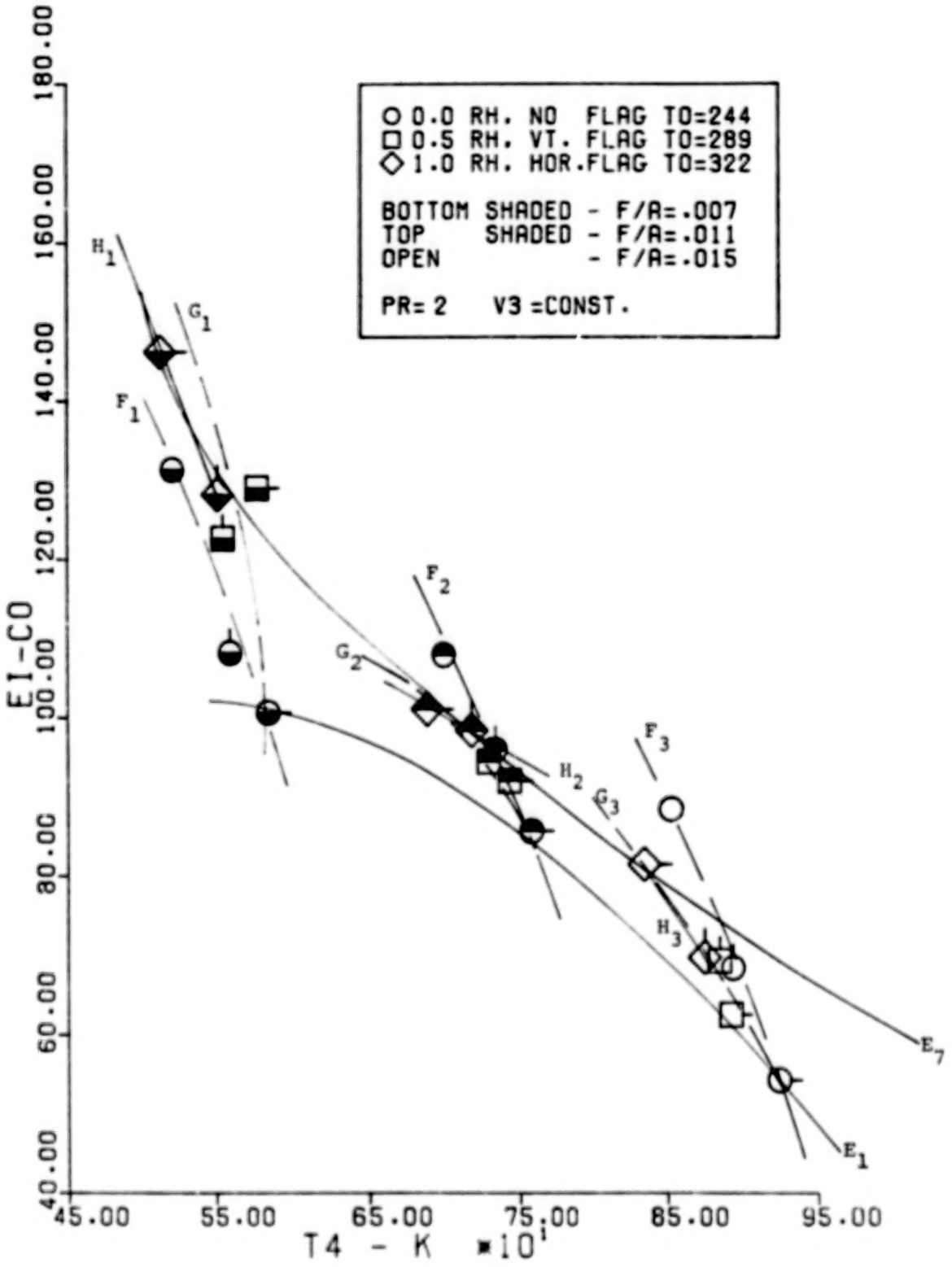

Figure 12. Carbon Monoxide Emission Index for a Constant Reference Velocity at a Pressure Ratio of Two

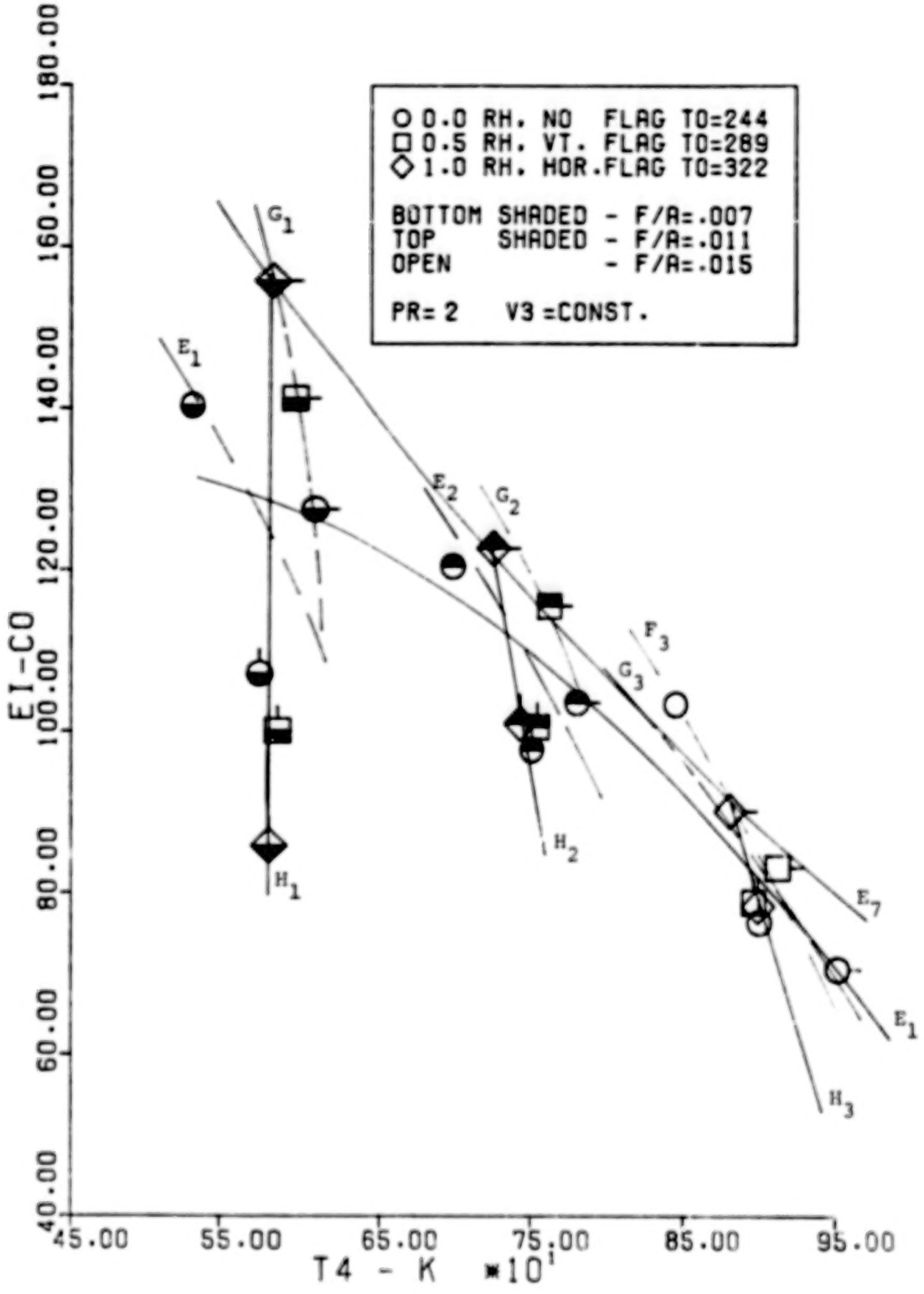

Figure 13. Carbon Monoxide Emission Index Rerun for a Constant Reference Velocity at a Pressure Ratio of Two

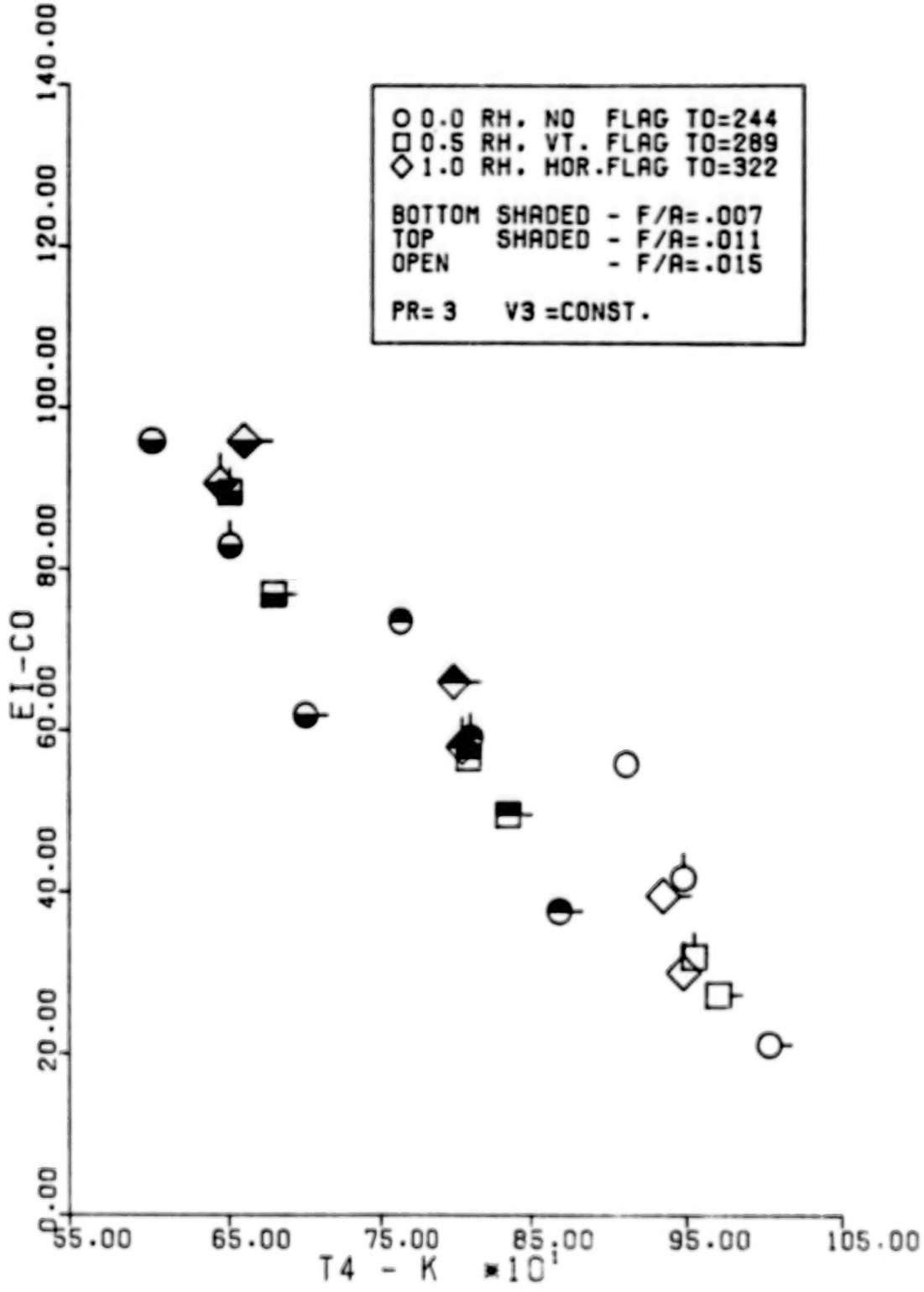

Figure 14. Carbon Monoxide Emission Index for a Constant Reference Velocity at a Pressure Ratio of Three

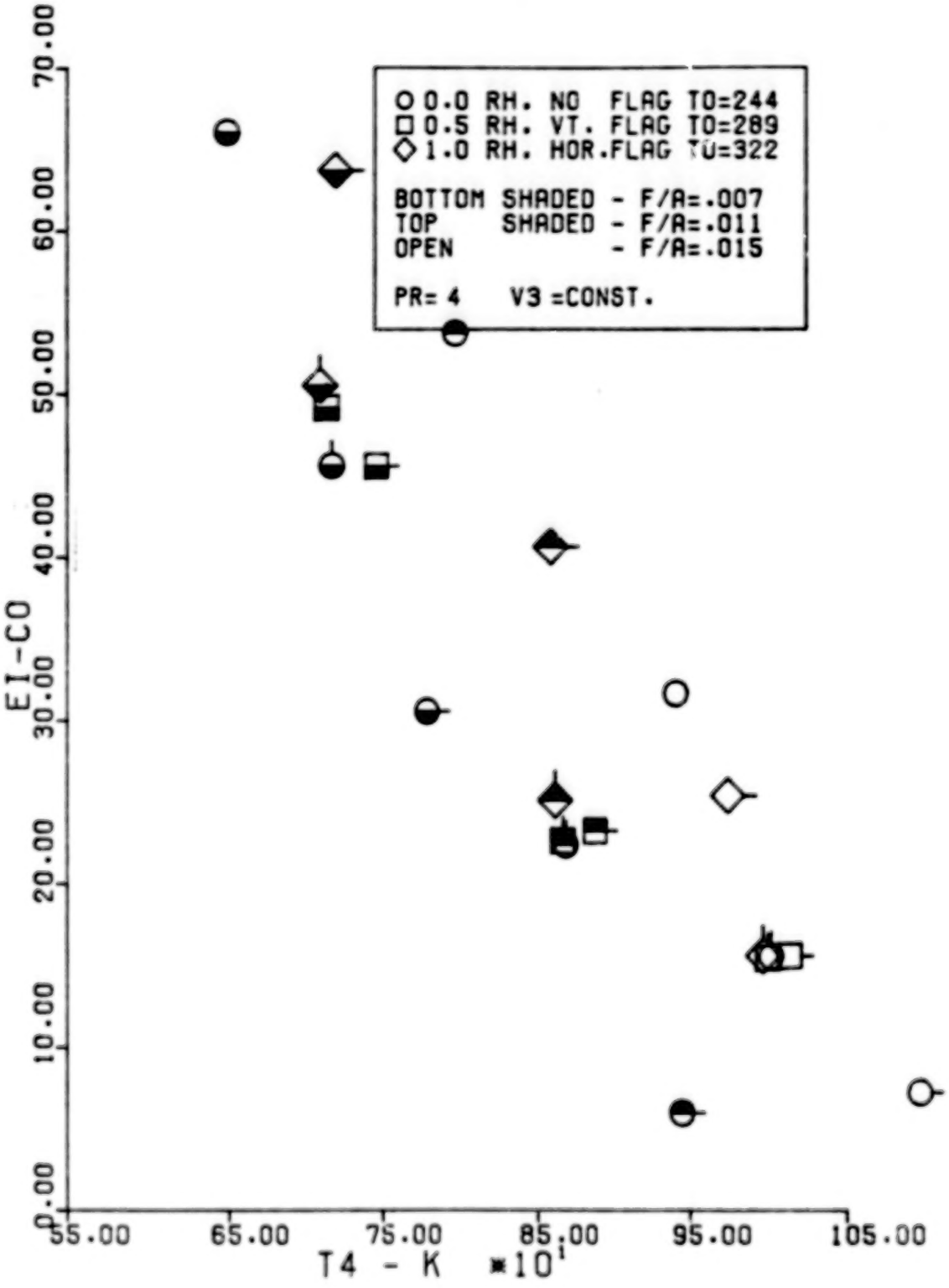

Figure 15. Carbon Monoxide Emission Index for a Constant Reference Velocity at a Pressure Ratio of Four

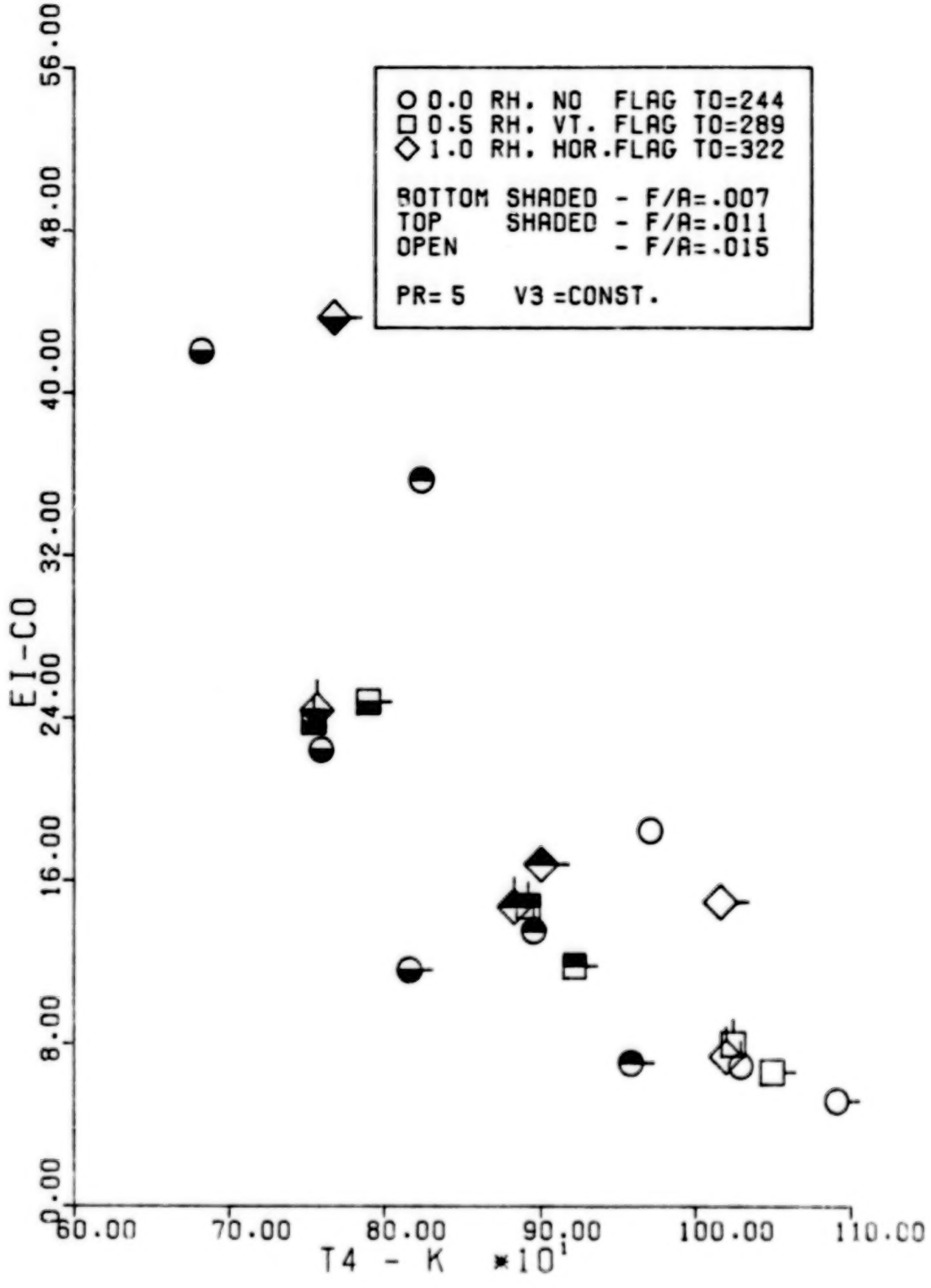

Figure 16. Carbon Monoxide Emission Index for a Constant Reference Velocity at a Pressure Ratio of Five

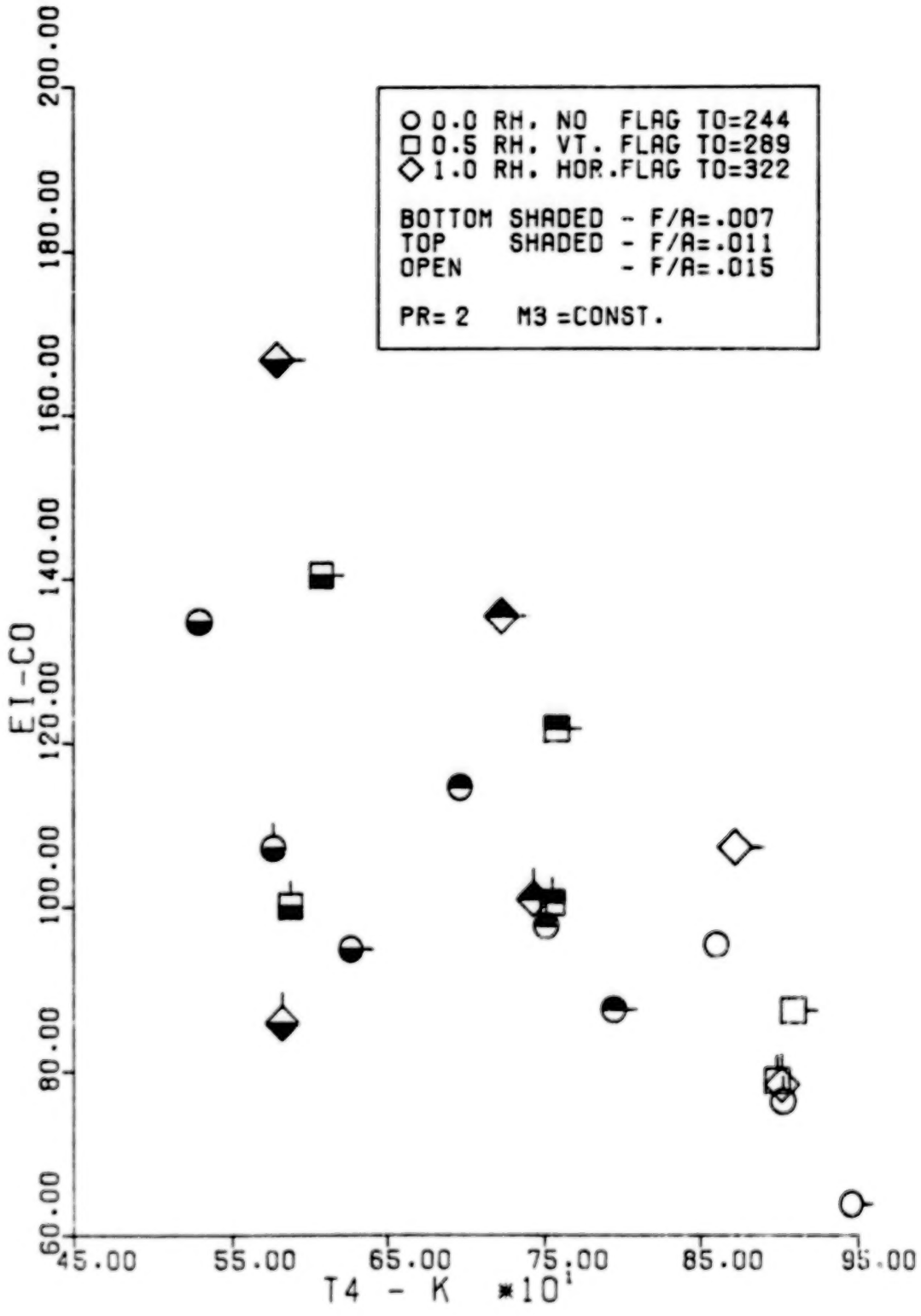

Figure 17. Carbon Monoxide Emission Index for a Constant Compressor Discharge Mach Number at a Pressure Ratio of Two

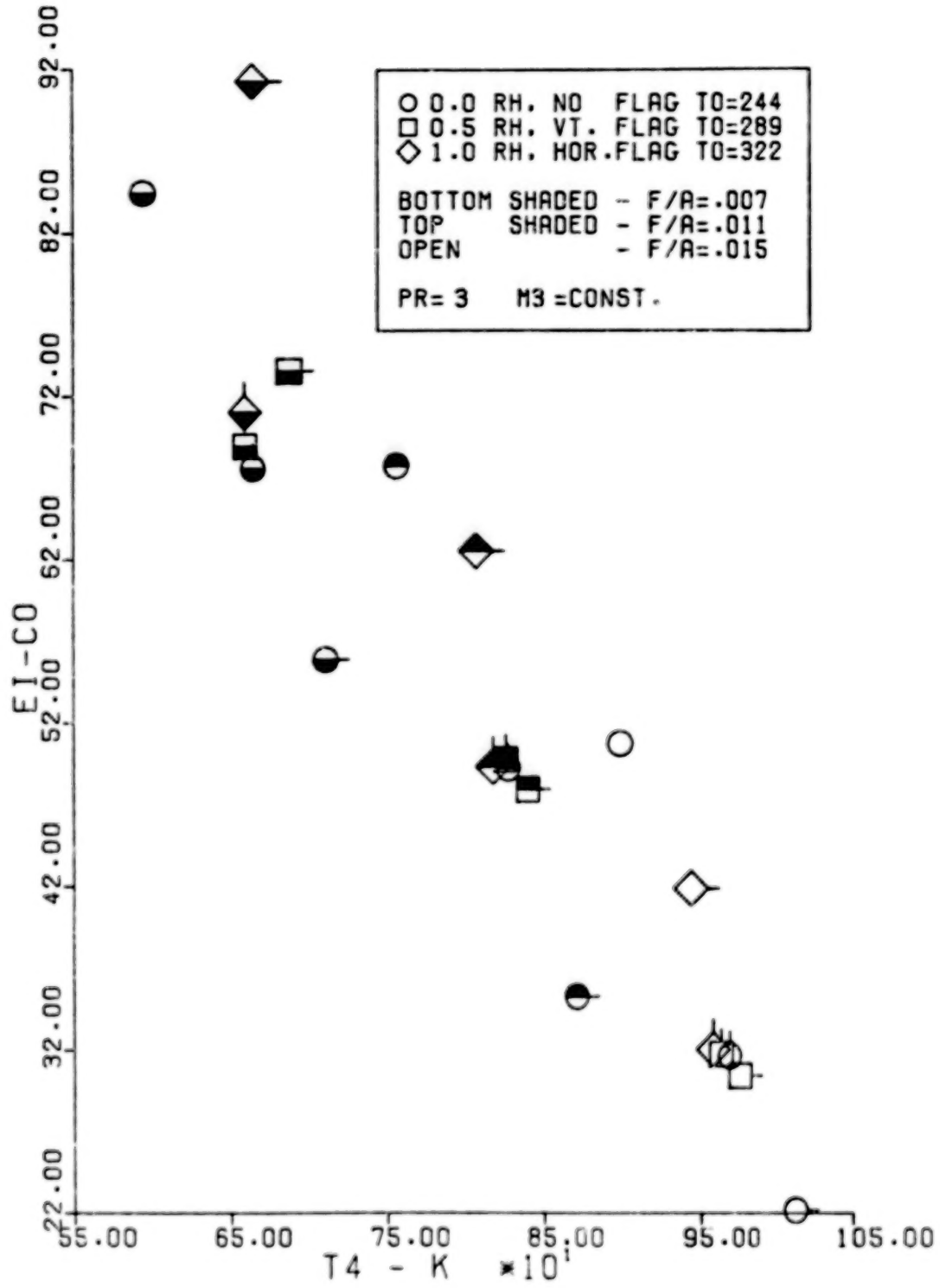

Figure 18. Carbon Monoxide Emission Index for a Constant Compressor Discharge Mach Number at a Pressure Ratio of Three

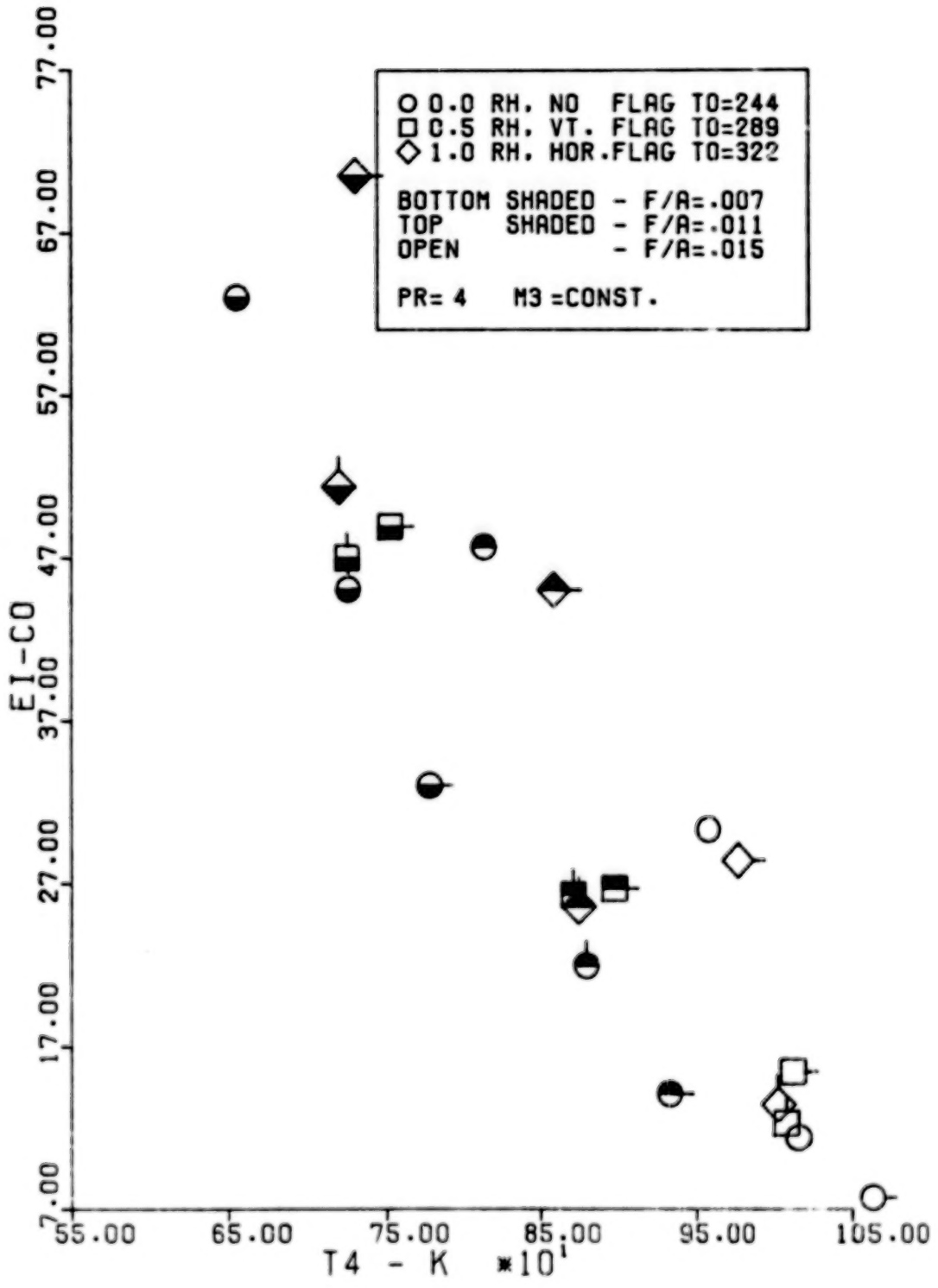

Figure 19. Carbon Monoxide Emission Index for a Constant Compressor Discharge Mach Number at a Pressure Ratio of Four

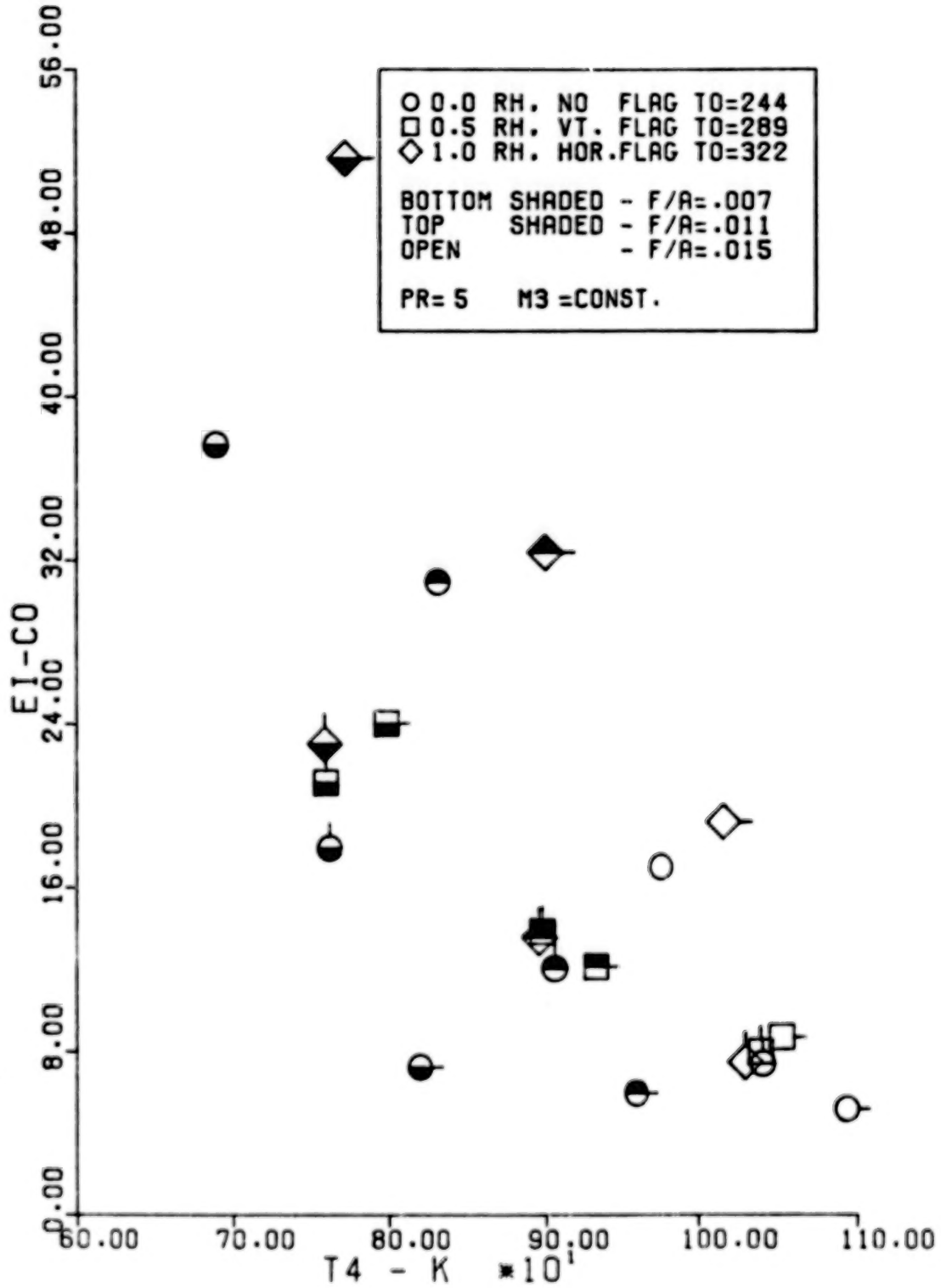

Figure 20. Carbon Monoxide Emission Index for a Constant Compressor Discharge Mach Number at a Pressure Ratio of Five

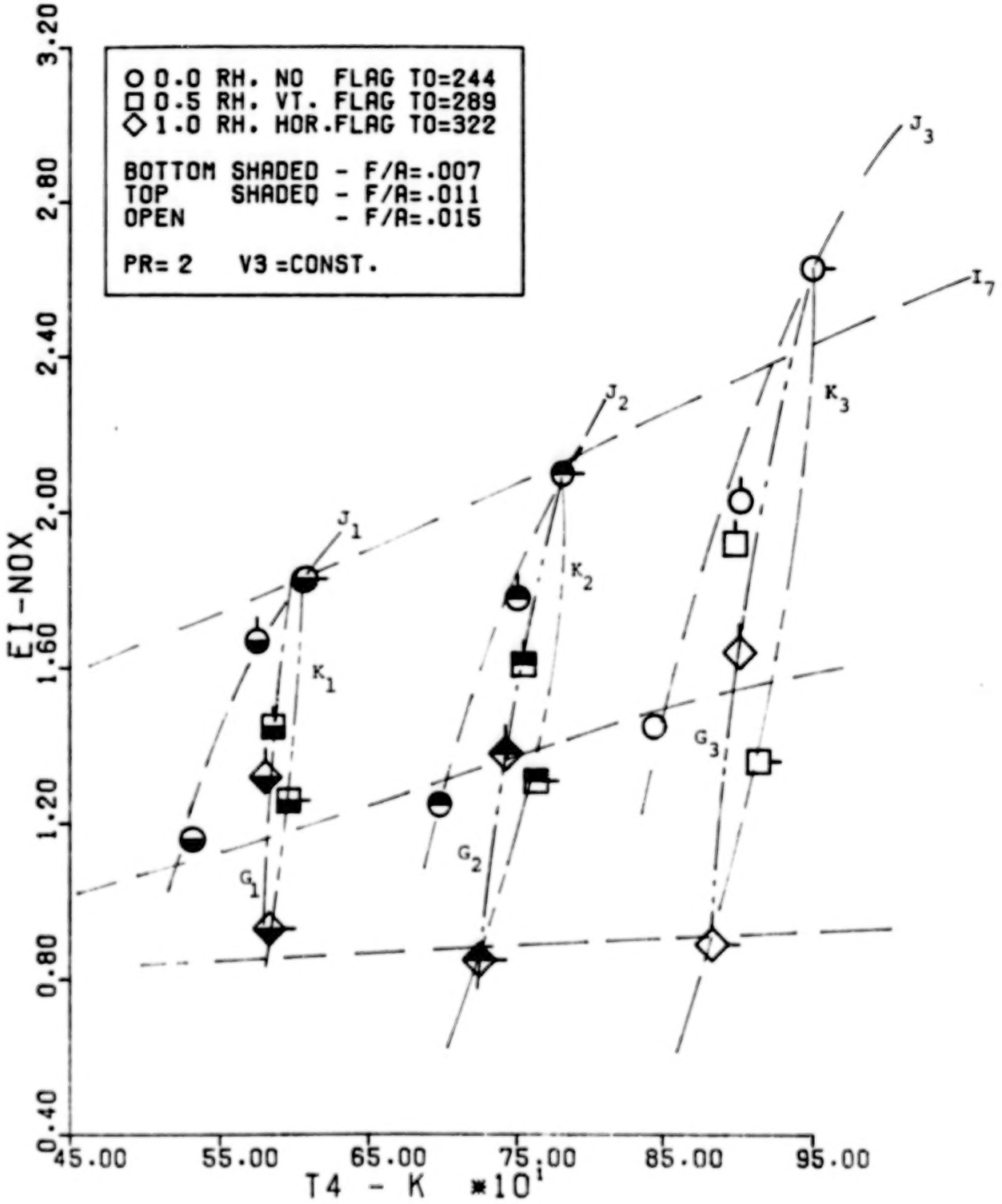

Figure 21. Oxides of Nitrogen Emission Index for a Constant Reference Velocity at a Pressure Ratio of Two

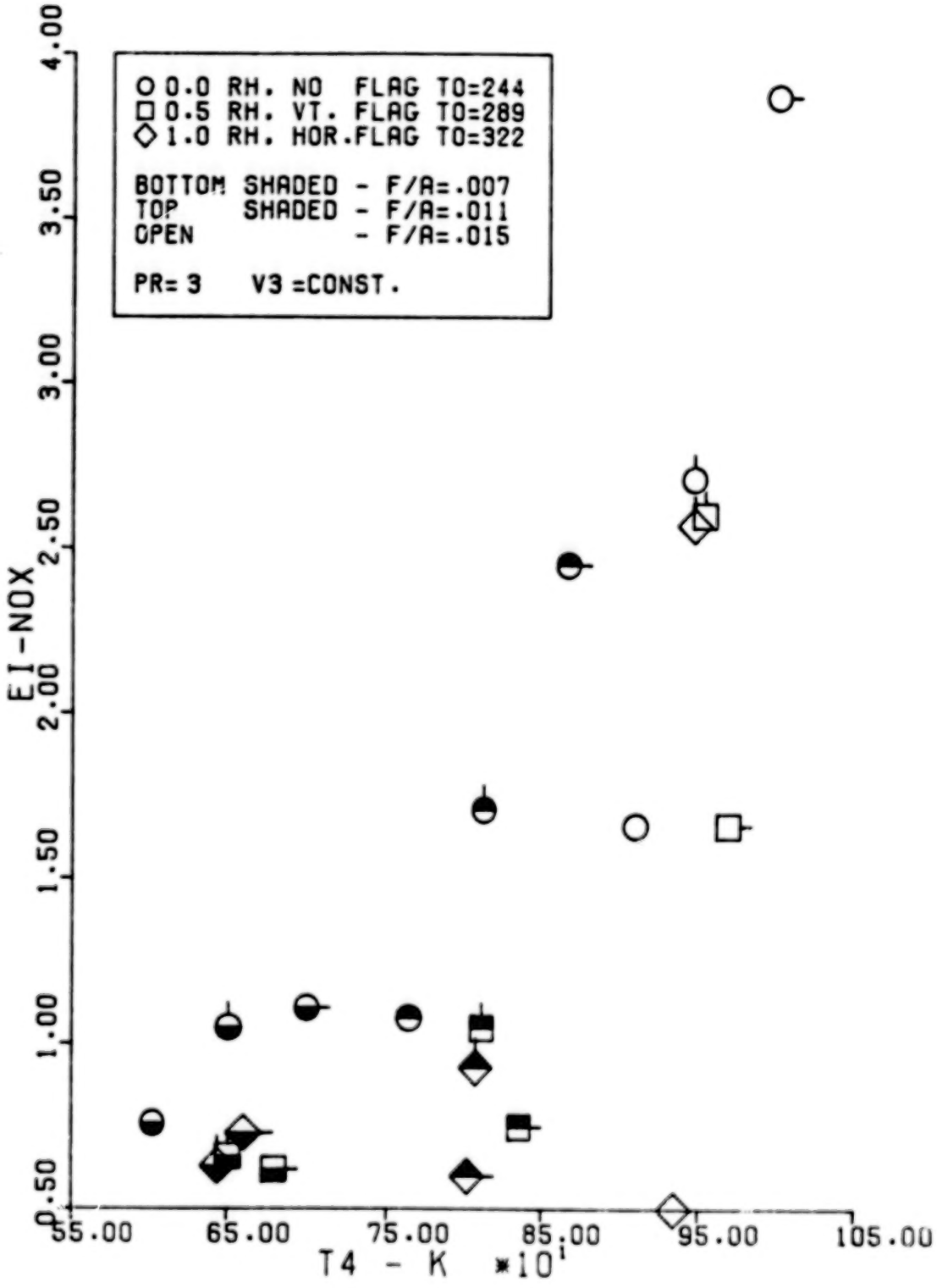

Figure 22. Oxides of Nitrogen Emission Index for a Constant Reference Velocity at a Pressure Ratio of Three

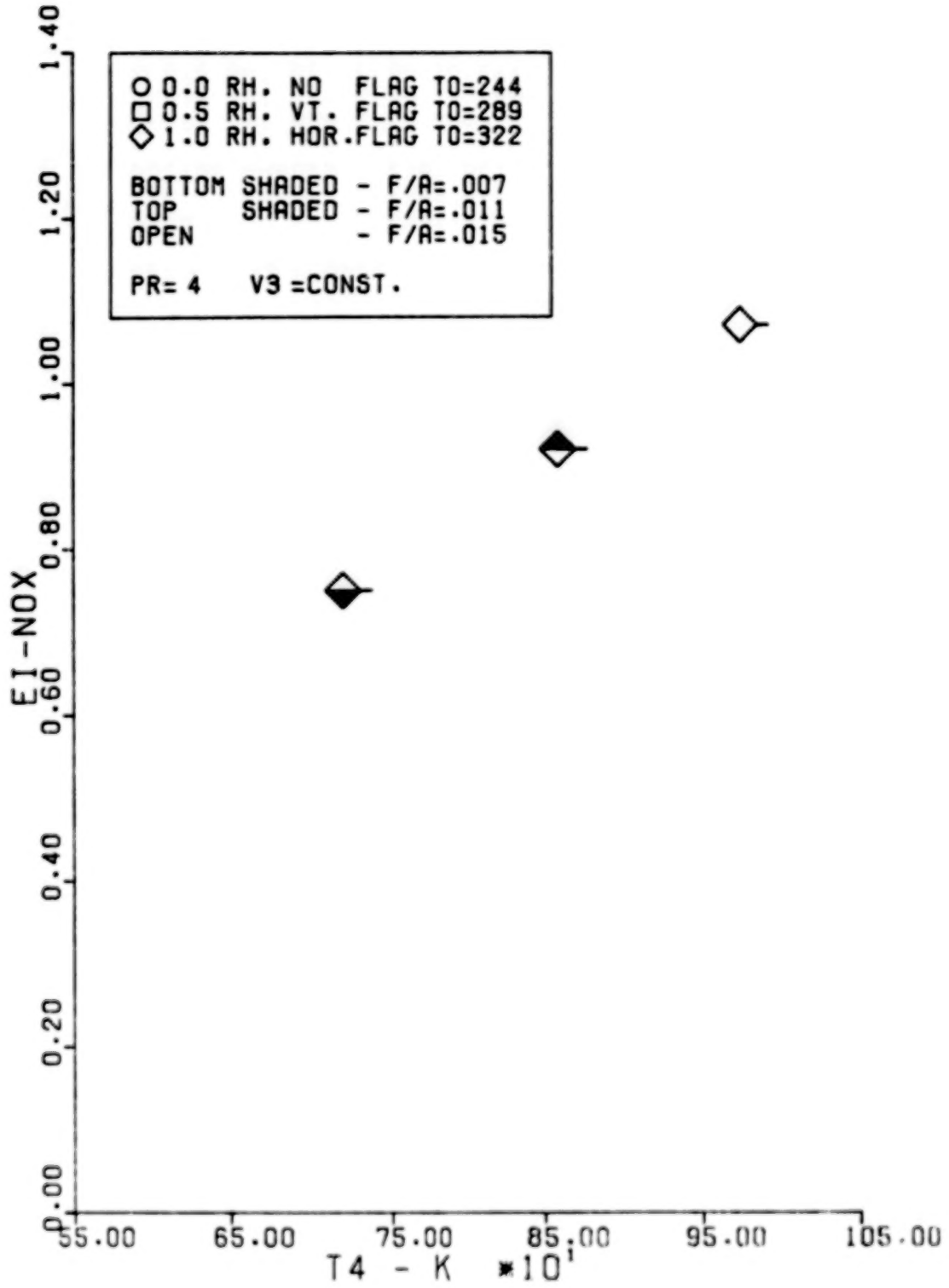

Figure 23. Oxides of Nitrogen Emission Index for a Constant Reference Velocity at a Pressure Ratio of Four

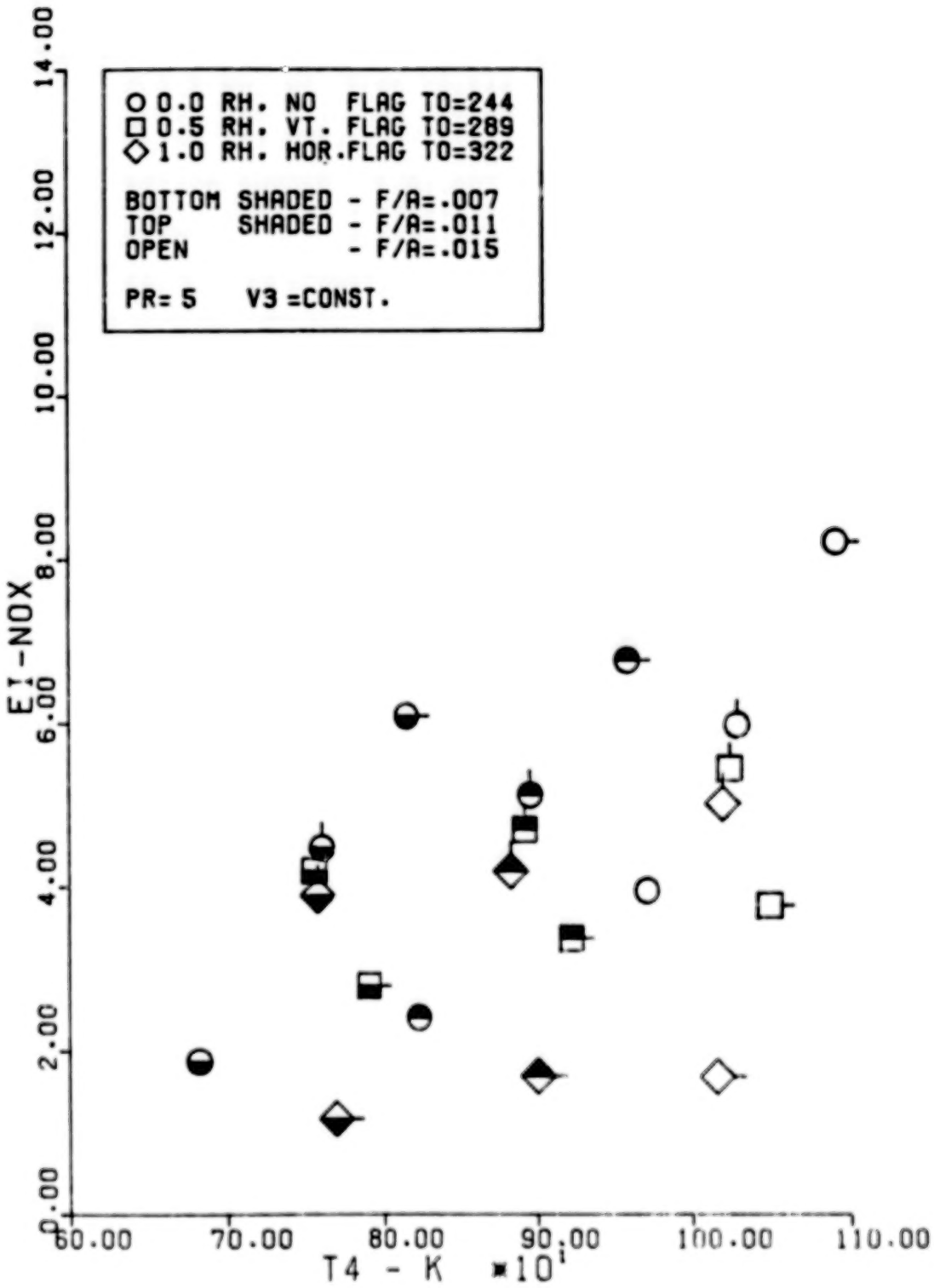

Figure 24. Oxides of Nitrogen Emission Index for a Constant Reference Velocity at a Pressure Ratio of Five

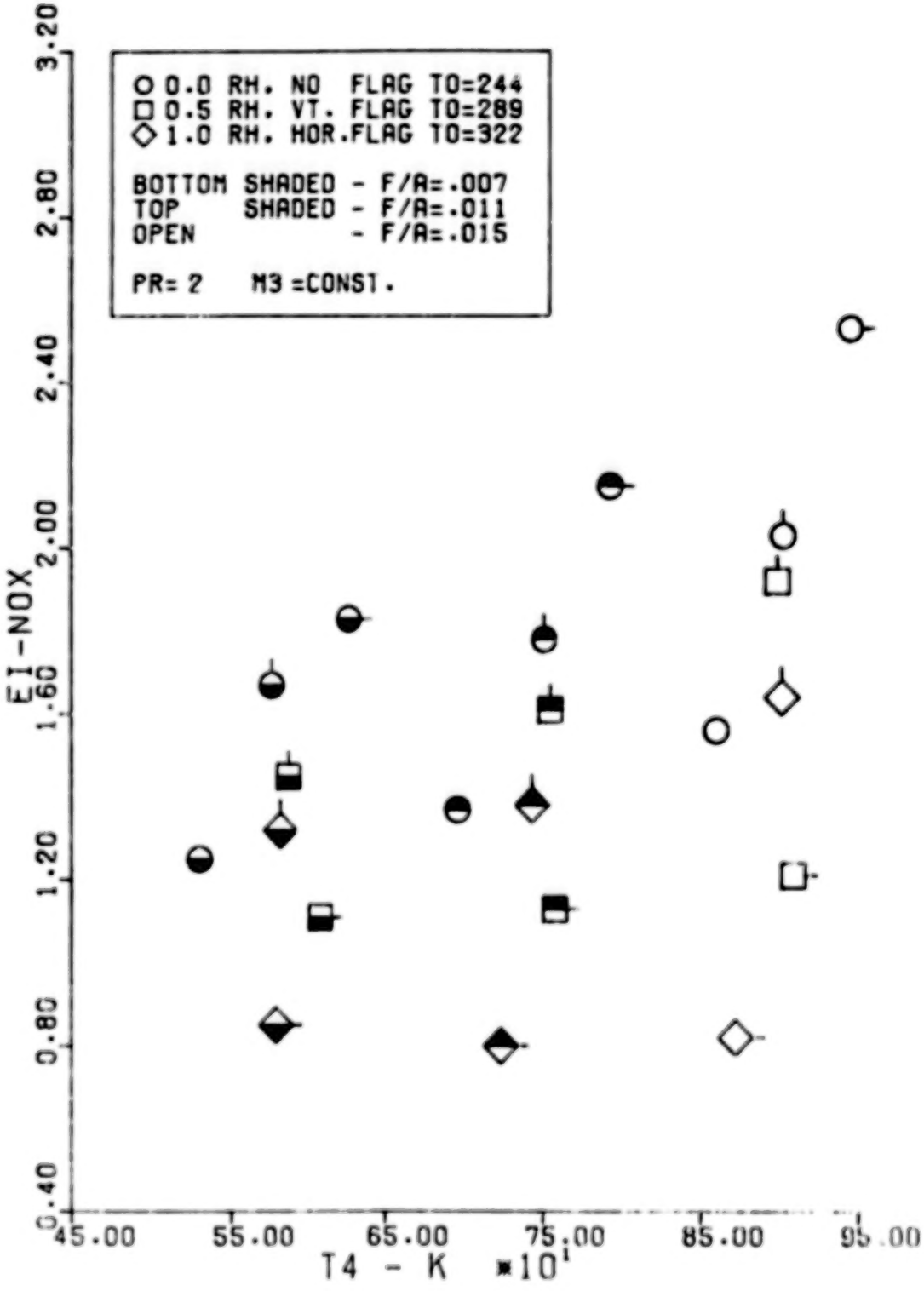

Figure 25. Oxides of Nitrogen Emission Index for a Constant Compressor Discharge Mach Number at a Pressure Ratio of Two

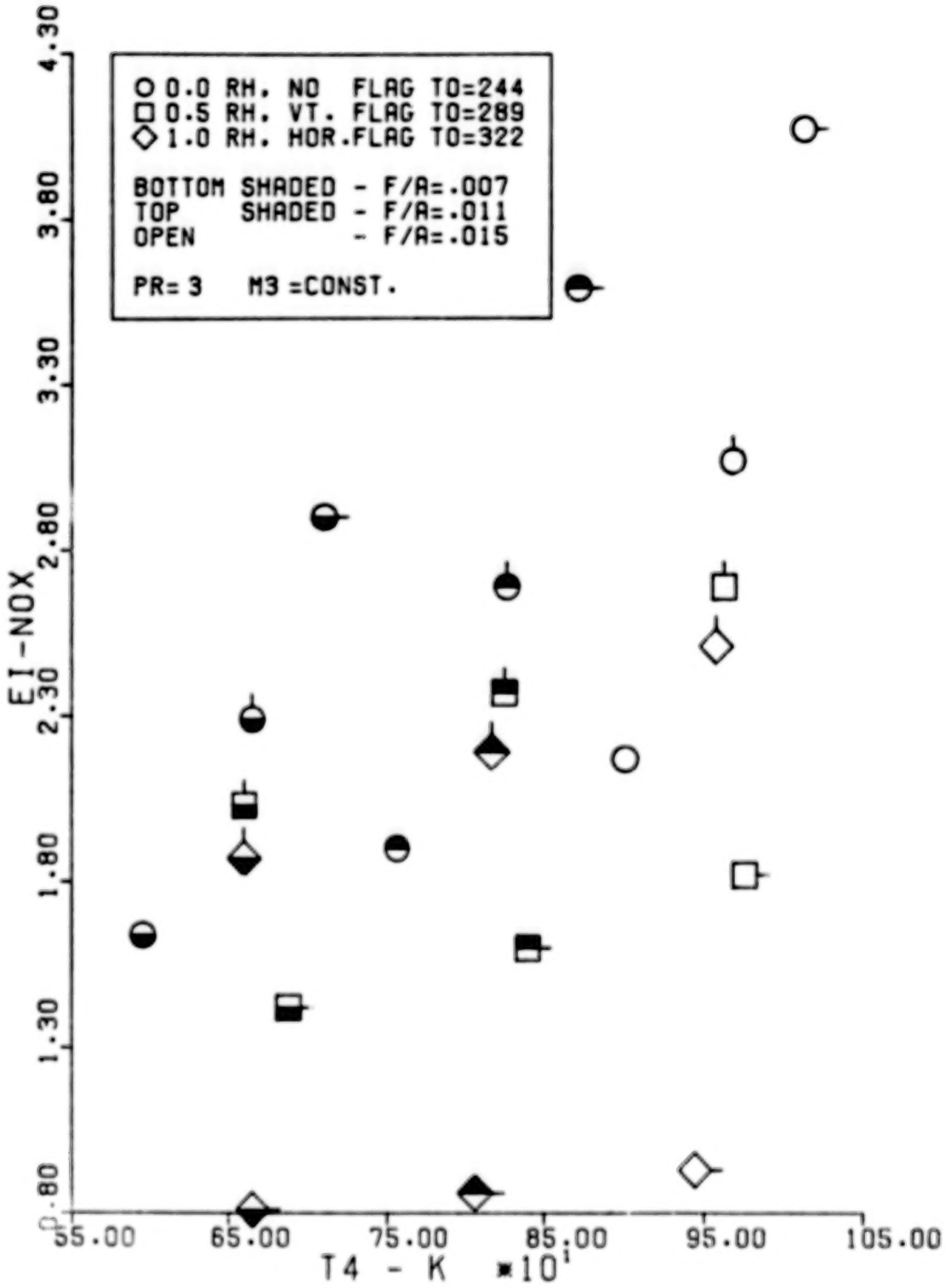

Figure 26. Oxides of Nitrogen Emission Index for a Constant Compressor Discharge Mach Number at a Pressure Ratio of Three

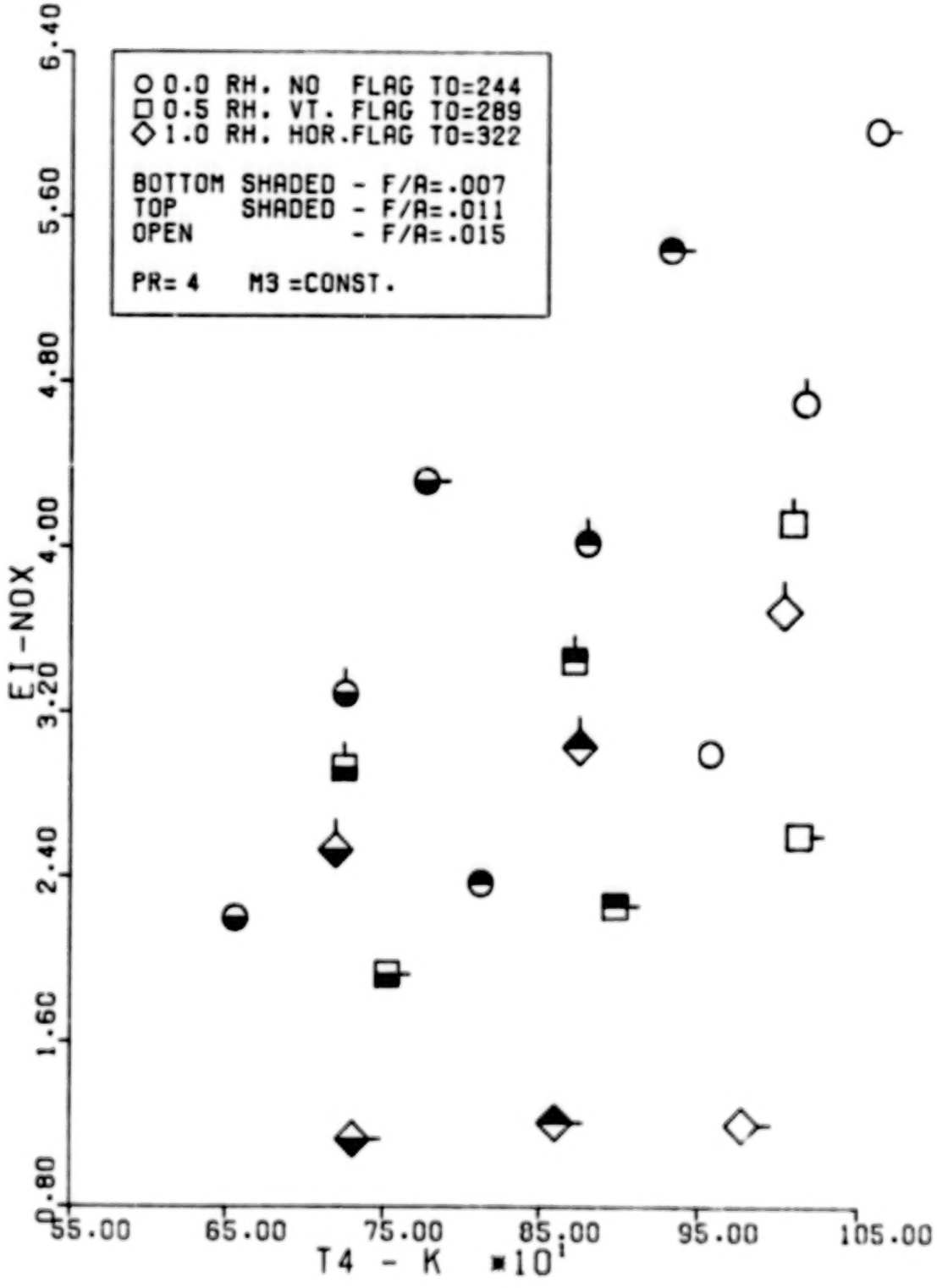

Figure 27. Oxides of Nitrogen Emission Index for a Constant Compressor Discharge Mach Number at a Pressure Ratio of Four

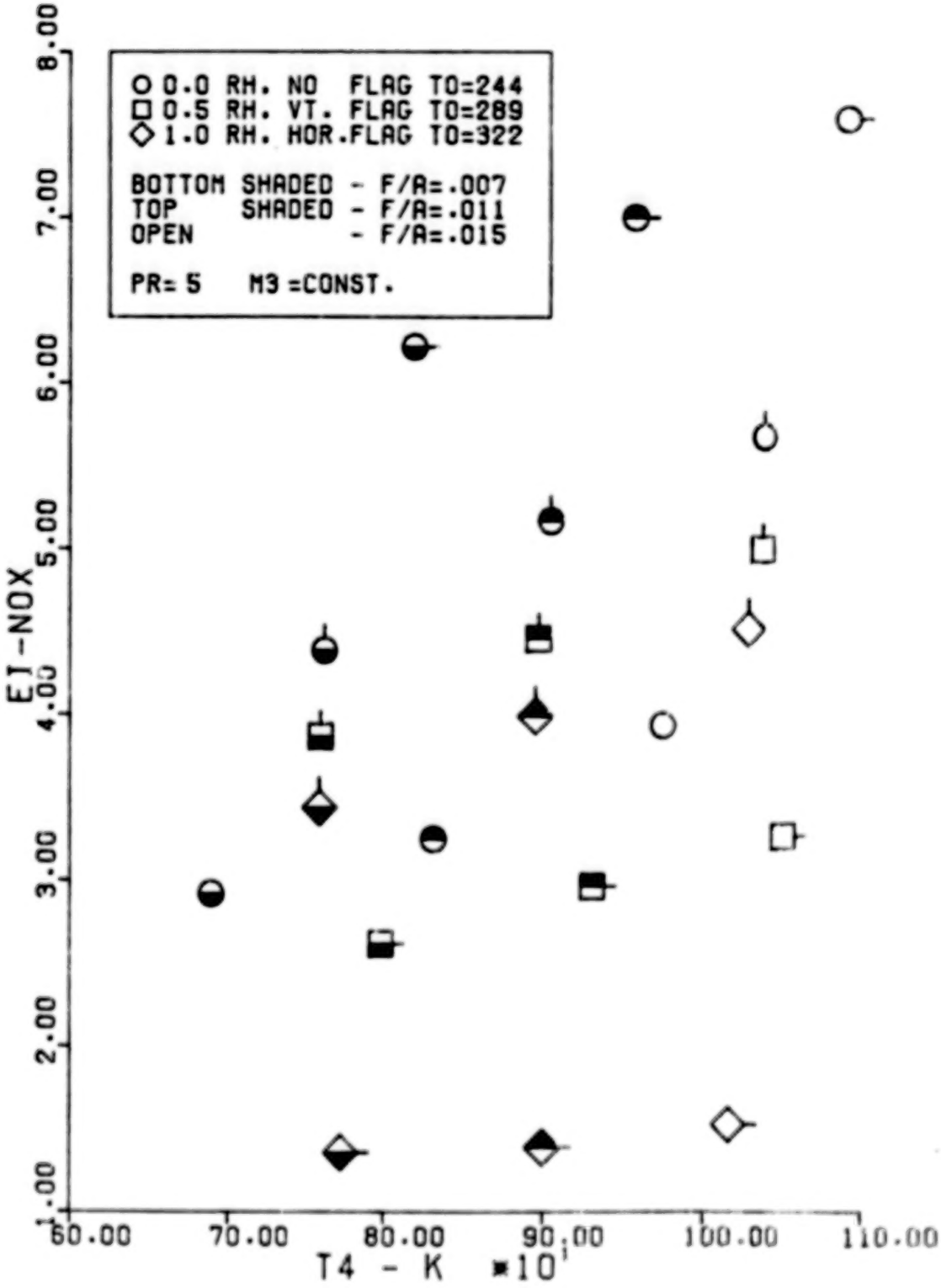

Figure 28. Oxides of Nitrogen Emission Index for a Constant Compressor Discharge Mach Number at a Pressure Ratio of Five

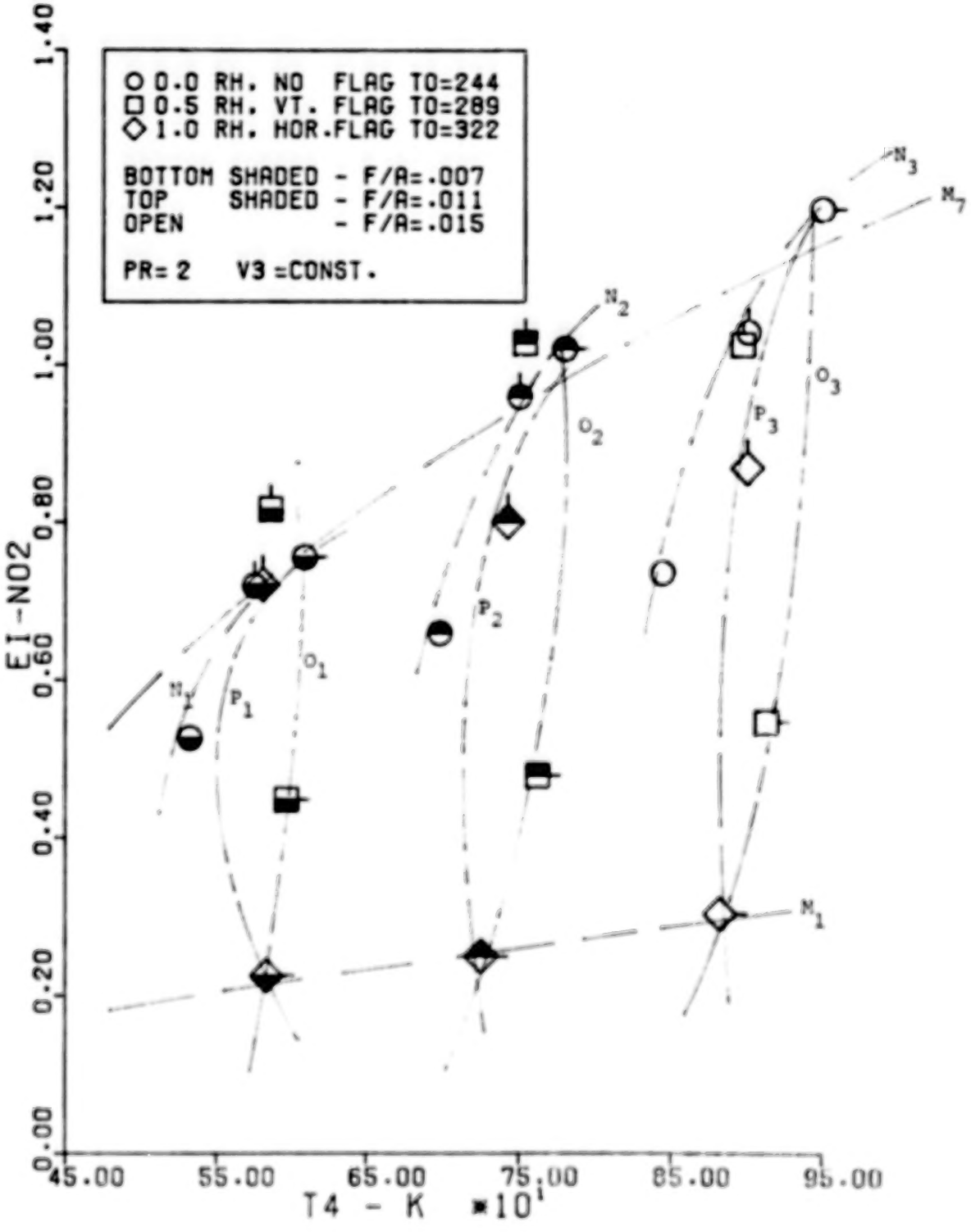

Figure 29. Nitrogen Dioxide Emission Index for a Constant Reference Velocity at a Pressure Ratio of Two

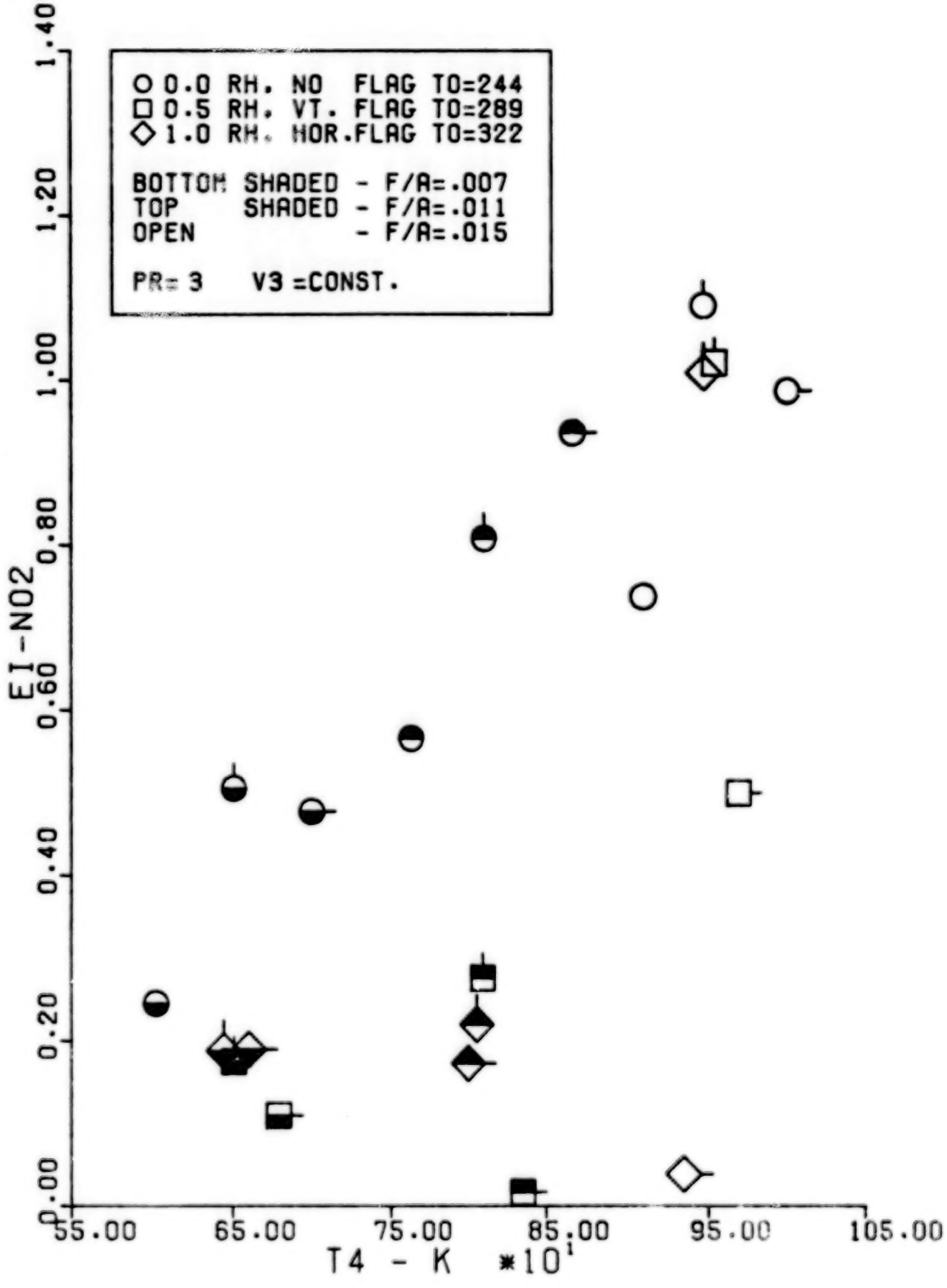

Figure 30. Nitrogen Dioxide Emission Index for a Constant Reference Velocity at a Pressure Ratio of Three

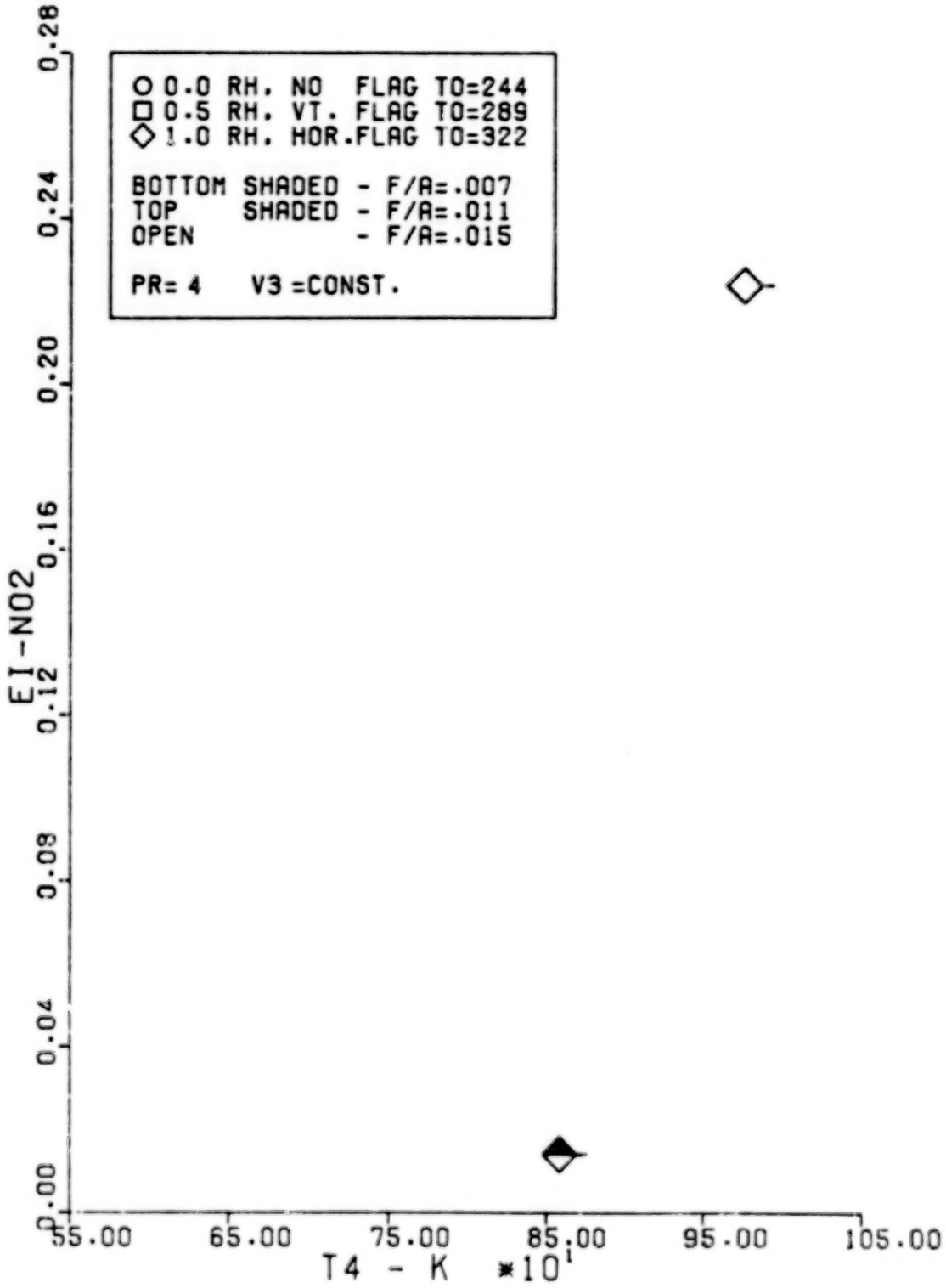

Figure 31. Nitrogen Dioxide Emission Index for a Constant Reference Velocity at a Pressure Ratio of Four

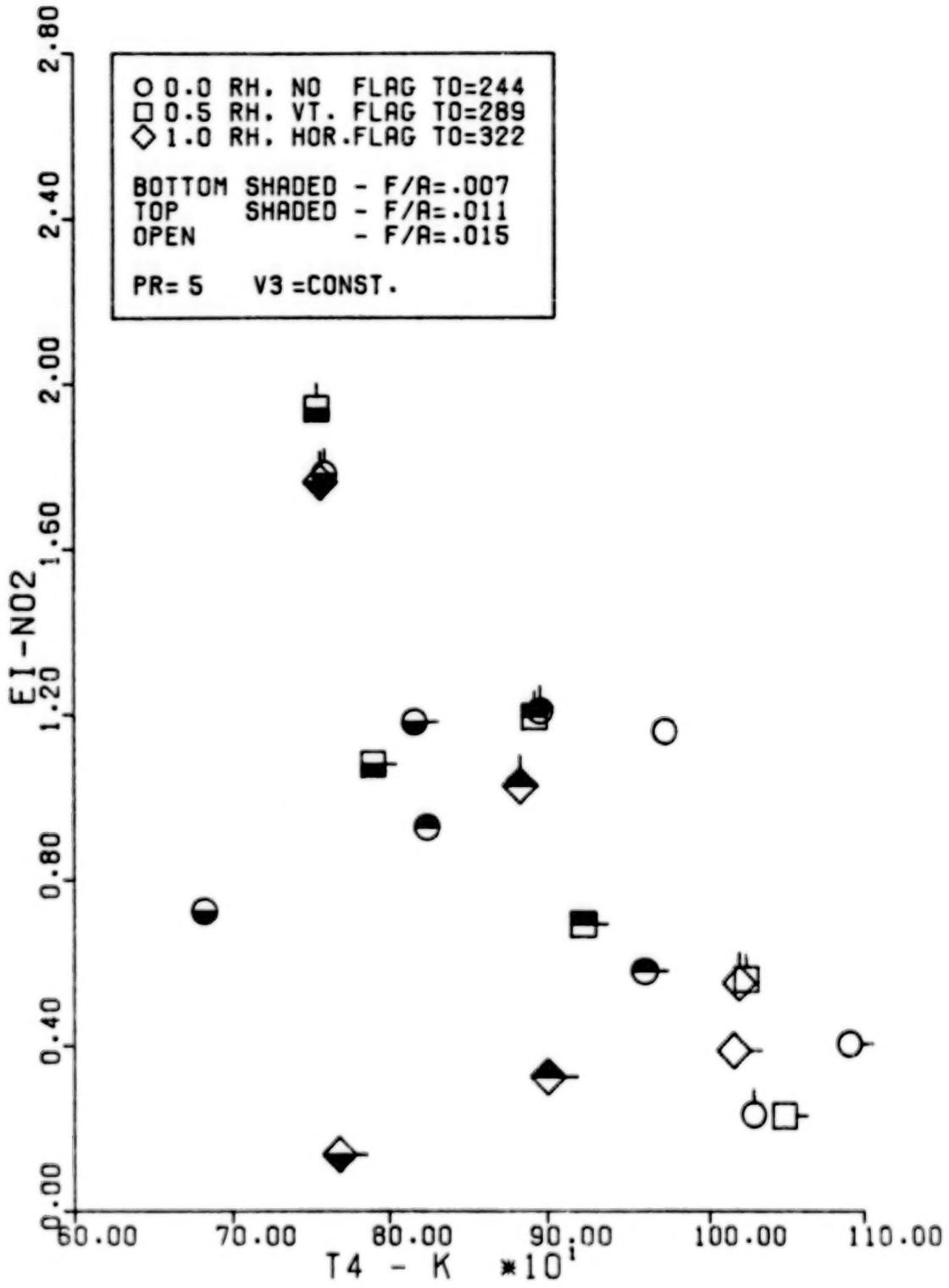

Figure 32. Nitrogen Dioxide Emission Index for a Constant Reference Velocity of a Pressure Ratio of Five

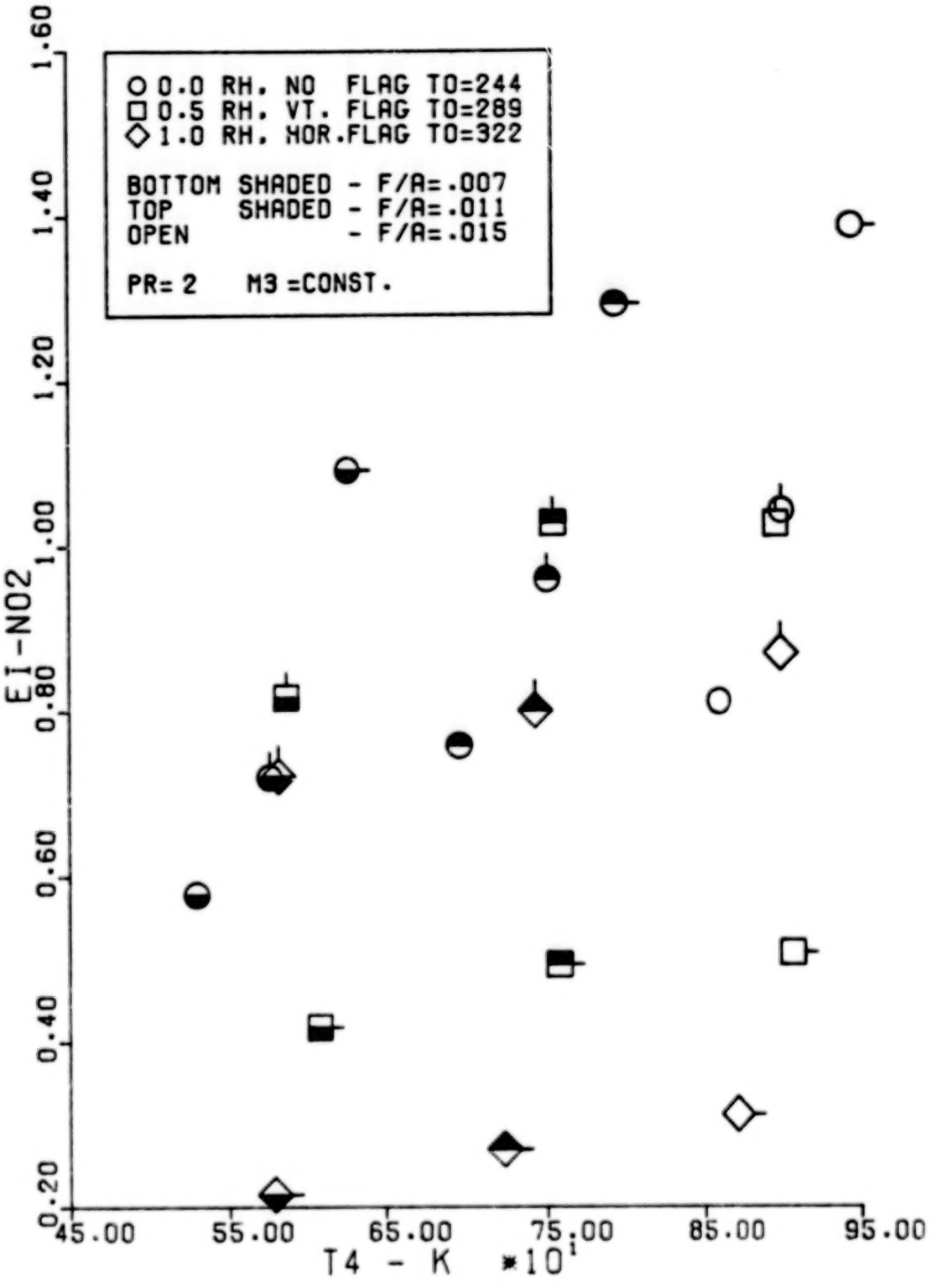

Figure 33. Nitrogen Dioxide Emission Index for a Constant Compressor Discharge Mach Number at a Pressure Ratio of Two

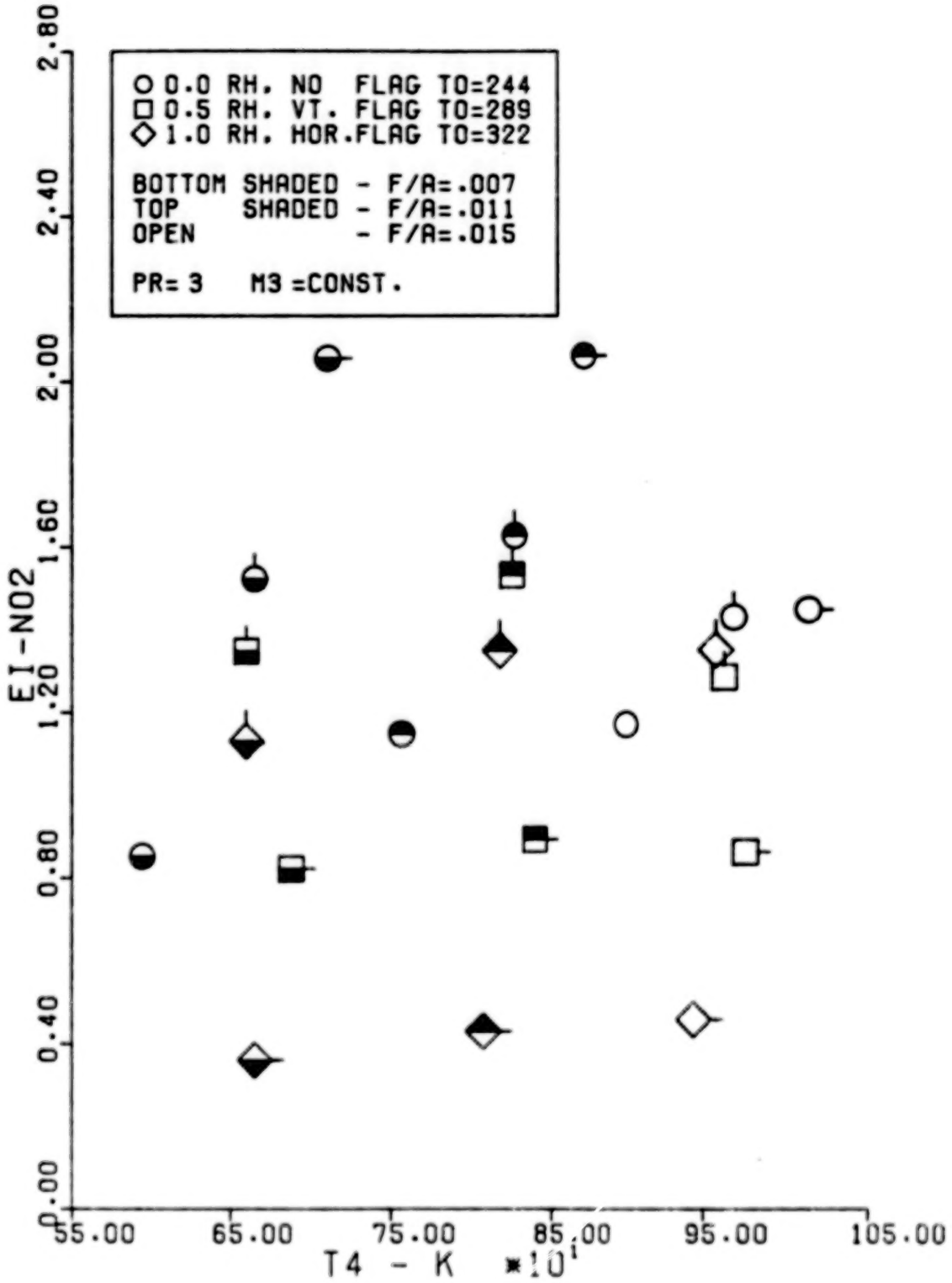

Figure 34. Nitrogen Dioxide Emission Index for a Constant Compressor Discharge Mach Number at a Pressure Ratio of Three

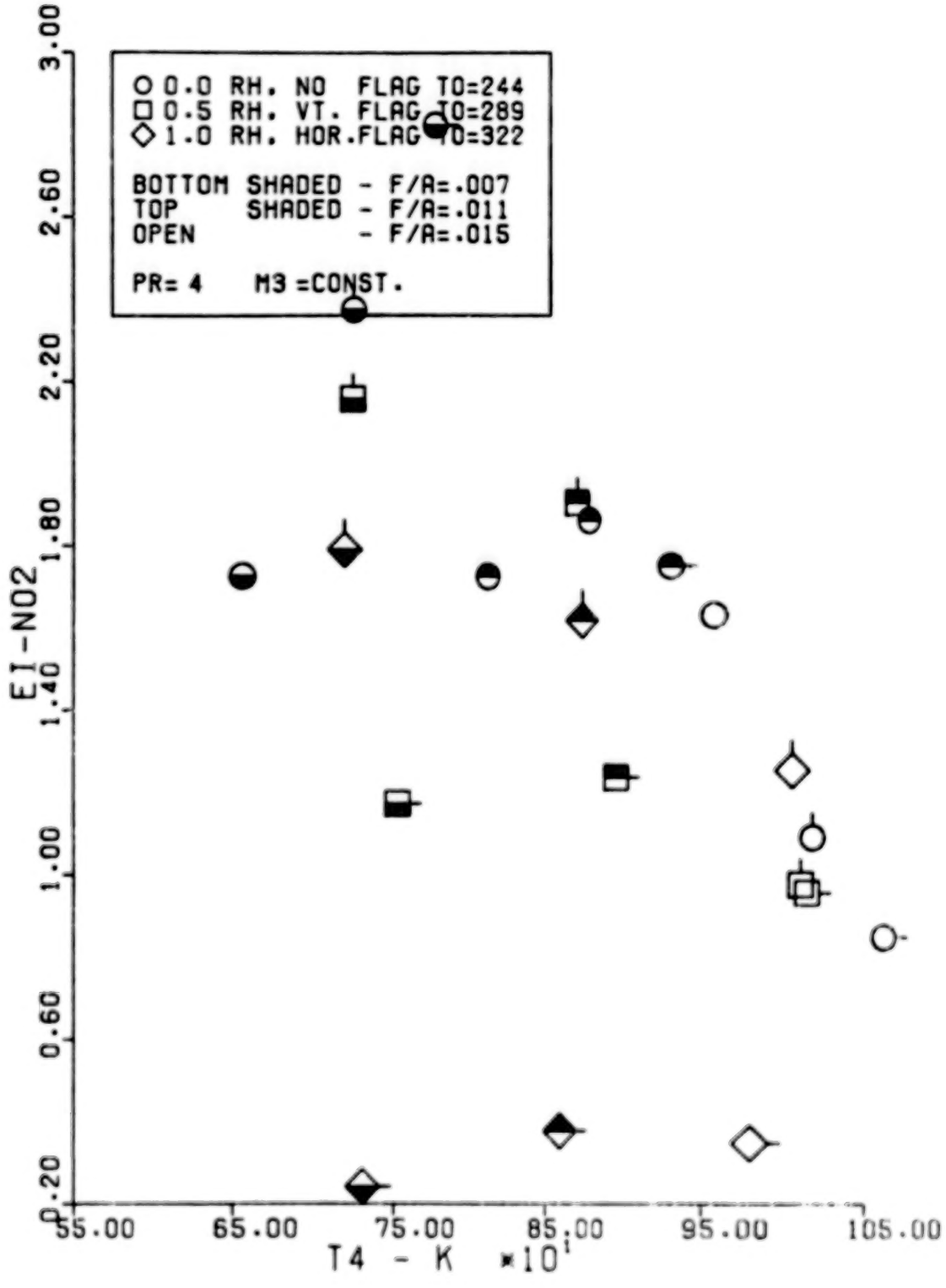

Figure 35. Nitrogen Dioxide Emission Index for a Constant Compressor Discharge Mach Number at a Pressure Ratio of Four

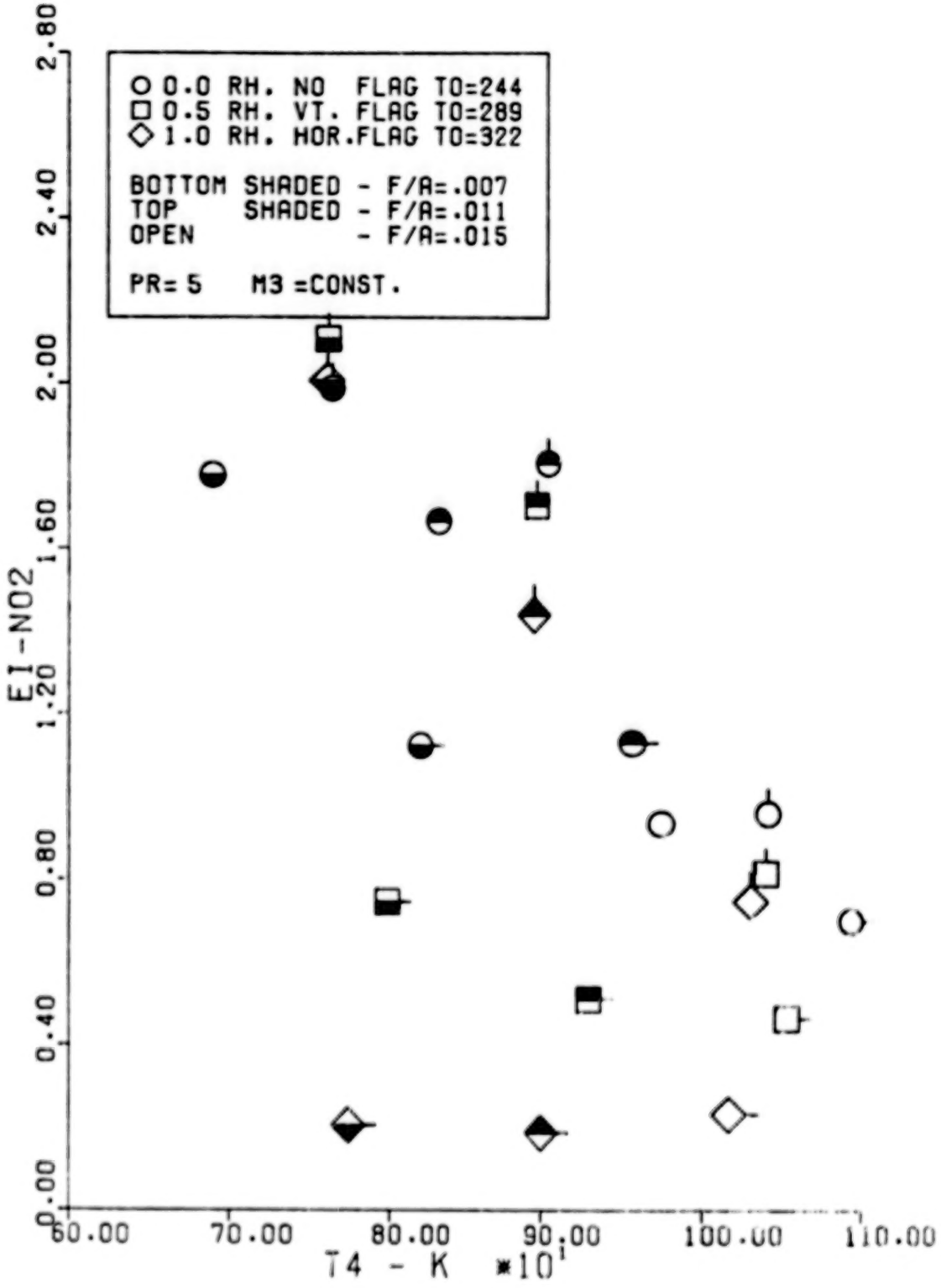

Figure 36. Nitrogen Dioxide Emission Index for a Constant Compressor Discharge Mach Number at a Pressure Ratio of Five

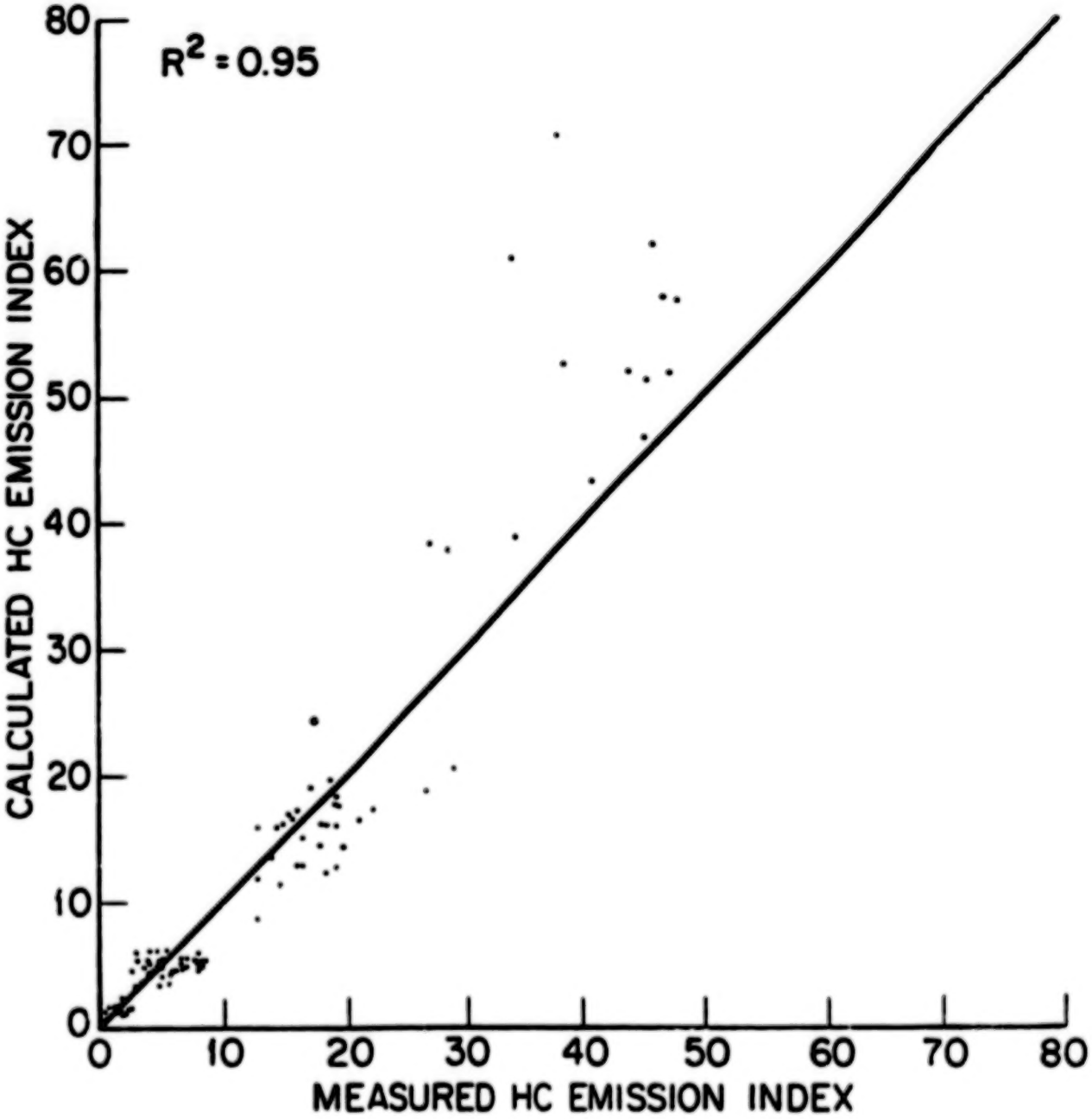

Figure 37. Hydrocarbon Emission Curve Fit

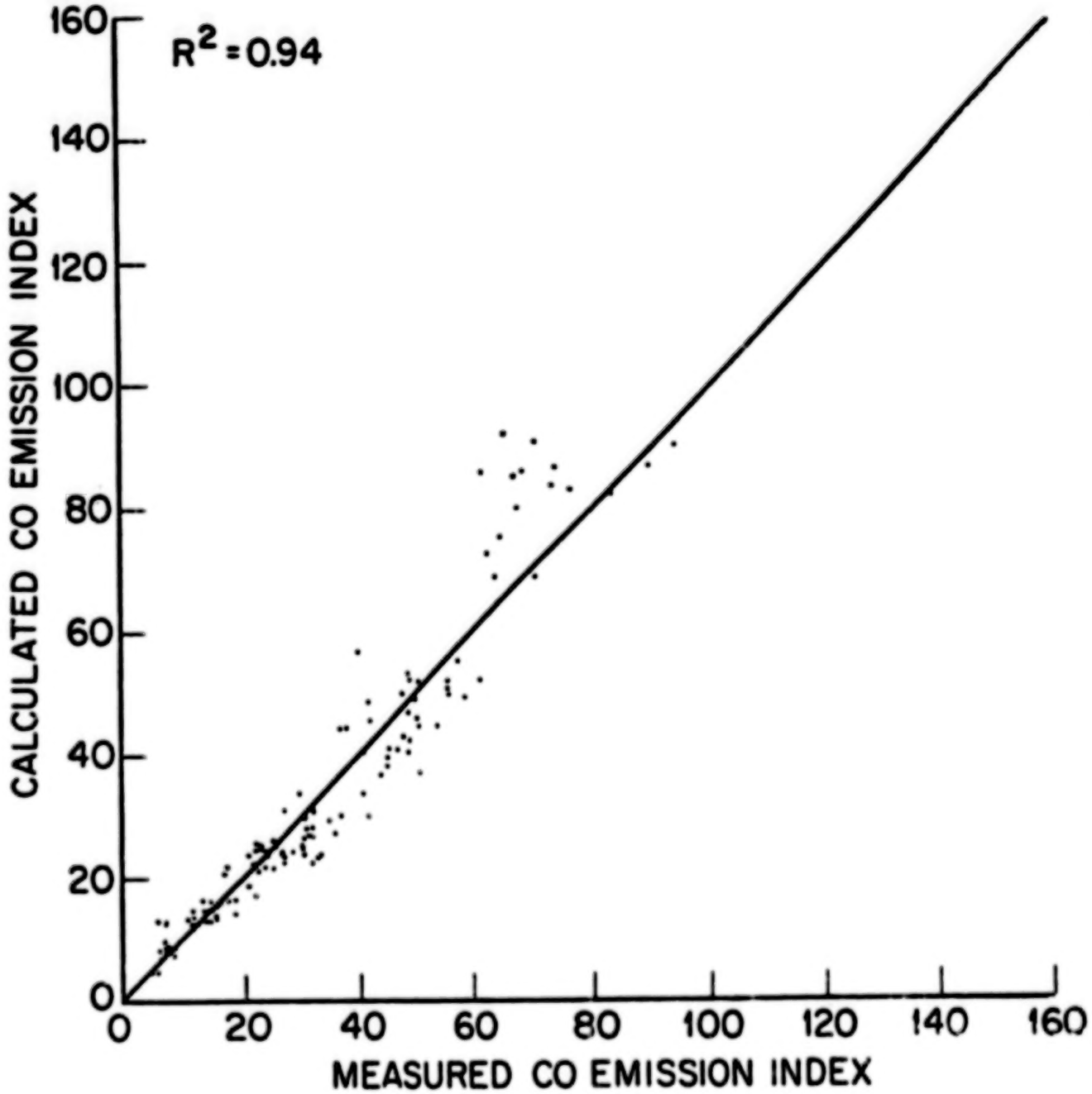

Figure 38. Carbon Monoxide Emission Curve Fit

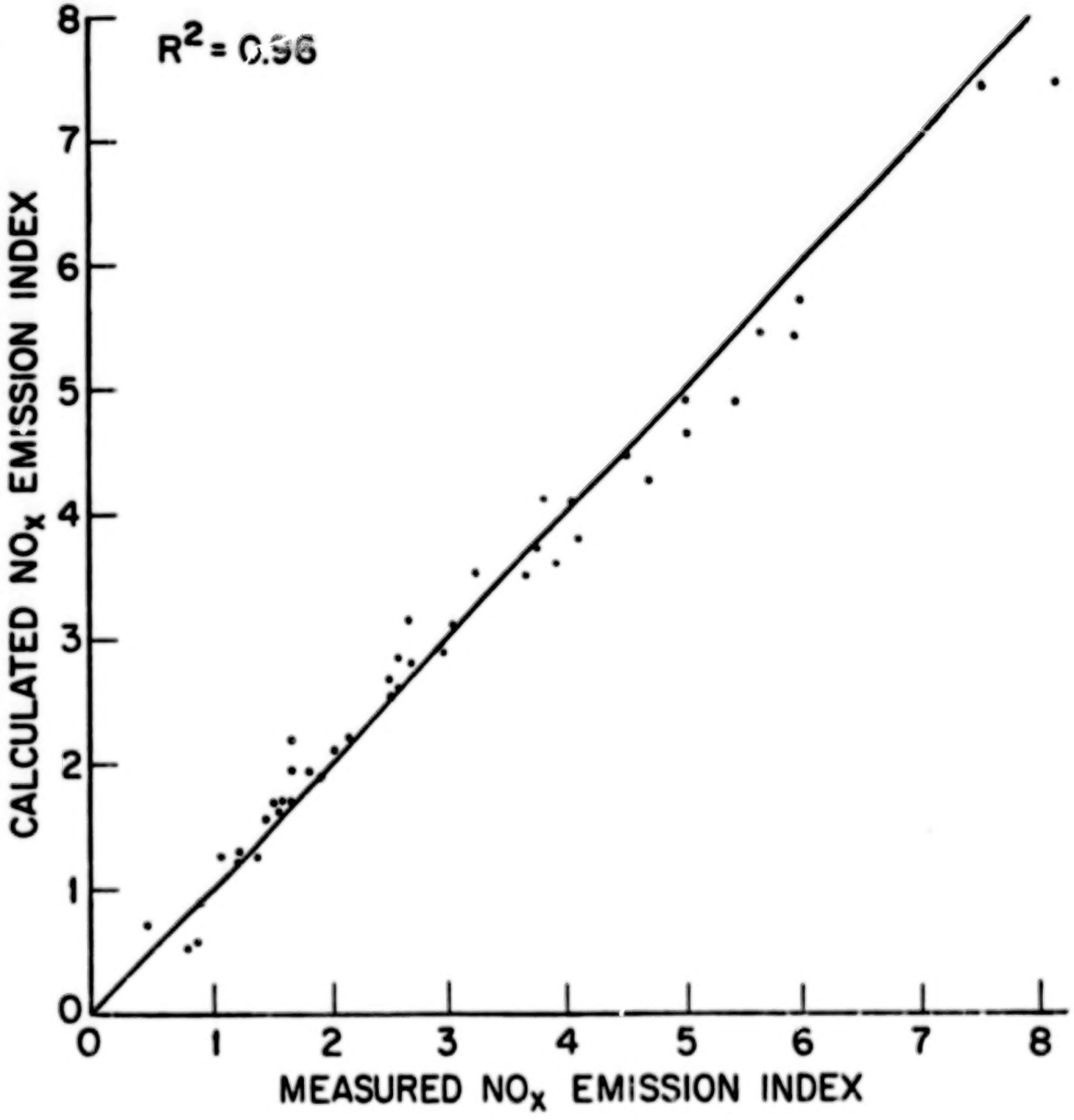

Ficure 39. Oxides of Nitrogen Emission Curve Fit

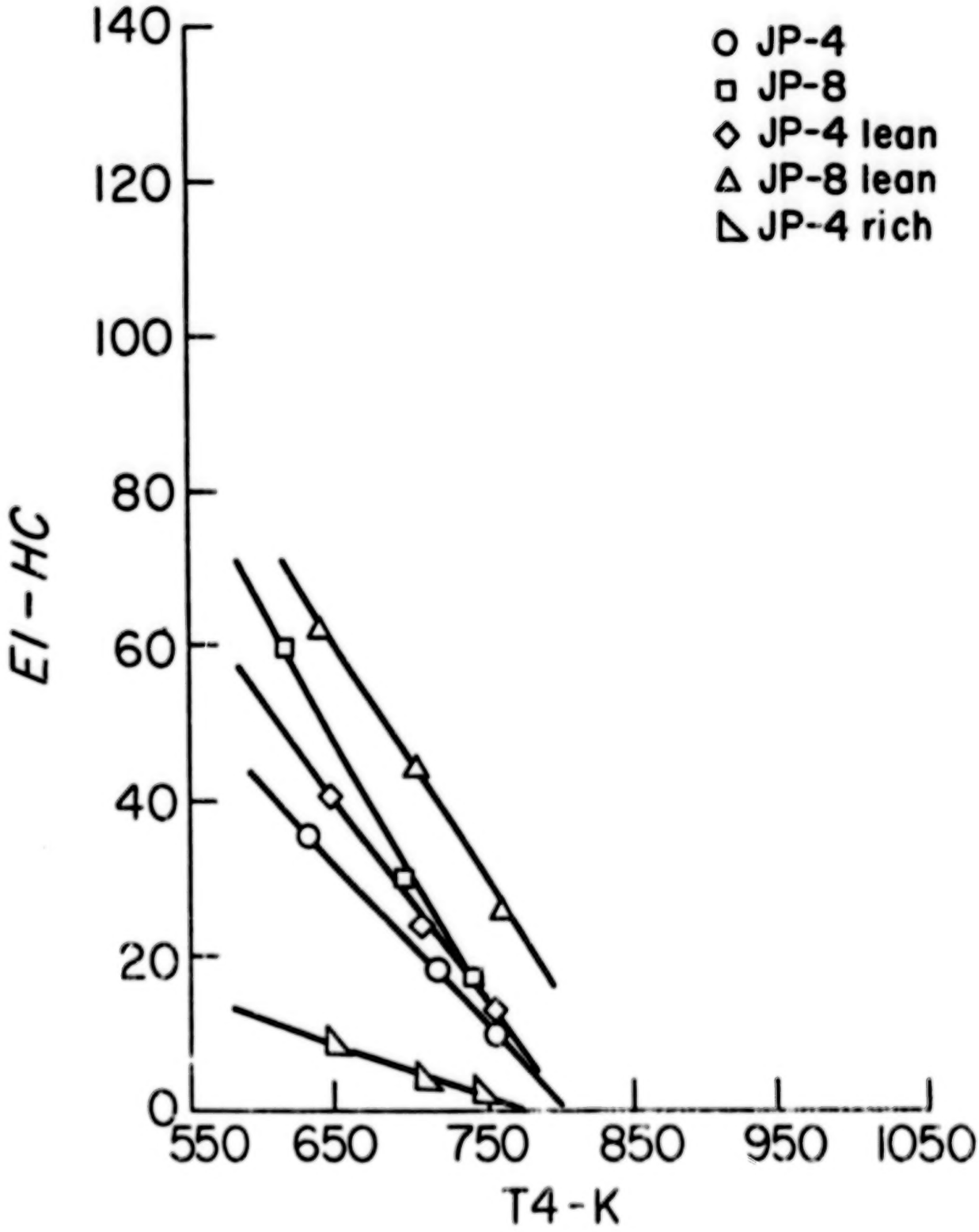

Figure 40. Hydrocarbon Emission Index, T-56

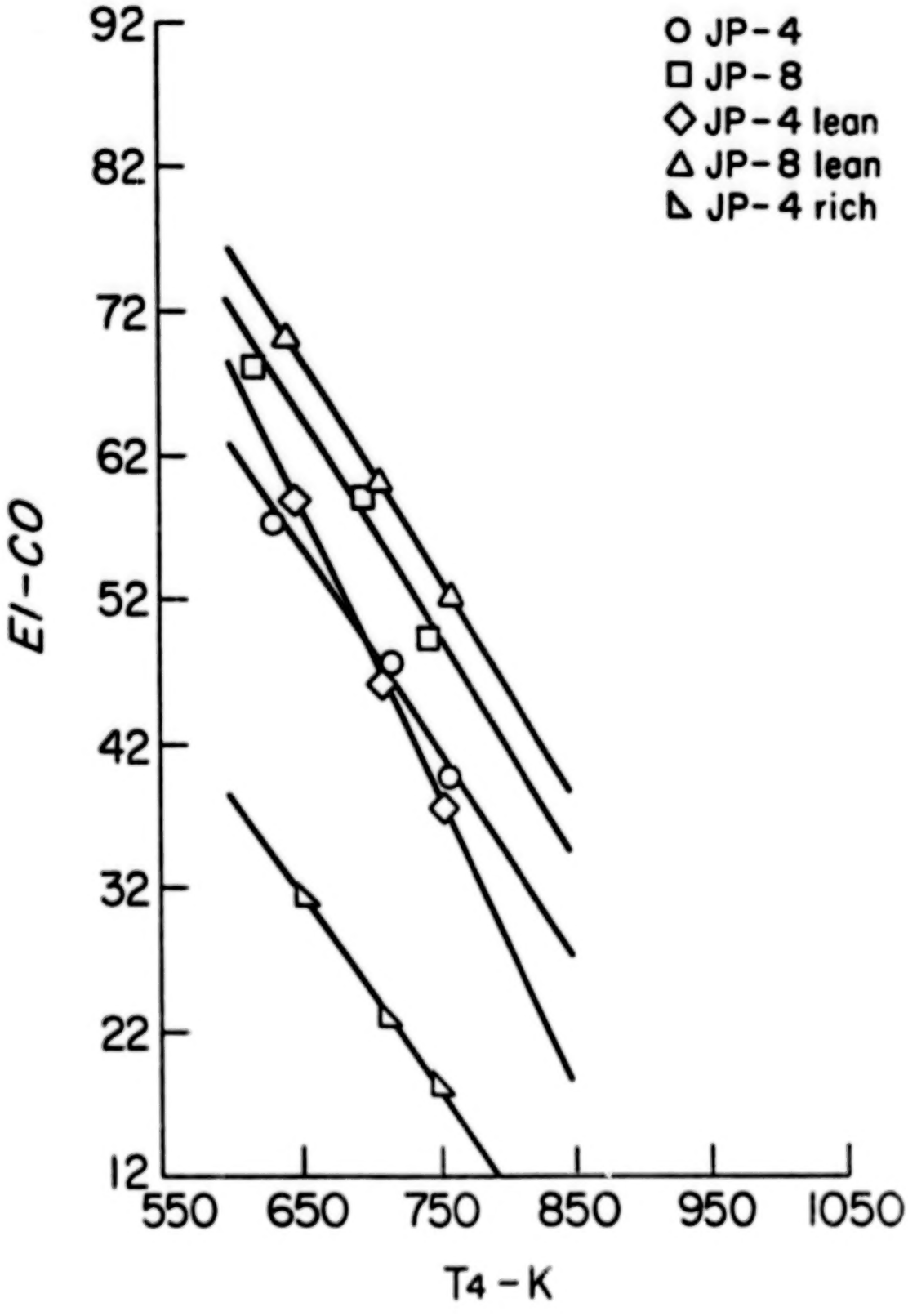

Figure 41. Carbon Monoxide Emission Index, T-56

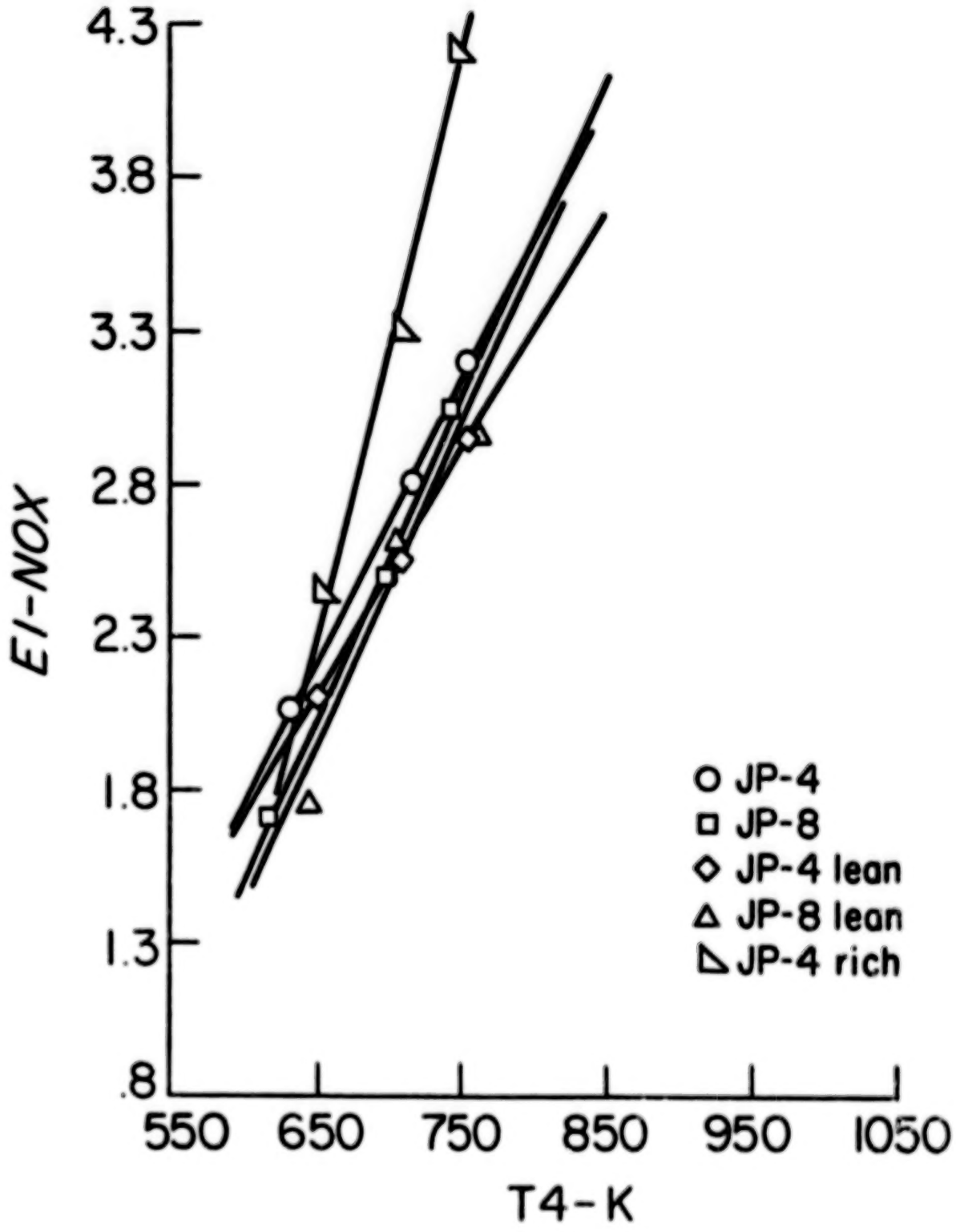

Figure 42. Oxides of Nitrogen Emission Index, T-56

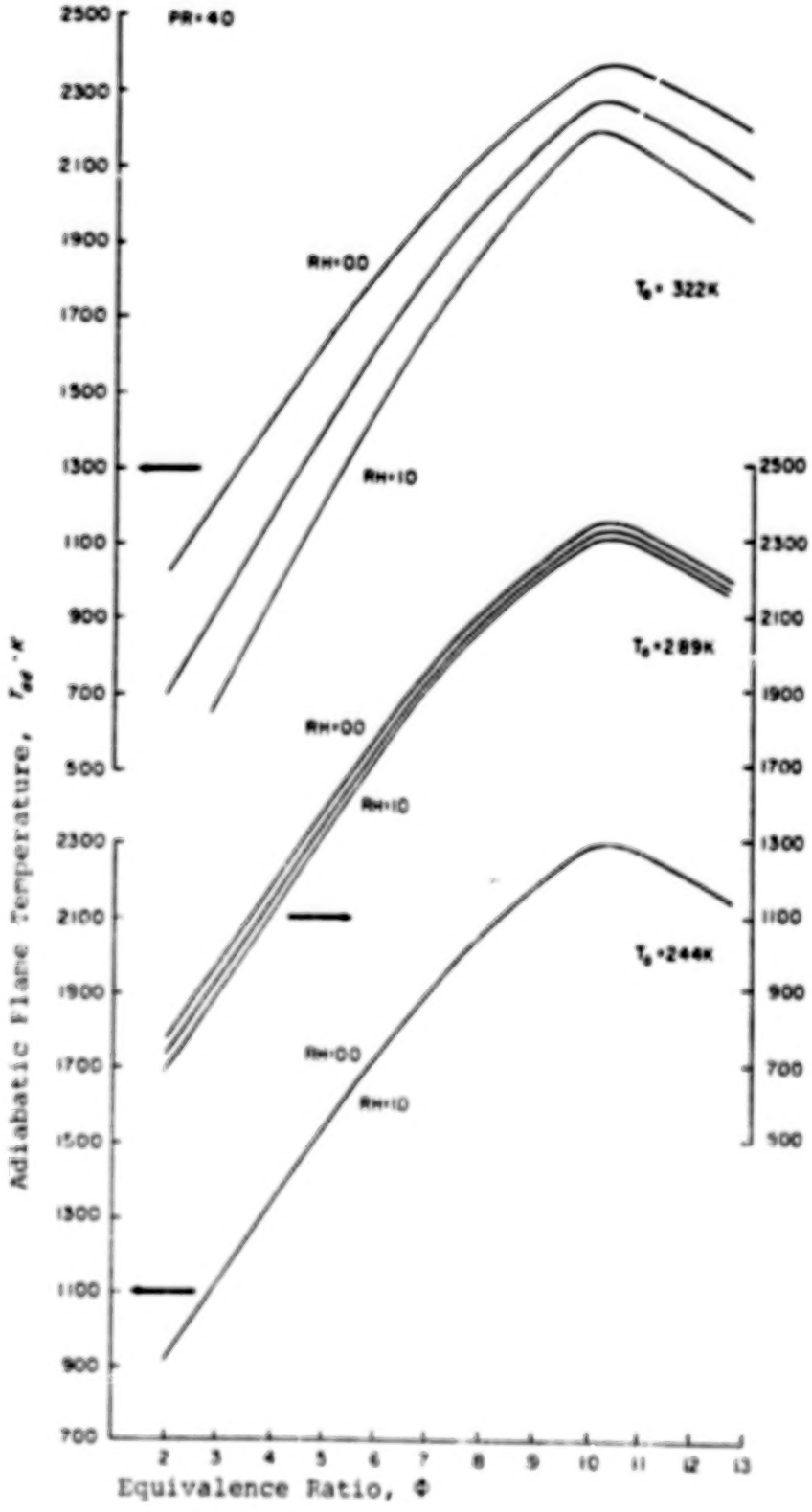

Figure 43. Methane Adiabatic Flame Temperature

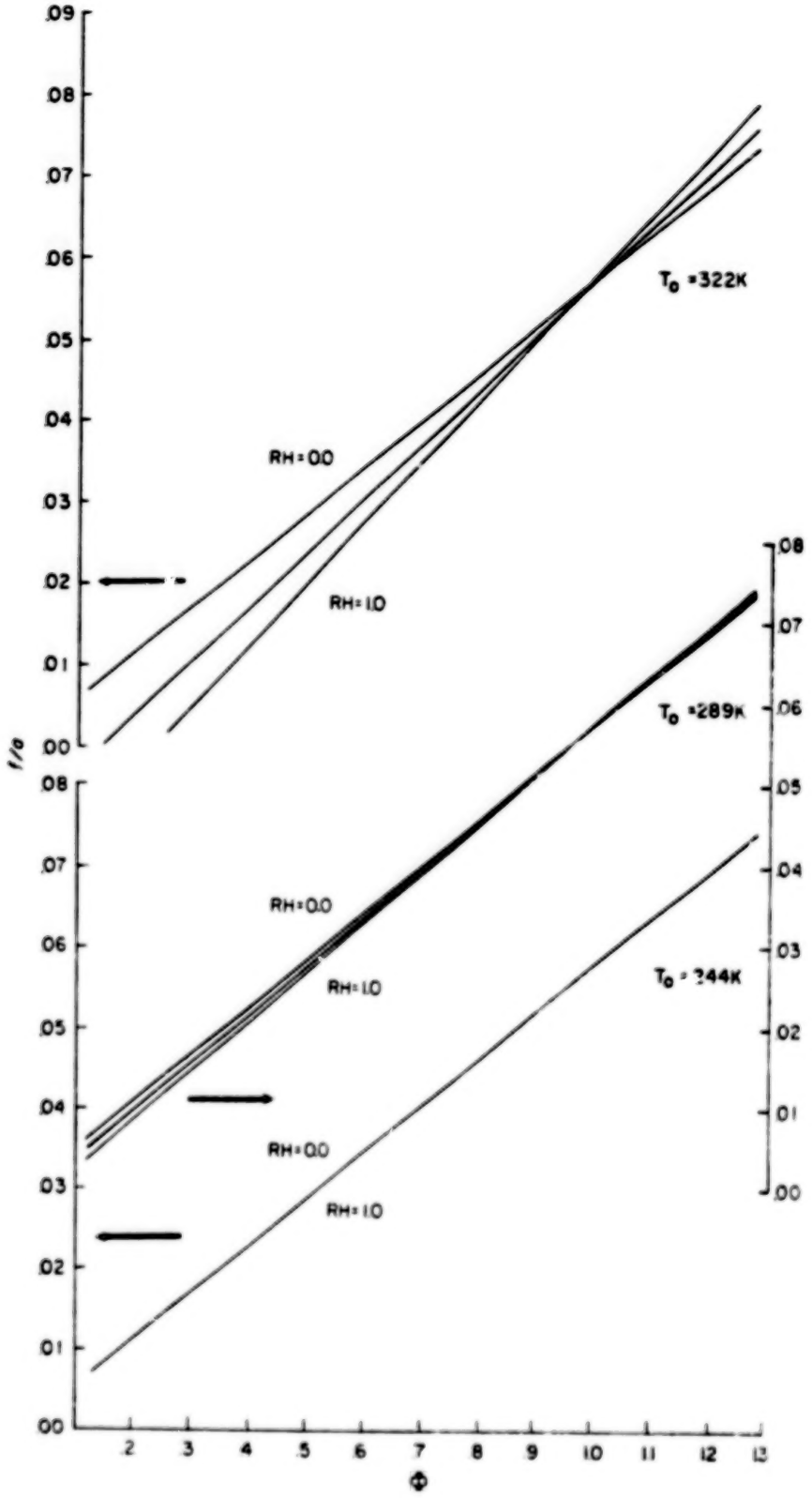

Figure 44. Methane Fuel-Air Ratio

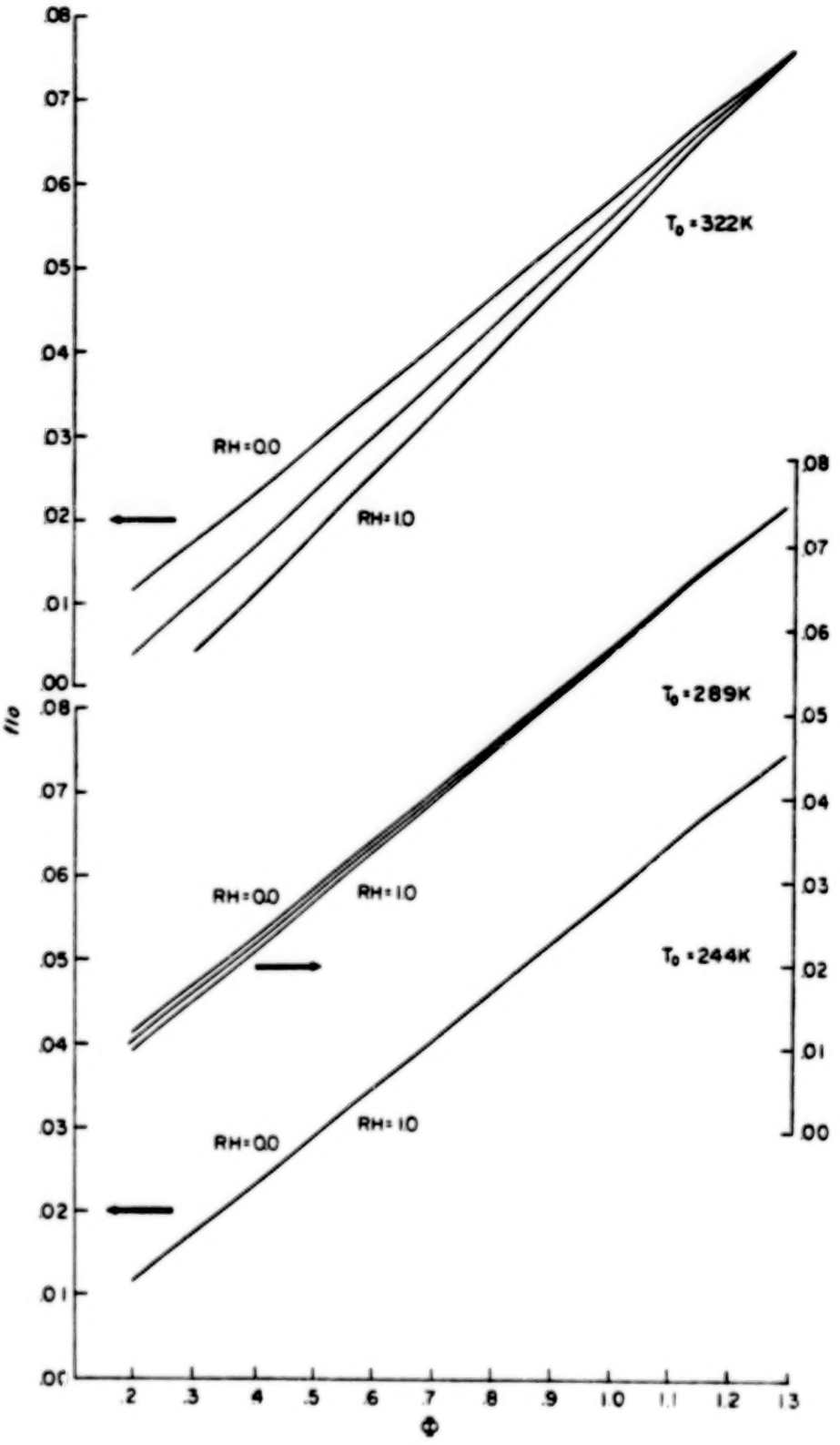

Figure 45. Methane Fuel-Oxidizer Ratio

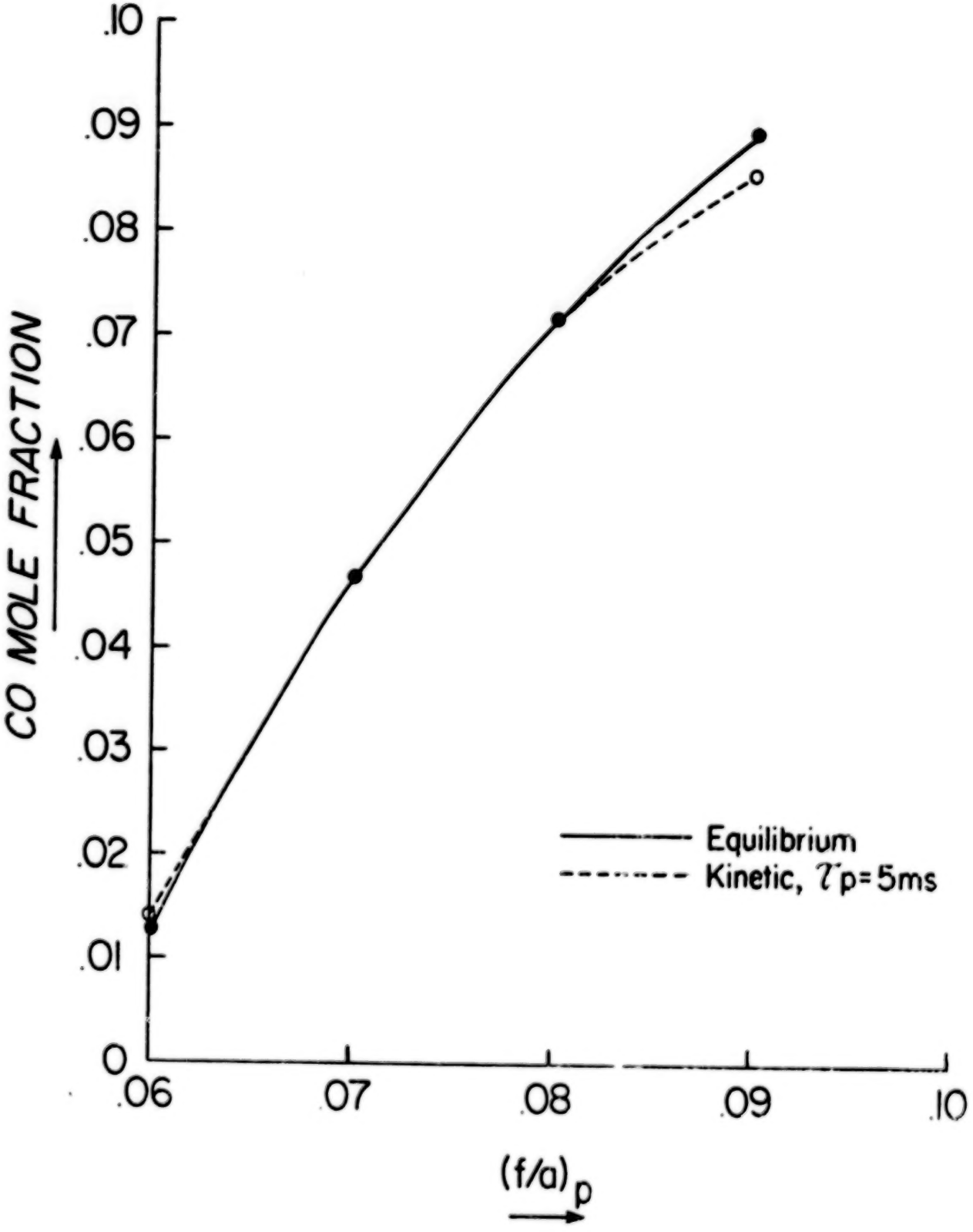

Figure 46. Primary Zone Carbon Monoxide Mole Fraction

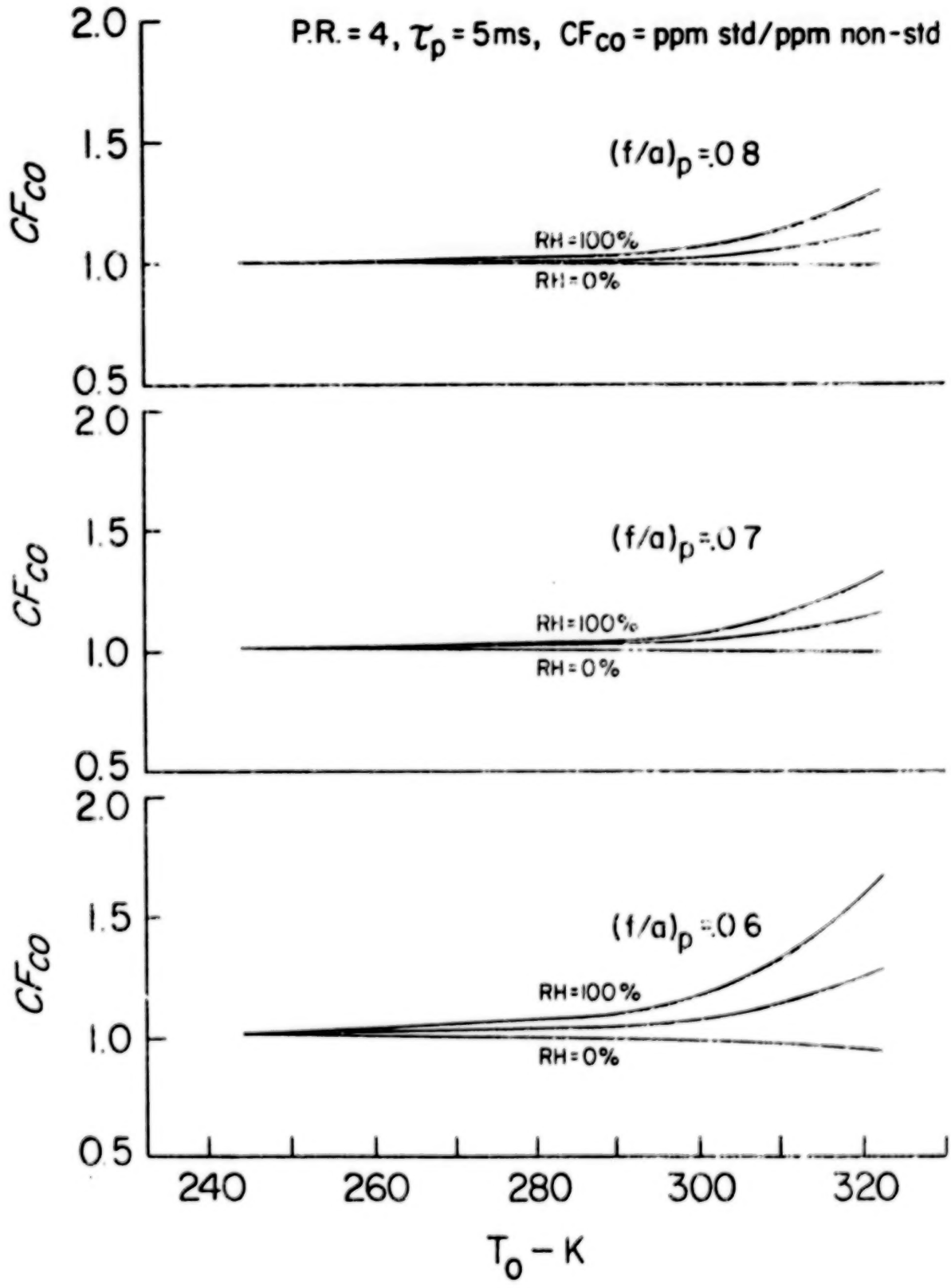

Figure 47. Normalized Primary Zone Carbon Monoxide Emissions

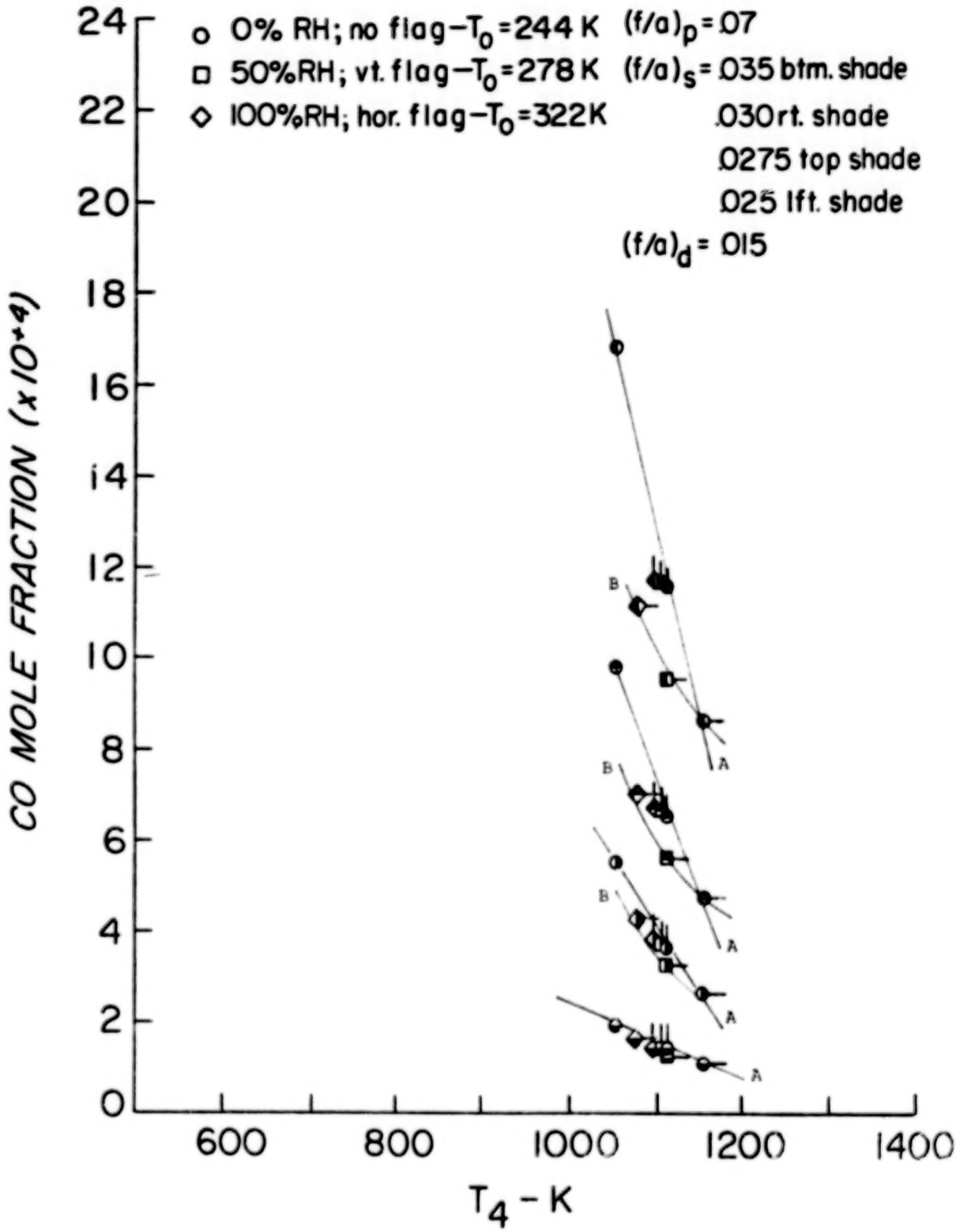

Figure 48. Carbon Monoxide Emissions as Determined by Secondary Zone Fuel-Air Ratio

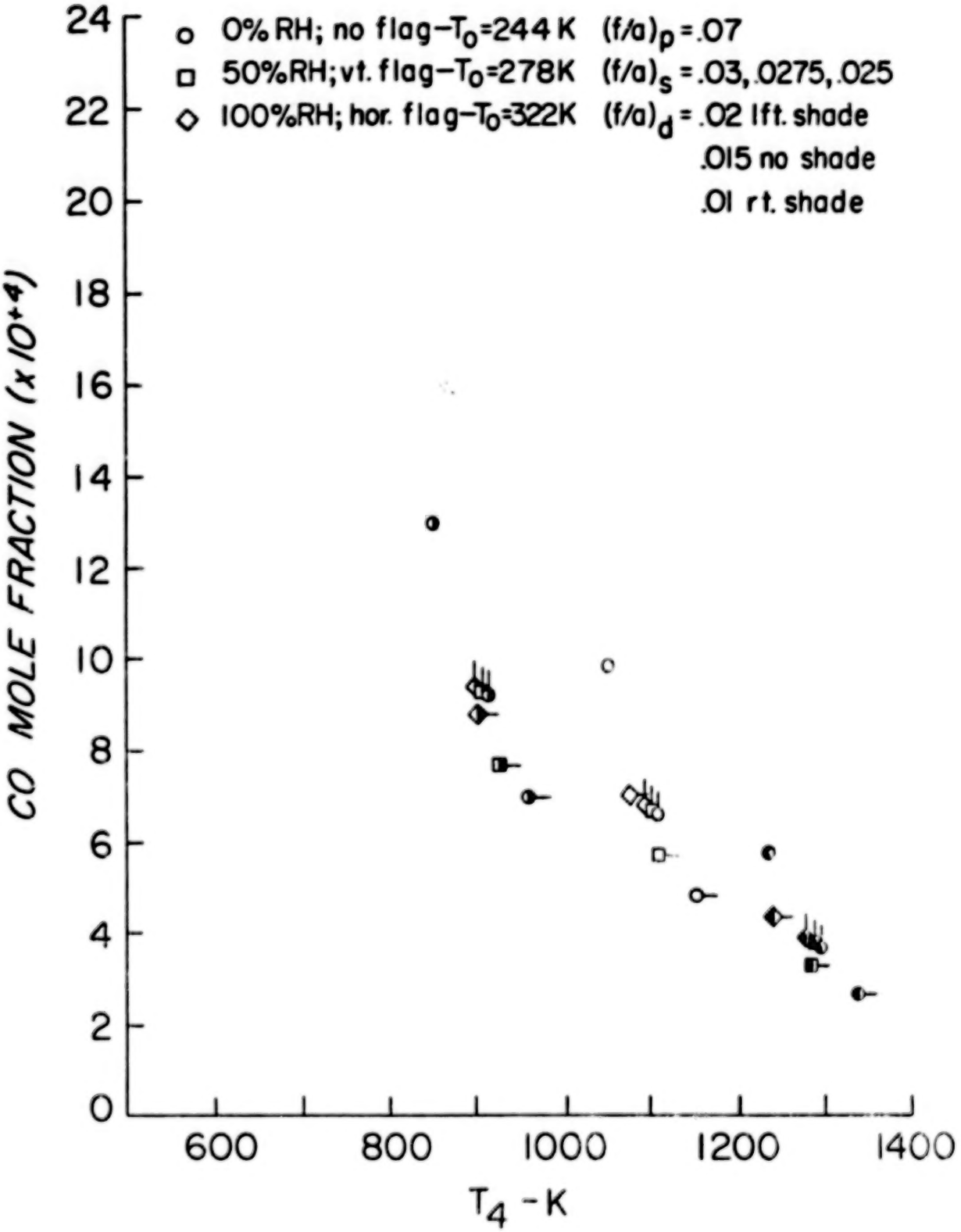

Figure 49. Carbon Monoxide Emissions for a Primary Zone Fuel-Air Ratio of .07

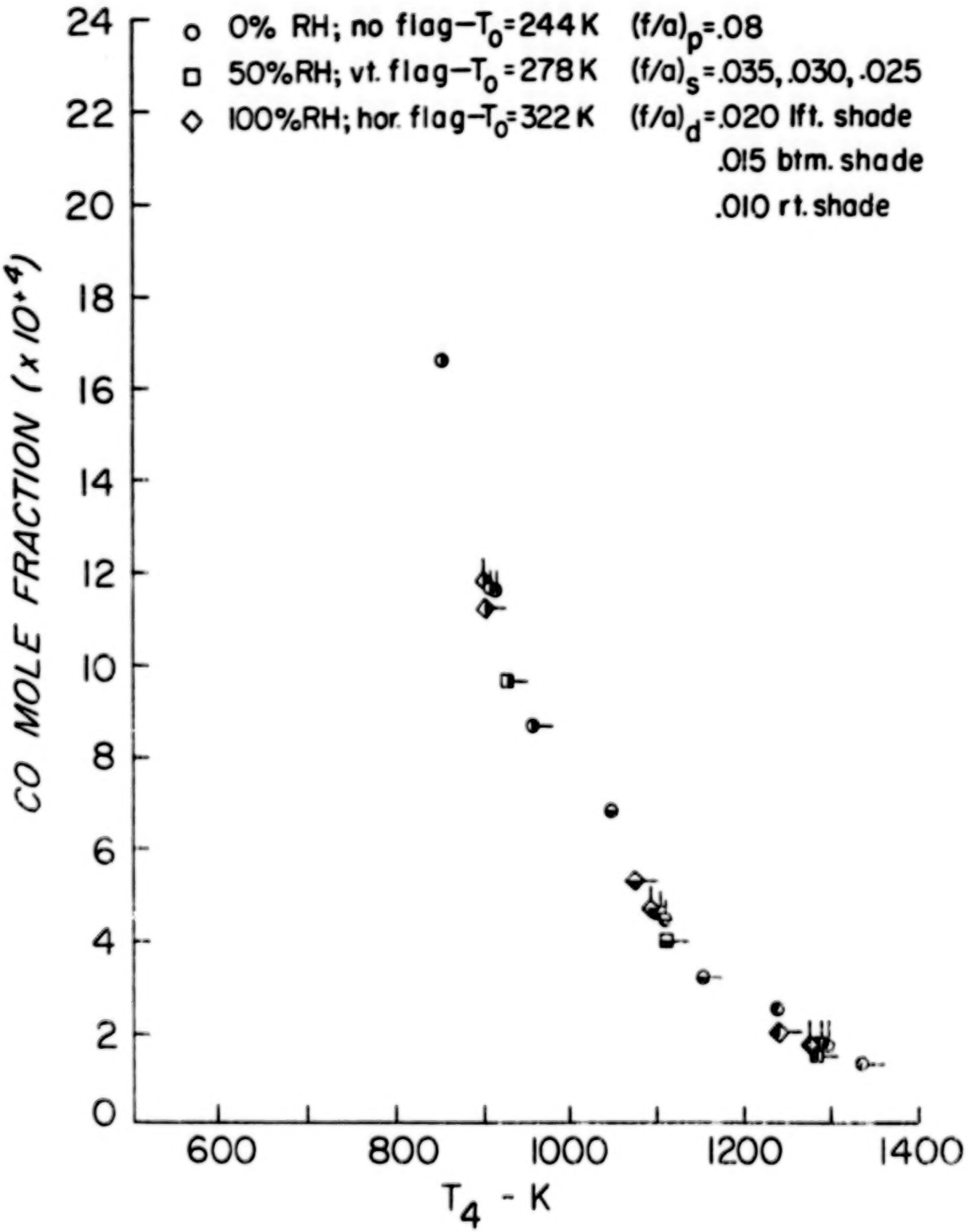

Figure 50. Carbon Monoxide Emissions for a Primary Zone Fuel-Air Ratio of .08

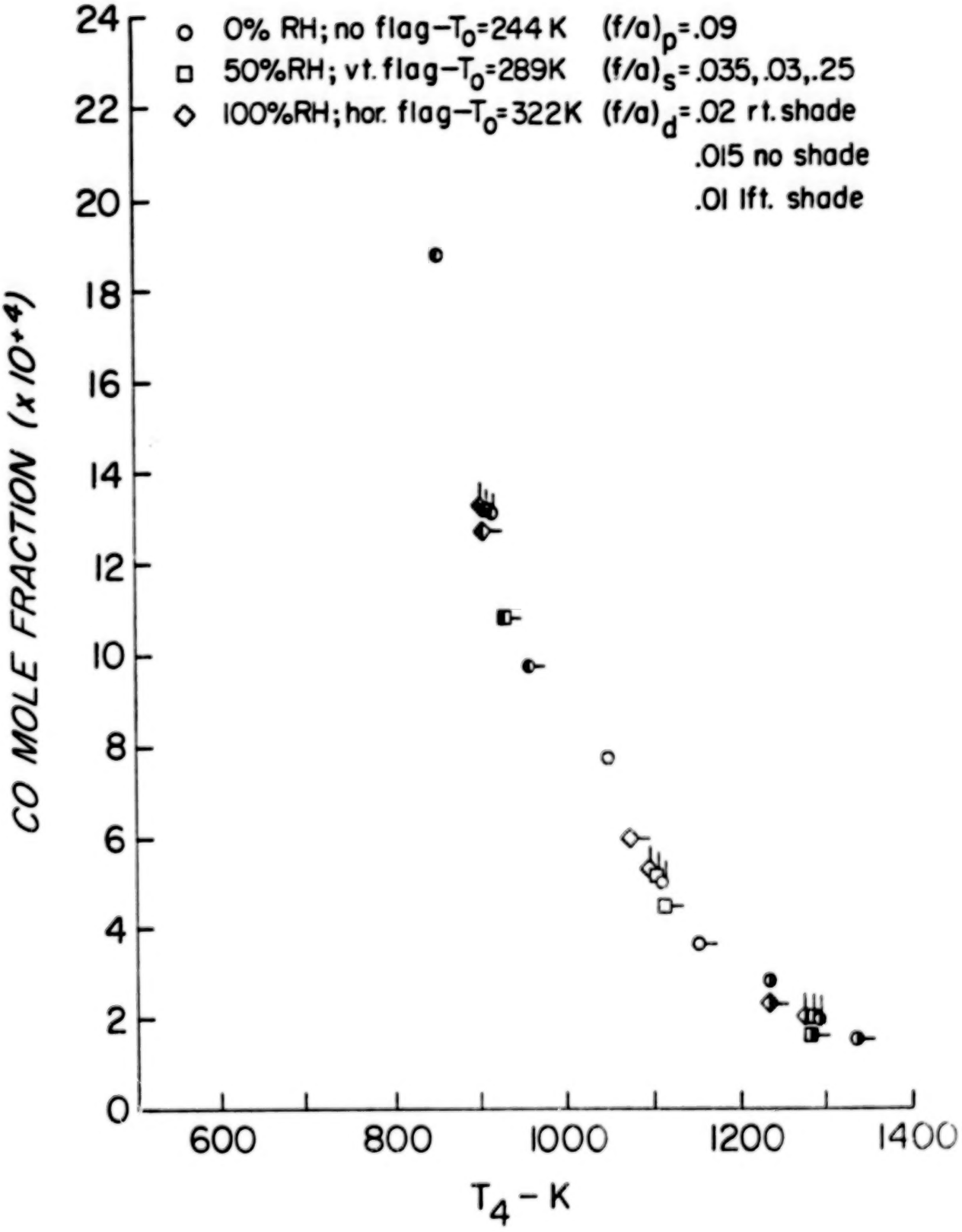

Figure 51. Carbon Monoxide Emissions for a Primary Zone Fuel-Air Ratio of .09

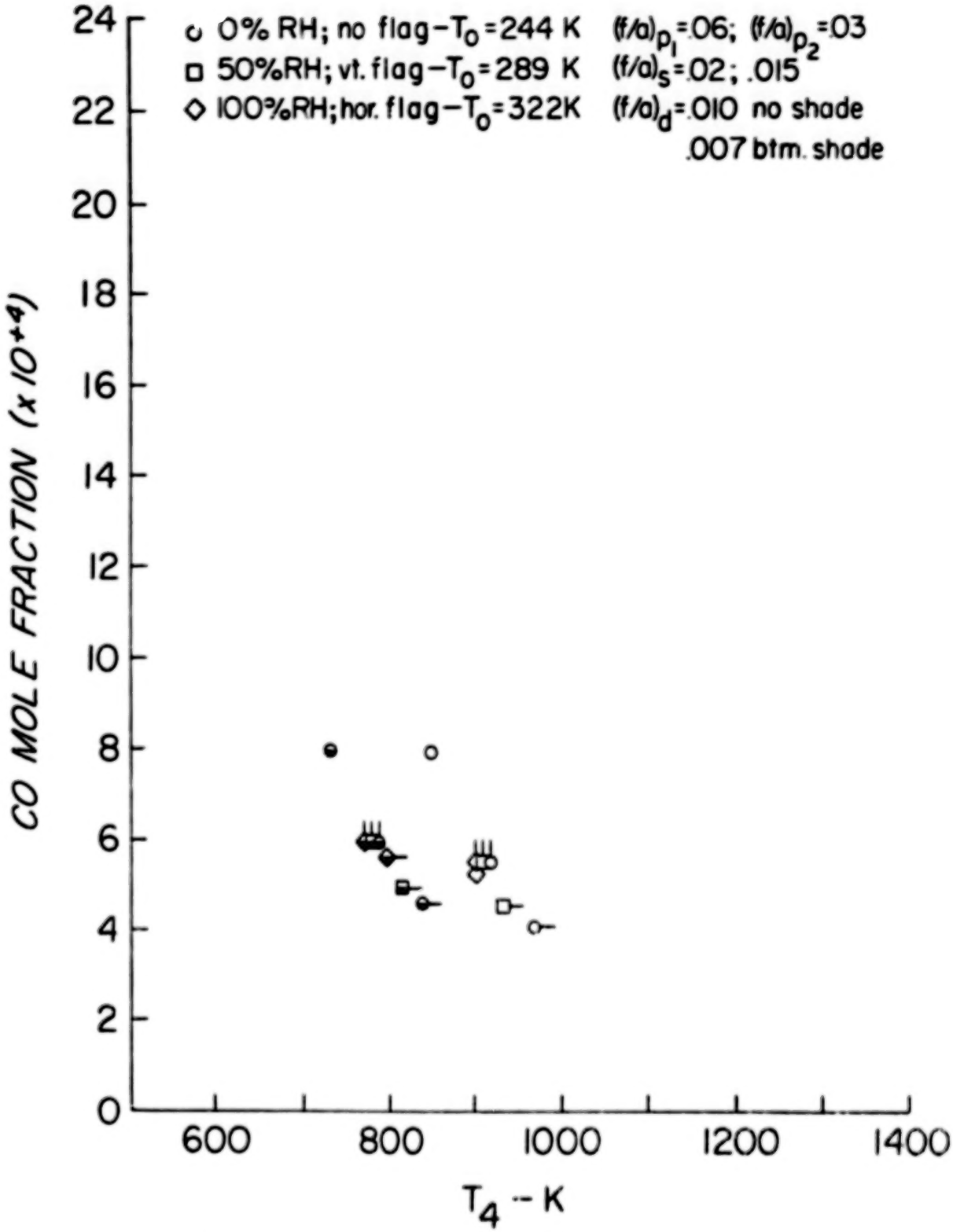

Figure 52. Carbon Monoxide Emissions for a Primary Zone Fuel-Air Ratio of .06

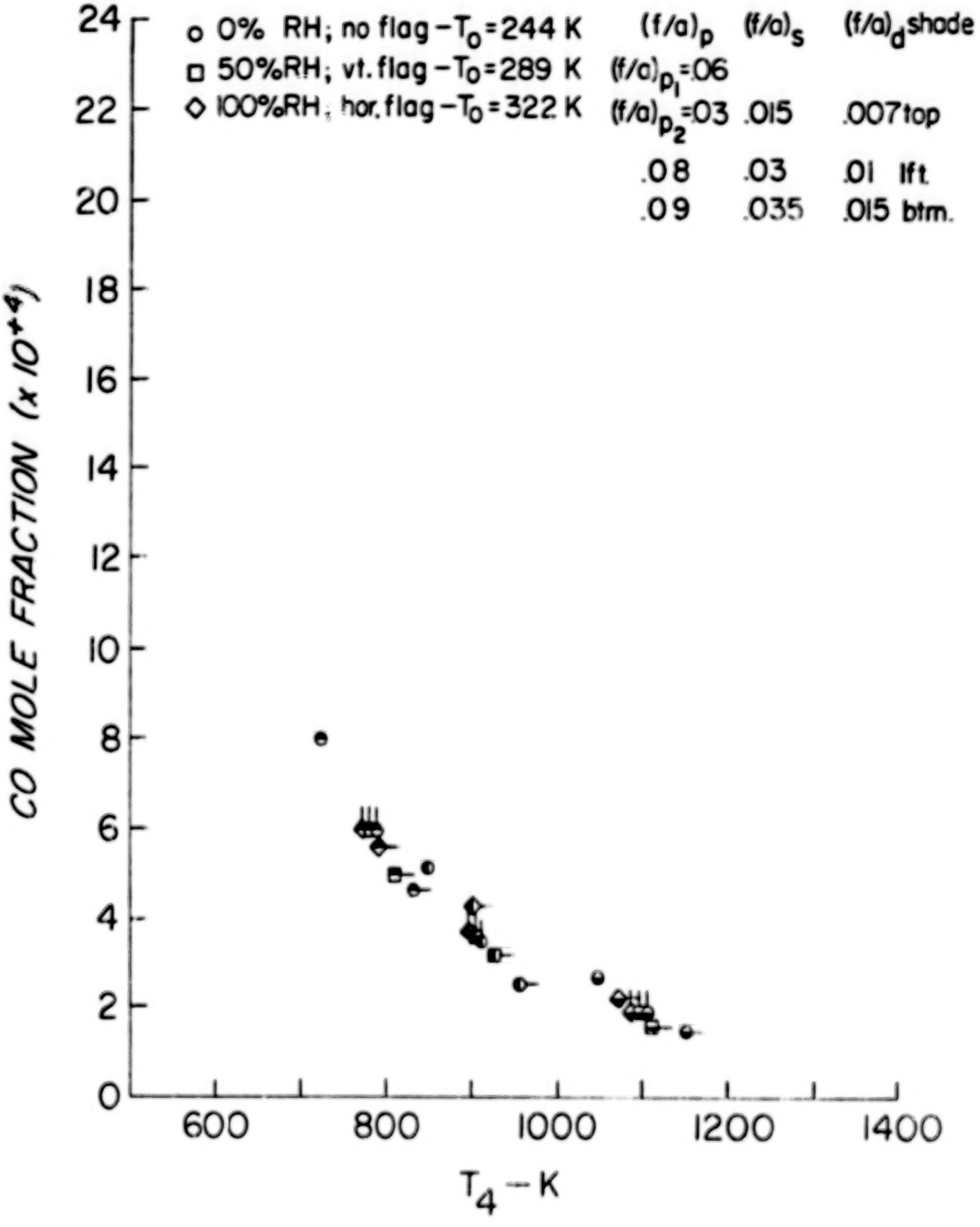

Figure 53. Carbon Monoxide Emissions for Different Primary Zones

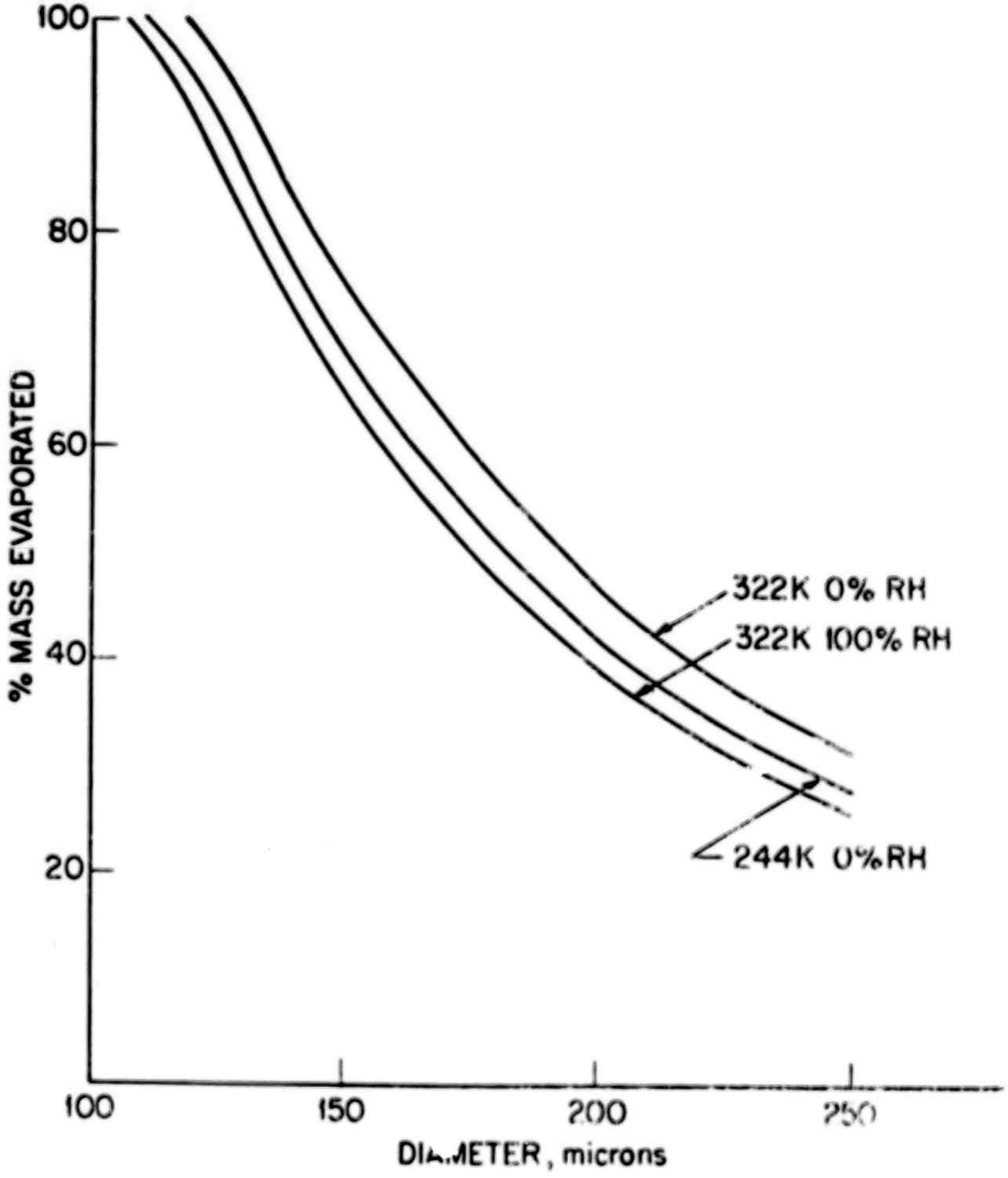

Figure 54. Fuel Drop Evaporation

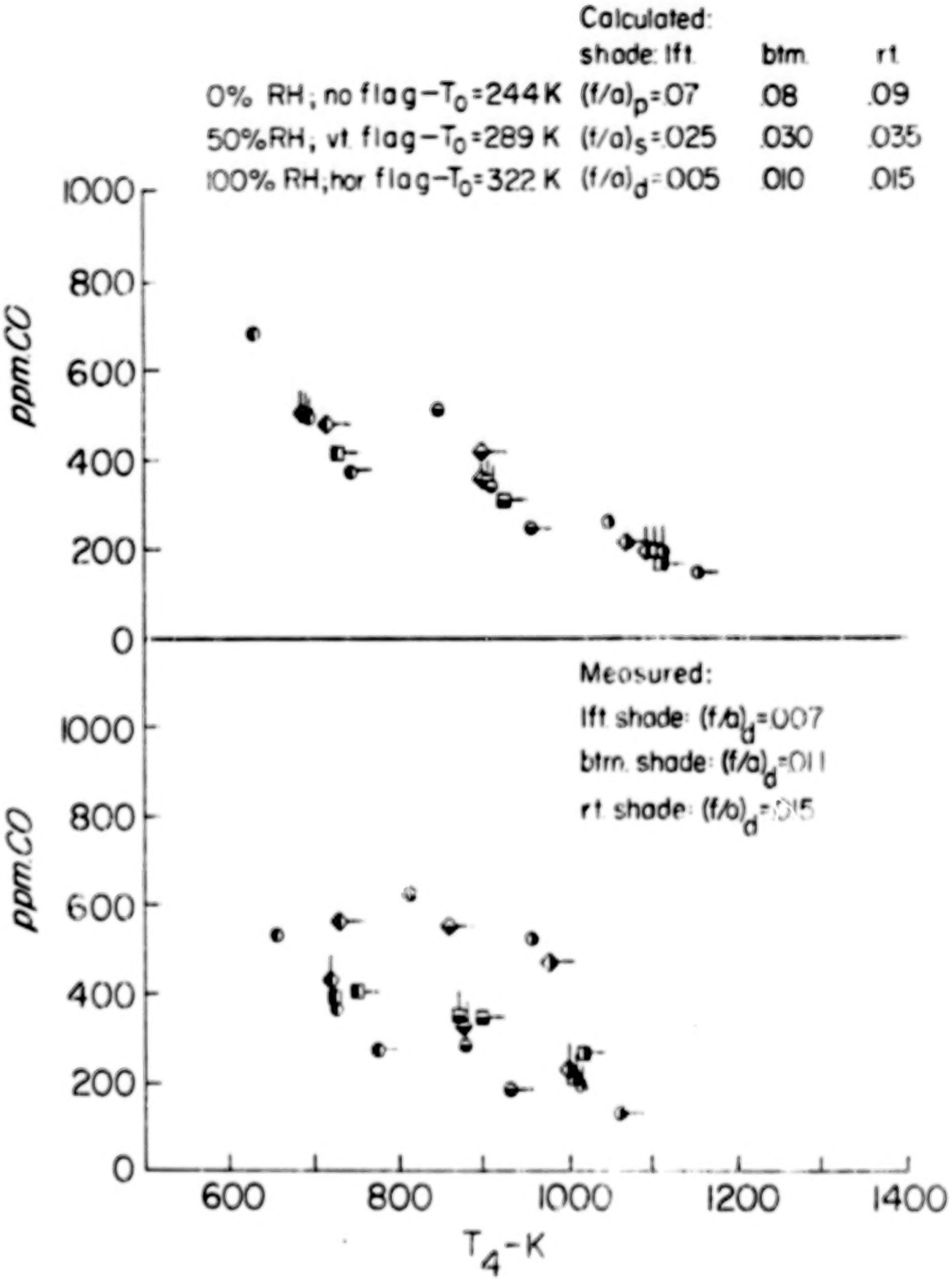

Figure 55. Comparison of Calculated and Measured Carbon Monoxide Emissions

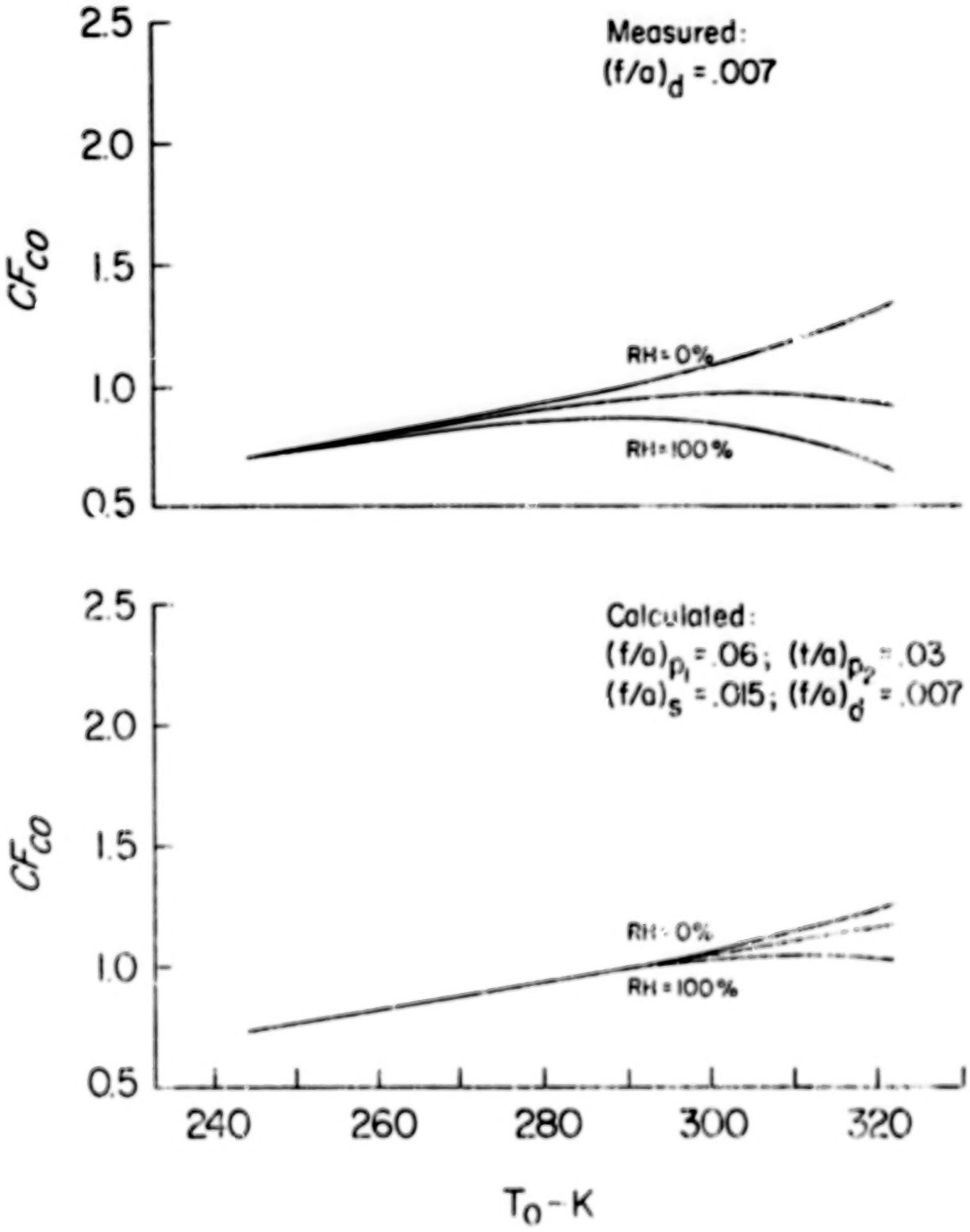

Figure 56. Ambient Temperature and Humidity Correction Factor for a Dilution Zone Fuel-Air Ratio of .007

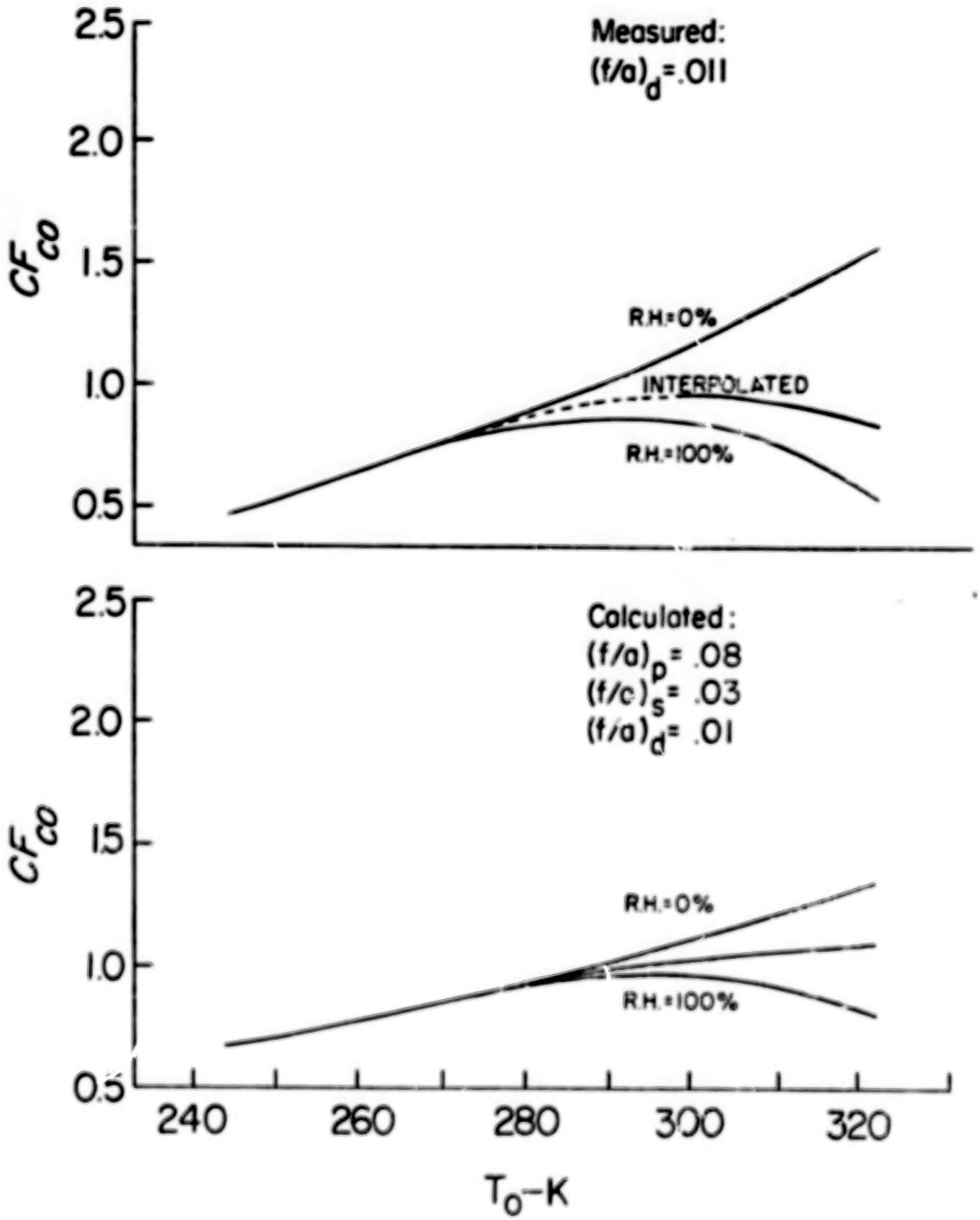

Figure 57. Ambient Temperature and Humidity Correction Factor for a Dilution Zone Fuel-Air Ratio of .011

TABLE OF CONTENTS

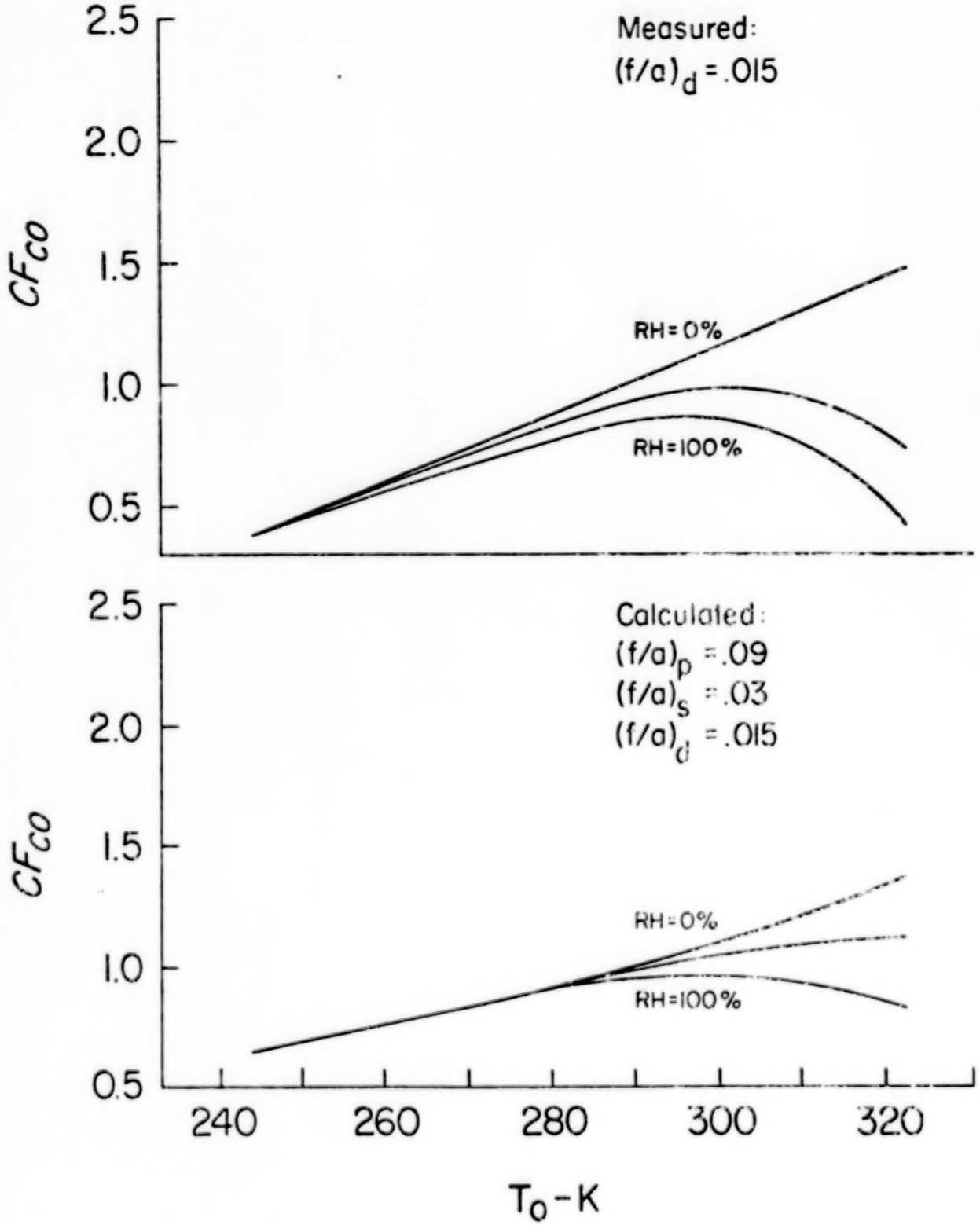

Figure 58. Ambient Temperature and Humidity Correction Factor for a Dilution Zone Fuel-Air Ratio of .015

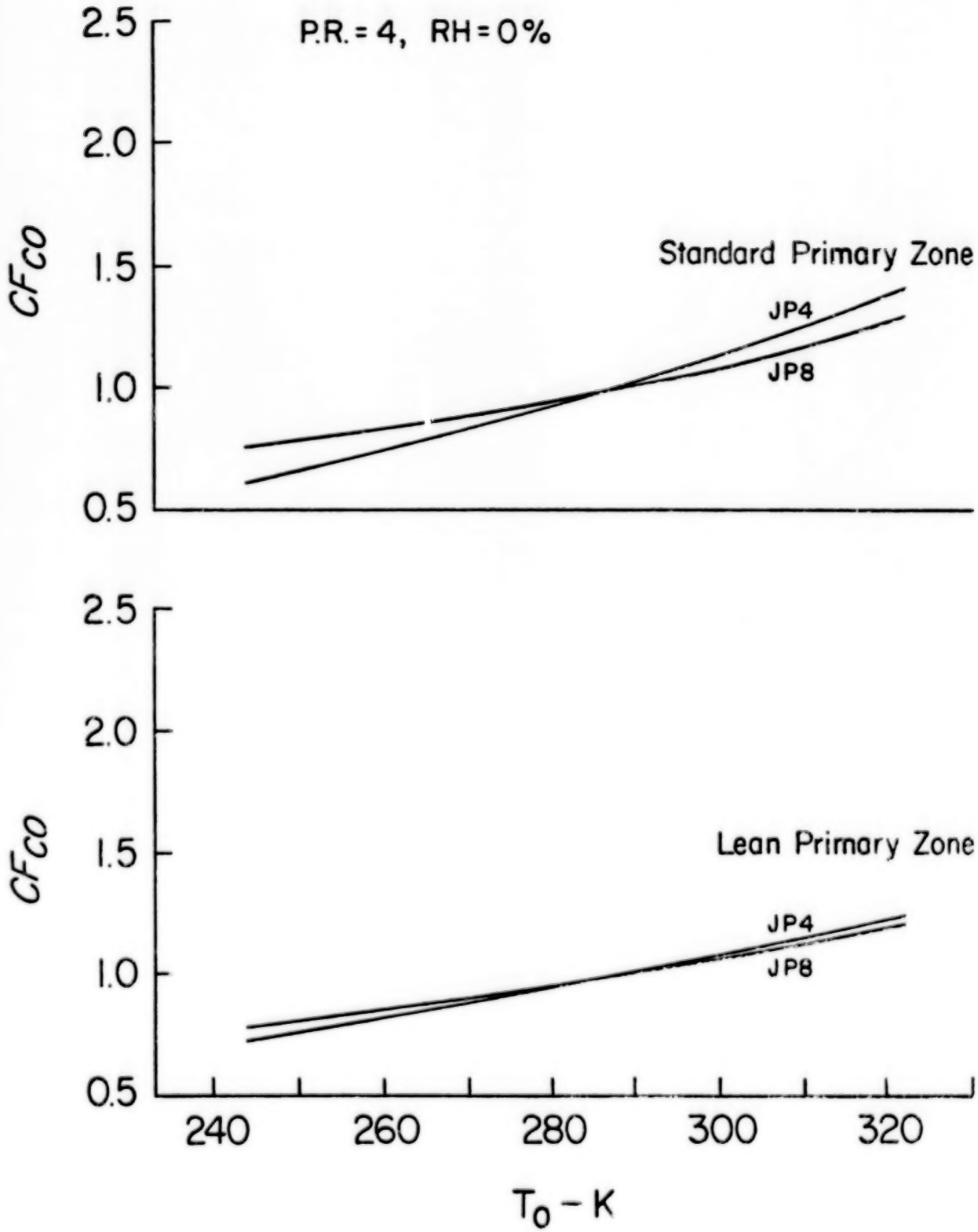

Figure 59. Ambient Temperature and Humidity Correction Factor, T-56

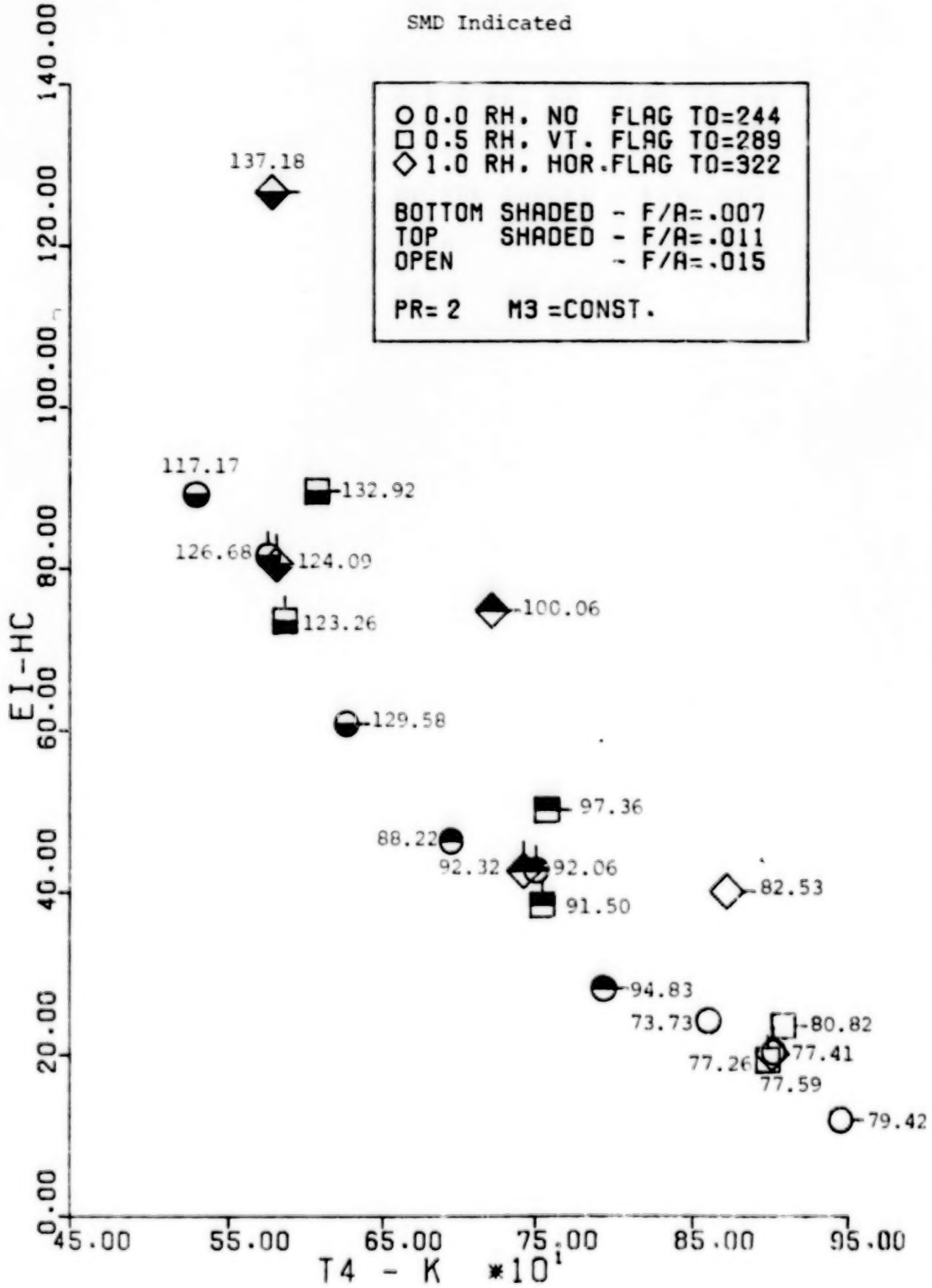

Figure 60. Hydrocarbon Emissions, SMD Effect for a Constant Compressor Discharge Mach Number at a Pressure Ratio of Two

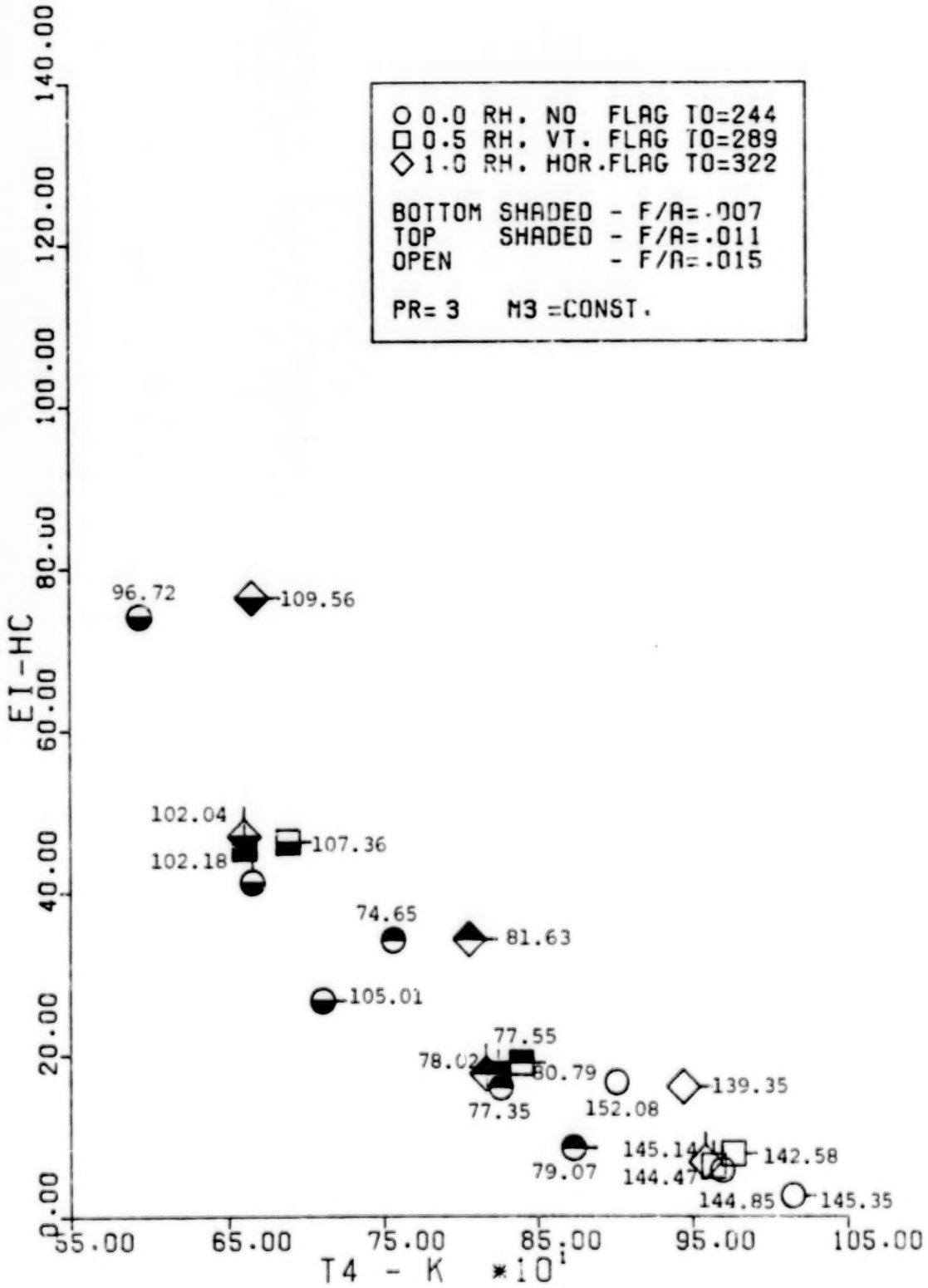

Figure 61. Hydrocarbon Emissions, SMD Effect for a Constant Compressor Discharge Mach Number at a Pressure Ratio of Three

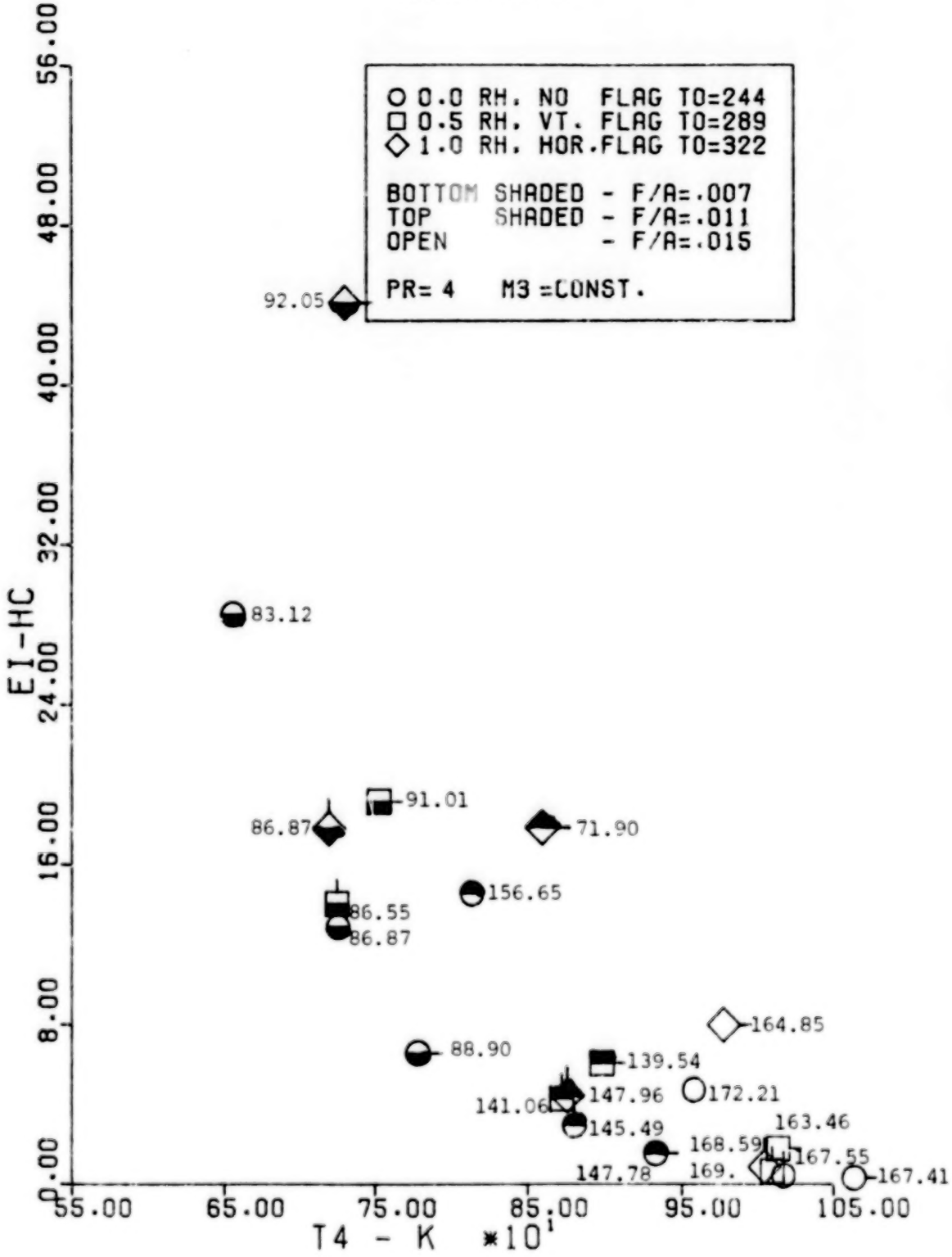

Figure 62. Hydrocarbon Emissions, SMD Effect for a Constant Compressor Discharge Mach Number at a Pressure Ratio of Four

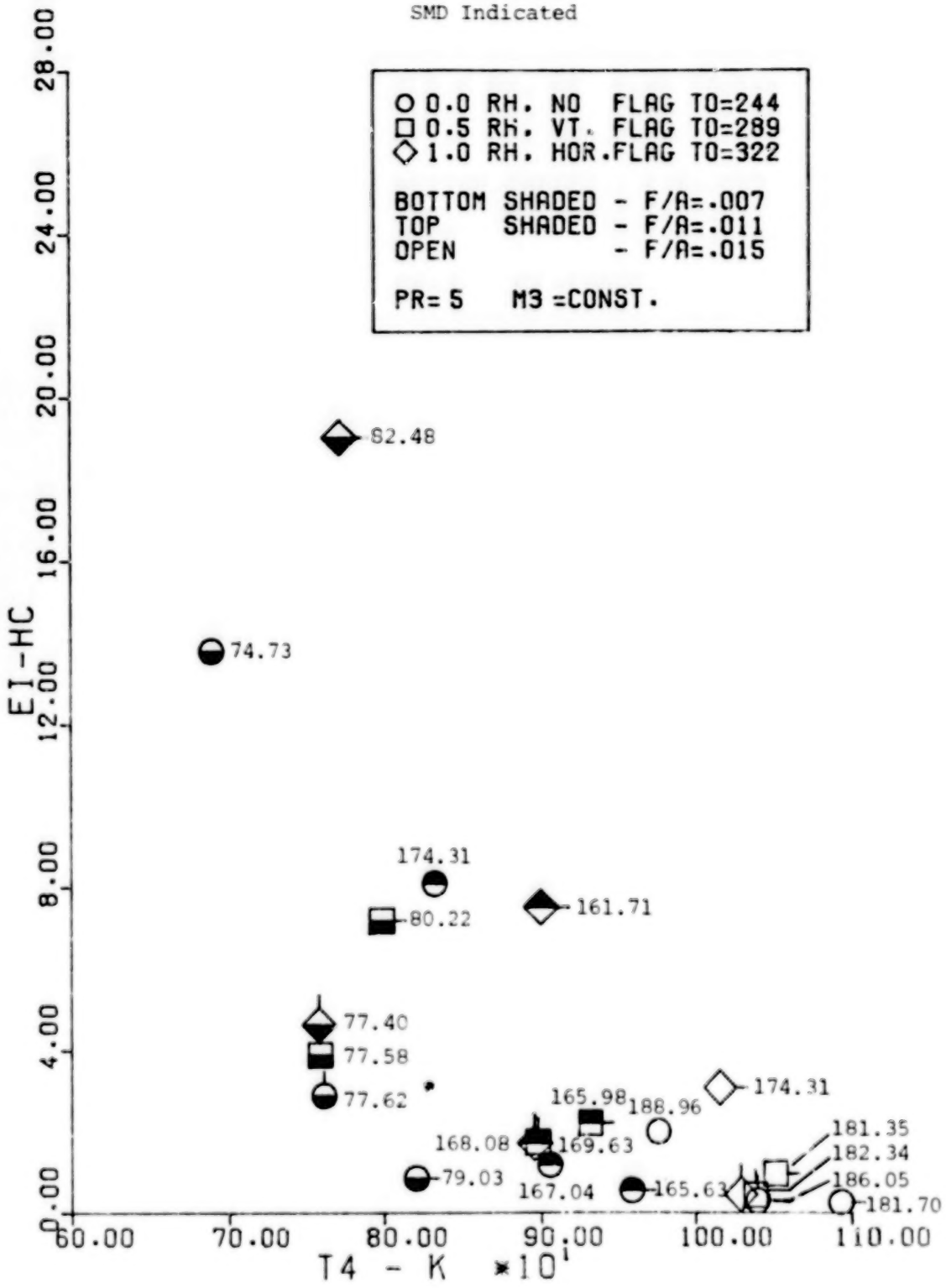

Figure 63. Hydrocarbon Emissions, SMD Effect for a Constant Compressor Discharge Mach Number at a Pressure Ratio of Five

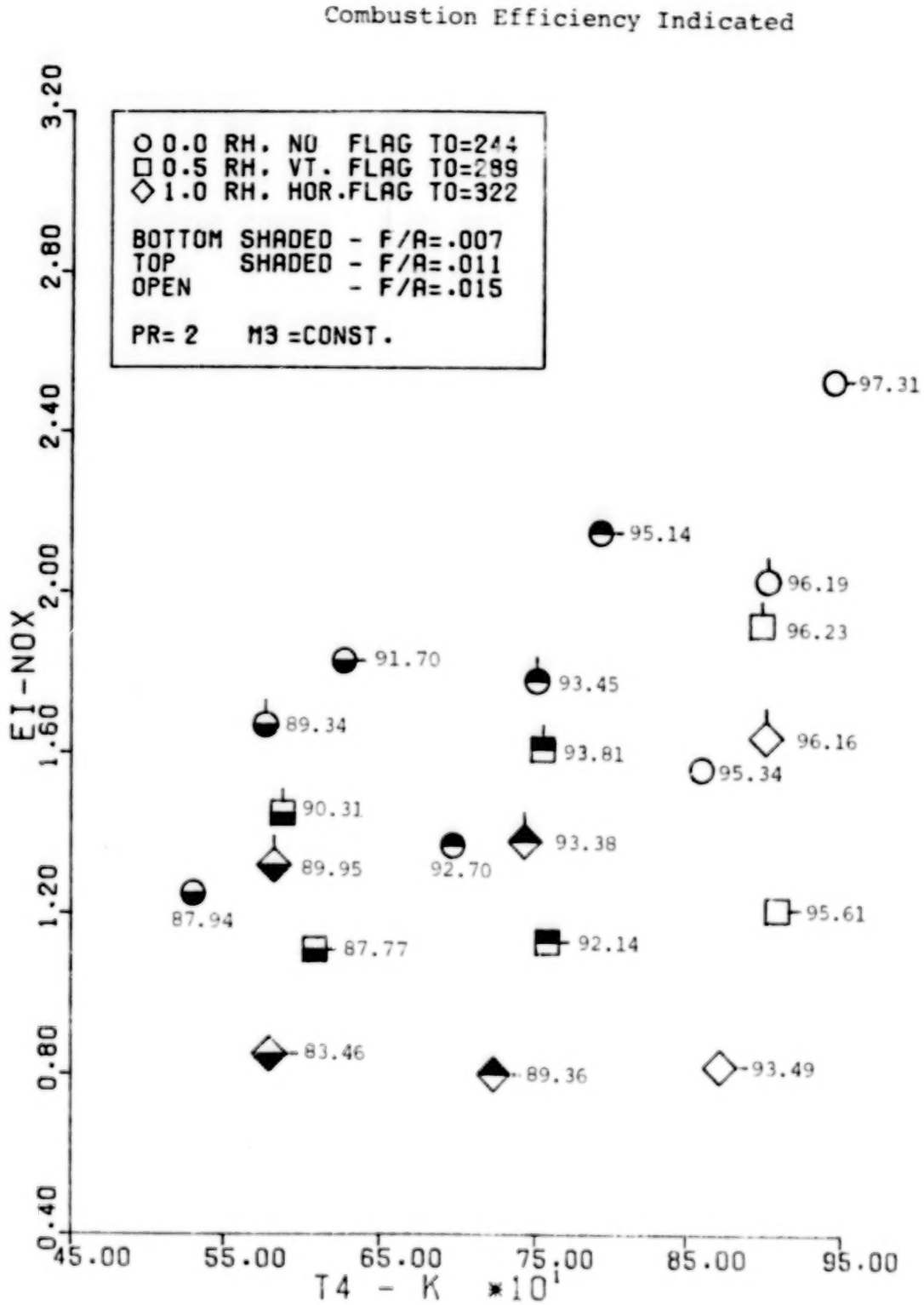

Figure 64. Oxides of Nitrogen, Combustion Efficiency for a Constant Compressor Discharge Mach Number at a Pressure Ratio of Two

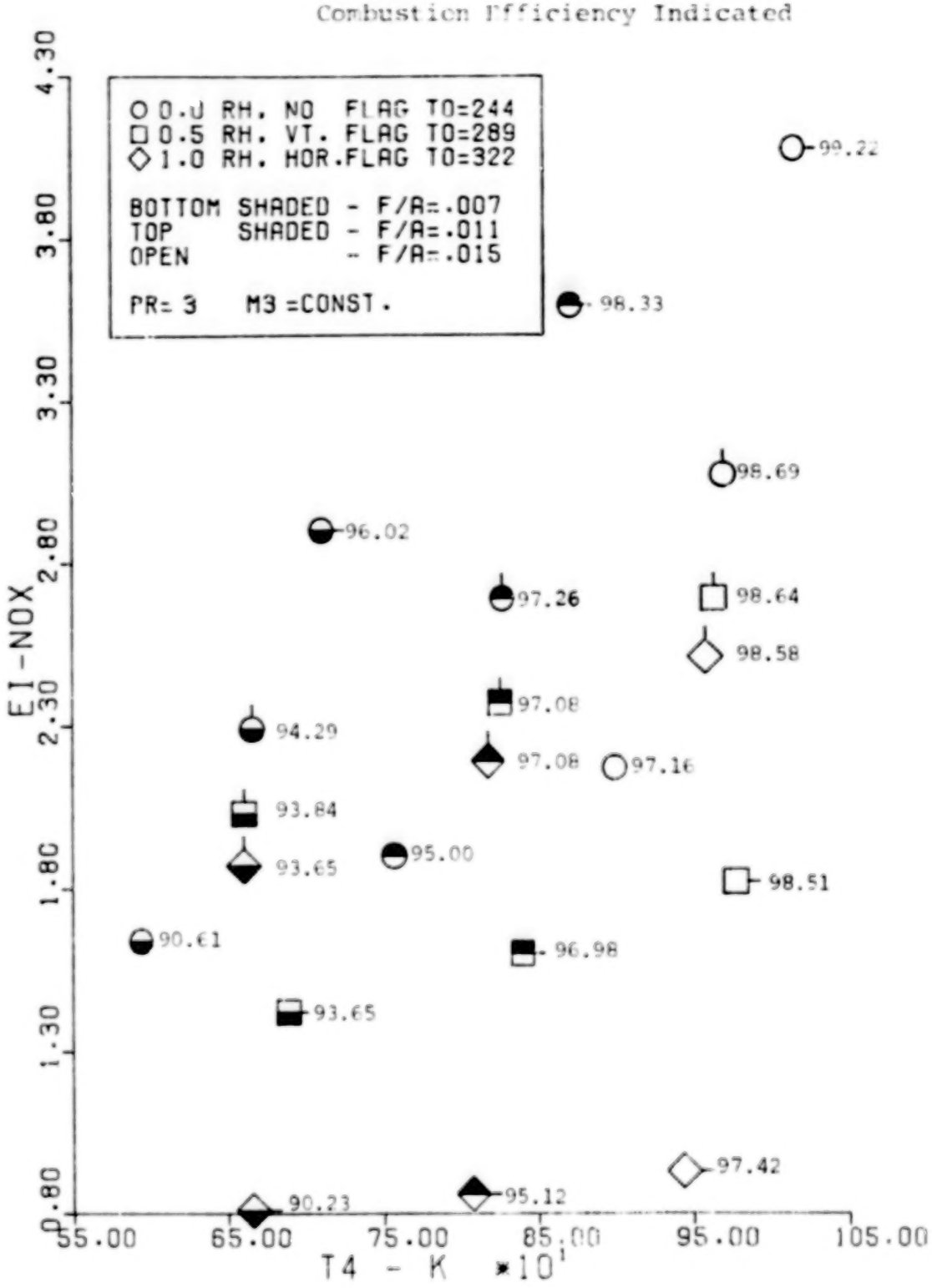

Figure 65. Oxides of Nitrogen, Combustion Efficiency for a Constant Compressor Discharge Mach Number at a Pressure Ratio of Three

Combustion Efficiency Indicated

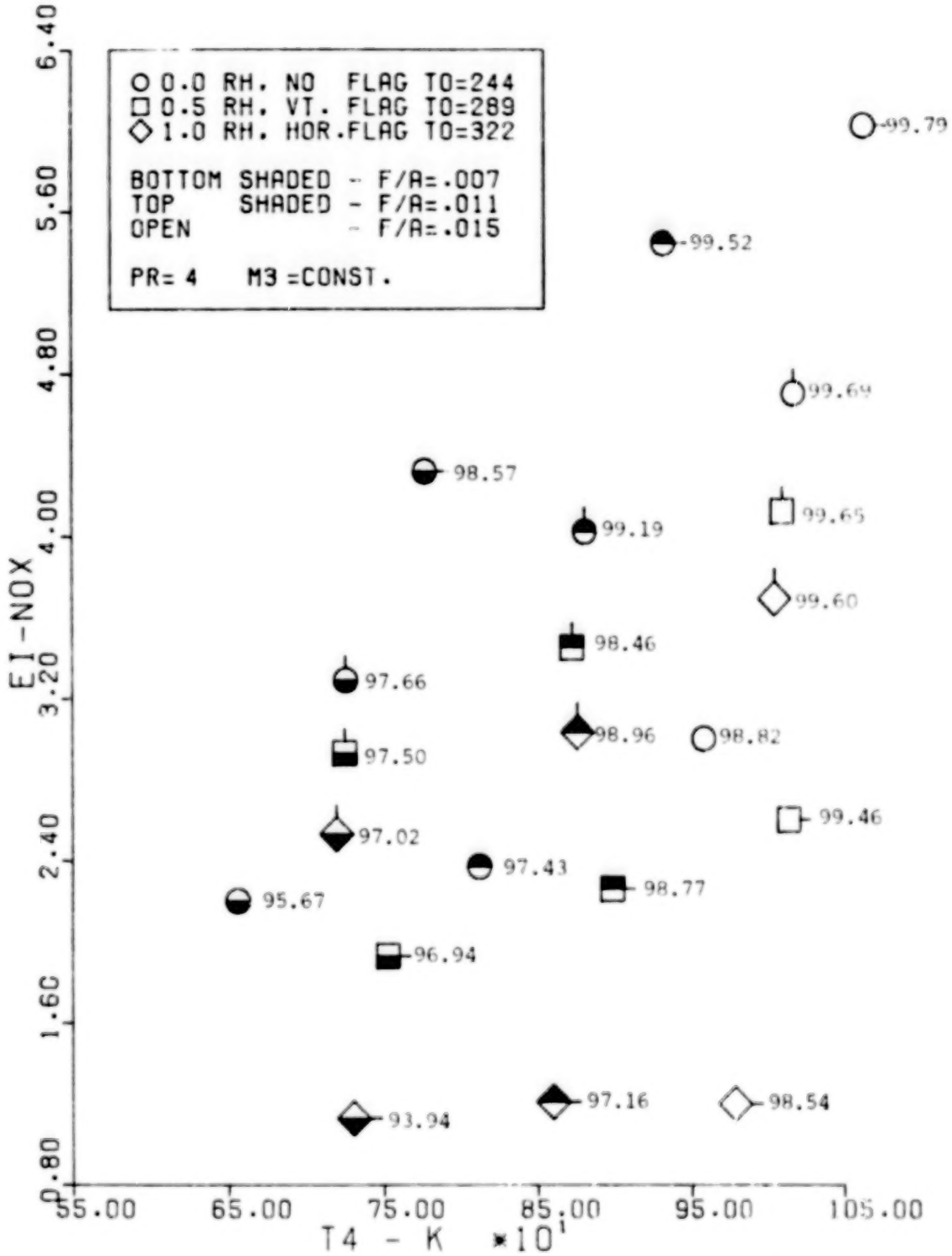

Figure 66. Oxides of Nitrogen, Combustion Efficiency for a Constant Compressor Discharge Mach Number at a Pressure Ratio of Four

Combustion Efficiency Indicated

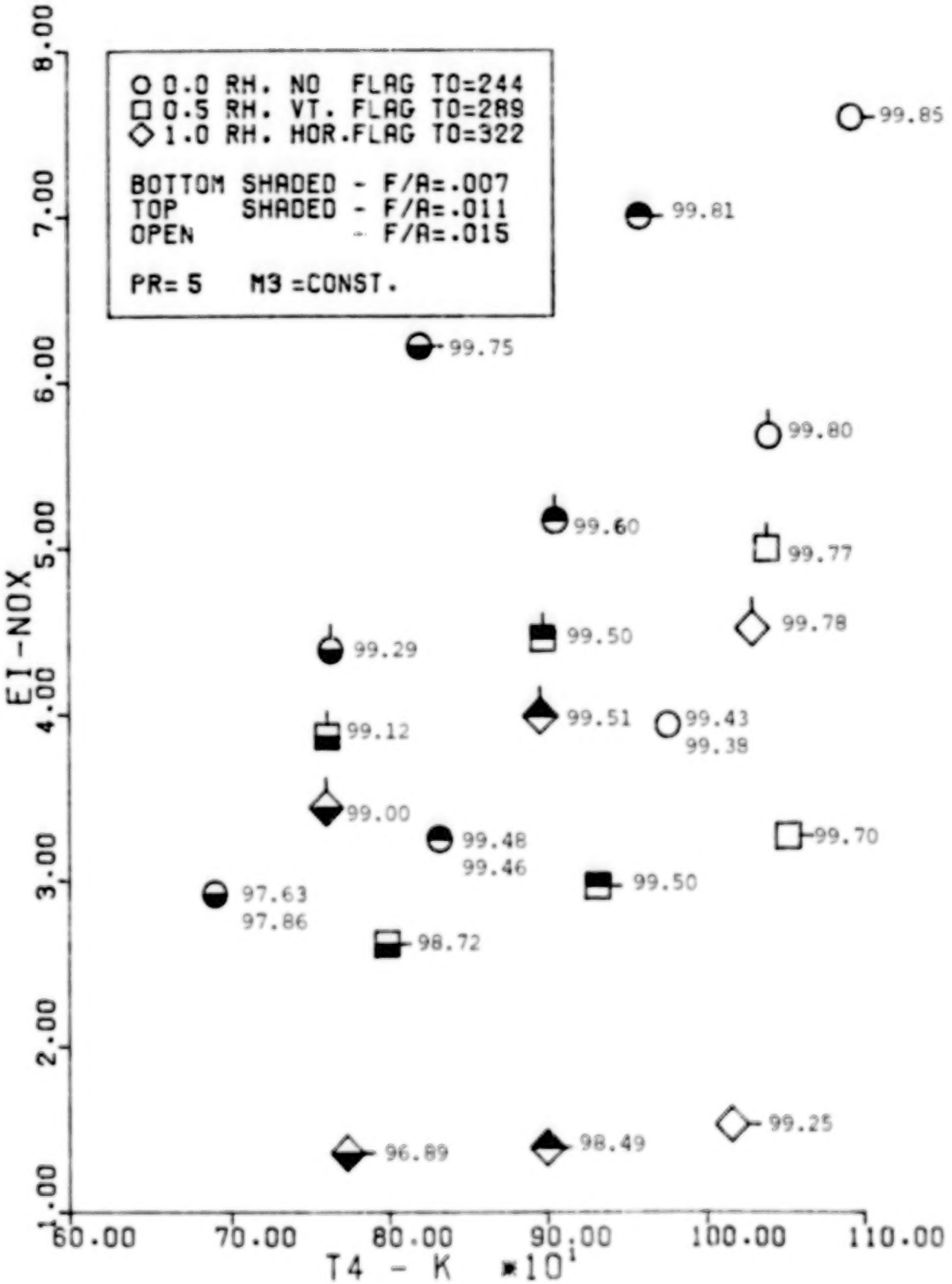

Figure 67. Oxides of Nitrogen, Combustion Efficiency for a Constant Compressor Discharge Mach Number at a Pressure ratio of Five

1. Report No.	2. Government Accession No.	3. Recipient's Catalog No.
NASA CR-3355		

4. Title and Subtitle	5. Report Date
EFFECT OF AMBIENT CONDITIONS ON THE EMISSIONS FROM A GAS TURBINE COMBUSTOR	November 1980
	6. Performing Organization Code

7. Author(s)	8. Performing Organization Report No.
C. W. Kauffman	None
	10. Work Unit No.

9. Performing Organization Name and Address	11. Contract or Grant No.
University of Cincinnati Cincinnati, Ohio 45219	NSG-3045
	13. Type of Report and Period Covered
12. Sponsoring Agency Name and Address	Contractor Report
National Aeronautics and Space Administration Washington, D.C. 20546	14. Sponsoring Agency Code

15. Supplementary Notes
Final report. Project Managers, Robert E. Jones, Aerothermodynamics and Fuels Division, Lewis Research Center, and David B. Ercegovic, U.S. Army Research and Technology Laboratories (AVRADCOM), Propulsion Laboratory, Lewis Research Center, Cleveland, Ohio 44135.

16. Abstract

An experimental and analytical investigation was initiated to determine, in a systematic way and under controlled conditions, the effect of variations in the ambient conditions of pressure, temperature, and relative humidity upon the emissions of a gas turbine combustor. A single combustor can from a Pratt and Whitney JT8D-17 engine was run at parametric inlet conditions bracketing the actual engine idle conditions. Data were correlated to determine the functional relationships between the emissions and ambient conditions. Mathematical modelling was used to determine the mechanism for the carbon monoxide and hydrocarbon emissions. Carbon monoxide emissions were modelled using finite rate chemical kinetics in a plug flow scheme. Hydrocarbon emissions were modelled by a vaporization scheme throughout the combustor.

17. Key Words (Suggested by Author(s))	18. Distribution Statement
Emissions Combustors Modelling	Unclassified - unlimited STAR Category 07

19. Security Classif. (of this report)	20. Security Classif. (of this page)	21. No. of Pages	22. Price*
Unclassified	Unclassified	106	A06

* For sale by the National Technical Information Service, Springfield, Virginia 22161

NASA-Langley, 1980

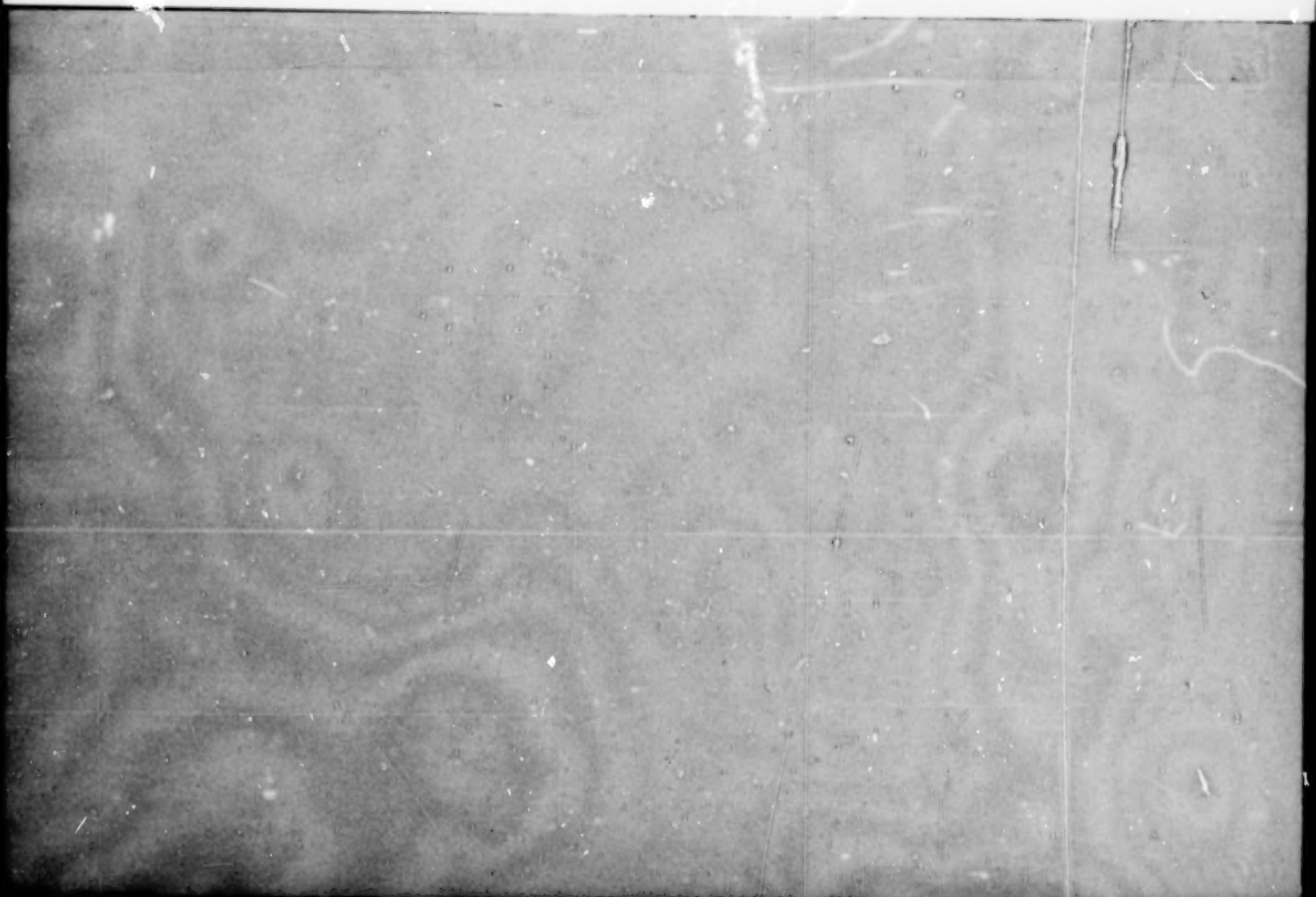

END

February 23/1981